The Dissertation Committee for Derek Scott Hernandez Certifies that this is the approved version of the following dissertation:

Multiphoton Techniques for Dynamic Manipulation of Cellular Microenvironments

Committee:

George Georgiou, Supervisor

Jason Shear, Co-Supervisor

Christine Schmidt

Christopher Ellison

Lydia Contreras

Wesley Thompson

Multiphoton Techniques for Dynamic Manipulation of Cellular Microenvironments

by

Derek Scott Hernandez B.S. Ch.E.

Dissertation

Presented to the Faculty of the Graduate School of

The University of Texas at Austin

in Partial Fulfillment

of the Requirements

for the Degree of

Doctor of Philosophy

The University of Texas at Austin

August, 2014

Acknowledgements

Multiphoton Techniques for Dynamic Manipulation of Cellular Microenvironments

Derek Scott Hernandez, Ph.D.

The University of Texas at Austin, 2014

Supervisors: George Georgiou and Jason Shear

A multitude of biophysical signals, including chemical, mechanical, and contact guidance cues, are embedded within the extracellular matrix (ECM) to dictate cell behavior and determine cell fate. To understand the complexity of the cell-matrix interaction and how changes to the ECM contribute to the development of tissues or diseases, three-dimensional (3D), culture systems that can decouple the effects of these cues on cell behavior are required. This dissertation describes the development and characterization of approaches based on multiphoton excitation (MPE) to control the chemical, mechanical, and topographical presentation of micro-3D-printed (μ-3DP) protein hydrogels independently. Protein hydrogels were chemically functionalized via the MPE-induced conjugation of benzophenone-biotin without altering the physical properties of the matrix. Complex, immobilized patterns and chemical gradients were generated within protein hydrogels with a high degree of spatial resolution in all axes. Hydrogel surfaces were also labeled with adhesive moieties to promote localized Schwann cell adhesion and polarization. Laser shrinking, a method based on MPE to manipulate the topographical and mechanical presentation of protein hydrogels after fabrication, is also presented. Topographical features on an originally flat substrate are created with depths approaching 6 μm. The Young's modulus of protein hydrogels can

also be increased by 6-fold (~15 – ~90 kPa) using laser shrinking, and parameters can be adjusted to create continuous gradient profiles for studying durotaxis. At determined scan conditions, the two properties can be adjusted independently of each other. Most importantly, the physical properties of the hydrogels can be manipulated *in situ* to study the effects of dynamic changes to the substrates on cells. As a potential tool to monitor cellular responses to presented cues, fluorescent probes that detect nitric oxide are characterized. Collectively, these technologies represent a key advance in hydrogel tunability, as the platforms presented offer independent, dynamic, and spatiotemporal control of the chemical, mechanical, and topographical features of protein hydrogels. The introduced technologies expand the possibilities of protein hydrogels to clarify underlying factors of cell-matrix interactions that drive morphogenesis and pathogenesis, and are broadly applicable to a multitude of physiological systems.

Table of Contents

List of Tables

List of Figures

Chapter 1: Biomimetic Cell Culture Platforms

1.1 BIOMATERIALS: A TRANSLATIONAL CHALLENGE

Cell culture was revolutionized in the early 1900's when Ross Harrison, Alexis Carrel, and Montrose Burrows introduced techniques to maintain living cells outside of the body [1, 2]. Since that time, the study of cells *in vitro* has led to the discovery of many biologically relevant mechanisms cells use to communicate with their surrounding environment. These experimental methods are the foundation that led to numerous discoveries to control cell phenomena such as morphology, gene expression, adhesion, and migration. However, as demonstrated by repeated failures to translate *in vitro* success to *in vivo* applications, two primary challenges continue to impede the progress of tissue engineering: 1) the two-dimensional nature of traditional cell-culture techniques is not representative of the native environment [3]; and 2) fact that current manufacturing methods lead to a coupling of many material properties, which prevents the evaluation of cellular responses to isolated signals [4].

Technologies such as photolithography, microfluidics, hydrogels, and three-dimensional (3D) printing have highlighted the importance of dimensionality in cell culture, and are driving the desire for more representative culture conditions [5]. A long list of material properties, such as chemical composition, topography, mechanical stimuli, and electrical conductivity have been studied to evaluate their roles in physiological systems. As our knowledge of what drives cellular outcomes continues to evolve, the ability to alter specific properties selectively is paramount to defining accurate cell-substrate interactions.

My research focuses on designing 3D platforms to engineer and manipulate culture systems in order to develop an understanding of the cell-matrix interaction. This

dissertation introduces novel approaches that seek to tune the chemical, mechanical, and topographical properties of protein hydrogels independently, and application of these techniques to influence fundamental cell behaviors such as adhesion and polarization. Understanding how cells function in dynamic environments also requires inventive methods to quantify chemical responses that accompany morphological and physiological changes. Toward this end, we have worked in concert with Eric Anslyn's Lab at the University of Texas at Austin, who develop fluorescent, nitric oxide (NO) probes, to evaluate the efficacy of NO sensing within and surrounding cultured cells. Ultimately, the use of probes for detecting various extracellular chemicals could be facilitated by conjugating such sensing molecules to 3D cell-culture scaffolds.

1.2 Environmental Signals to Direct Cellular Responses

The extracellular matrix (ECM) is a complex, 3D arrangement of chemical, mechanical, topographical, and electrical signals that dictate cell form and function. The composition and physical properties of the ECM are highly specific to the physiological system, and within individual tissues, subcellular heterogeneity exists in the combination and orientation of ECM components [6]. In an effort to encourage tissue regeneration, researchers across a number of fields have worked to recreate ECMs that mimic the native or developmental environment. Appropriate structural, chemical, and mechanical inputs are required to emulate the ECM; however, the complex, multidimensional, and dynamic environment is itself, difficult to characterize. Despite these challenges, the work conducted in this area of research has significantly contributed to the understanding of the cell-matrix interaction [7]. As a result, specific cellular responses to various matrix parameters, including chemical and biophysical cues, have been identified. A brief

review on how these inputs are integrated by cells and the types of responses they elicit is provided, focusing on the nervous system whenever appropriate.

1.2.1 Chemical Signaling

Cells have numerous recognition paradigms to respond to chemical signals in the extracellular environment [8-10]. For example, ECM proteins and growth factors bind to integrins and other receptors located on the cell membrane, activating various intracellular signaling pathways [11]. In addition to the extracellular composition, cells produce and secrete trophic factors, such as neurotransmitters or growth factors, to communicate with and support nearby cells [12]. Signaling molecules are known to influence a multitude of cell functions including adhesion, motility, differentiation, homeostasis, and cell death [13, 14]. For example, Schwann cells (SCs), the primary glial cells of the peripheral nervous system, secrete numerous growth factors and basement membrane proteins such as laminin, to support neurons and promote axogenesis during development and nerve repair [15-18]. More details regarding intracellular signaling pathways are beyond the scope of this document.

While certain chemical cues generate a common response across numerous cell phenotypes, many others elicit highly specific behaviors. Differential effects are attributed to variability in intracellular signaling cascades and receptor expression on the cell membrane [19-22]. For example, chondroitin sulfate proteoglycans (CSPGs), major components in glial scar tissue, recruit and activate macrophages but signal axons to degenerate [23, 24]. Furthermore, simultaneous exposure to more than one biomolecular species may be required to control cell organization and/or differentiation. Typically, combinations of growth factors and inducers are used to direct differentiation of pluripotent stem cells down specific lineages [25, 26]. Differential responses of cells to

3

various cues can offer opportunities for designing cell- or function-specific tissue scaffolds.

In addition to the type of signal presented, signal concentration also molds the cellular response. For instance, mesenchymal stem cells (MSCs) cultured with a higher concentration of fibroblast growth factor preferentially undergo neuronal differentiation as opposed to differentiation to other possible lineages [27, 28]. Kosaka *et al*. also increased the likelihood of neuronal differentiation of neural progenitor cells (NPCs) approximately three-fold over concentrations of fibroblast growth factor 4 (FGF-4) ranging from 0 – 5 ng/mL [29]. At a concentration of FGF-4 equal to 20 ng/mL, neuronal differentiation was reduced by 20% relative to 5 ng/mL. Another example highlighting the effect of cue concentration involves cell motility, where maximum velocities of smooth muscle cells are observed at intermediate ligand densities of collagen and fibronectin [30]. Similar biphasic distributions with respect to concentration have been reported for promoting axonal migration using nerve growth factor (NGF) gradients [31].

Since tissues and their component cells perform highly distinct functions, ECM composition is highly variable between physiological systems. For example, collagen is absent from the central nervous system, yet it makes up ~30% of the ECM elsewhere in the body [32]. To study effects of ECM composition on SC behavior, Suri and colleagues encapsulated SCs in hydrogels with an interpenetrating network of hyaluronic acid, collagen, and laminin, a primary ECM component of the peripheral nervous system. In the gels that contained laminin, the expression of S100 protein, a marker for SCs, and NGF secretion were significantly higher than for cells in laminin-free gels [33]. Deister *et al*. were also able to enhance neurite outgrowth from dorsal root ganglia (DRGs) simply by adjusting the composition of ECM proteins in hydrogels [34]. These studies highlight

4

the importance of developing scaffolds that reproduce certain aspects of native ECM composition in promoting appropriate tissue functions.

Additional biomolecules, beyond those contained within the ECM, can be presented to cells as soluble or bound cues to modify cell behavior in culture. For example, soluble cues can be dissolved within culture media in support of cell-culture maintenance. Gradients of soluble factors can also be generated using a combination of diffusion-based approaches and microfluidic devices [35-38]. Soluble gradients of permissive or inhibitory cues have been used to promote cell alignment and migration, a response referred to as chemotaxis. Seminal examples of chemotaxis demonstrated preferential migration and increased elongation of axons towards higher concentrations of NGF [39, 40]. Unlike soluble cues, bound cues are fixed to the substrate using bioconjugation chemistry or non-covalent adsorption. Bound cues are preferred for many tissue engineering applications where localized and sustained signaling is desired. In addition, the activity of many soluble cues is preserved when bound to a substrate [41-43]. For example, gradients of immobilized NGF are effective for directing neurite extension, a phenomenon known as haptotaxis, albeit at different concentrations than soluble NGF [31, 44]. Since cells cannot internalize bound cues, downstream signaling cascades associated with NGF internalization that promote additional neuronal outgrowth are limited; therefore, a nearly three-fold increase in the gradient slope is required for bound NGF to be effective [45, 46]. Ultimately the selected signal, its concentration, and its presentation have distinct impacts on the cellular response.

These examples highlight the importance of controlling the orientation and localized concentration of chemical cues within biomaterials to direct cell behavior. In **Chapter 2**, a platform to immobilize arbitrary, sub-cellular, 3D patterns of immobilized chemical cues on protein hydrogels is described. Protein hydrogels have previously been

investigated for biocompatibility, and their ability to serve as contact cues in tissue scaffolds was demonstrated [47-50]. Additional value of the immobilization technique is displayed by functionalizing protein hydrogels with adhesive peptides to improve cell adhesion and to promote cell patterning.

1.2.2 Mechanical Properties

Mechanical properties of the ECM are known to impact cell motility and direct stem cell differentiation through a process called mechanotransduction. Mechanotransduction refers to the transmission of tensile forces between cellular focal adhesion complexes and substrate binding motifs to intracellular signaling pathways. Cellular focal adhesions are dynamic protein complexes that link integrins with cytoskeletal filaments, including actin. As an external (or internal) force is applied to a cell, conformational changes to the focal adhesion complex impede its dissociation. The magnitude of the applied force depends on both the strength of the adhesion and the stiffness of the material, which ultimately dictates the stability of the focal adhesion complex. Application of force not only maintains the strong link between integrins and actin filaments, but also allows for the formation of more focal adhesion complexes that effectively fortify the interaction. Numerous proteins, including vinculin, phosphorylated focal adhesion kinase, Rho, Rac, and talin have been associated with the formation and subsequent signaling cascades of these complexes [51-53]. Most importantly, mechanotransduction must be viewed as an integration of both chemical and mechanical stimuli. Engineering approaches that can decouple the effects of these cues have the potential to improve understanding of cell-matrix interactions.

A commonly studied mechanical property of materials for cell applications is elastic modulus, and more specifically the Young's modulus or stiffness. Young's

modulus represents the ability of a material to reversibly deform under axial strain, often expressed in units of pascals (Pa) [1 kg/(m s^2)]. The modulus of tissues within the body range from as low as one hundred Pa in neural tissue [54], to kilopascals (kPa) in muscle fibers [55] and tendons [56], megapascals (MPa) for cartilage[57], and as high as gigapascals (GPa) for bones [58]. These innate differences highlight the importance of stiffness on form and function, and ultimately provide valuable clues to designing materials for targeted tissue regeneration.

The ability of cells to detect and respond to the mechanical properties of the surrounding matrix was first reported in 1997 by Pelham and Wang [59]. In this pioneering study, fibroblasts were cultured on polyacrylamide gels with a range of moduli and similar chemical presentation. Fibroblast motility, defined as migration speed, was significantly reduced from 0.55 to 0.1 μm/min as substrate stiffness increased from 15 to ~70 Pa. Lo *et al*. expanded on this work by creating gels with adjacent sections of low and high modulus, 14 and 30 kPa respectively. These studies revealed a directional bias of fibroblasts to preferentially localize on stiffer regions, a phenomena known as durotaxis [60]. A similar study by Gray also revealed a strong bias of fibroblasts to adhere and grow on stiffer substrates [61]. In contrast, neurite extension from DRGs was reduced in agarose hydrogels as gel stiffness increased from 2 to 140 Pa [62].

Engler and colleagues were the first to control stem cell fate using mechanical properties [63]. They cultured MSCs on polyacrylamide gels developed by Wang *et al*. with moduli of <1, 10, and 40 kPa. Significant differences in cell expression were observed after 7 days in culture. As Young's modulus was increased, cell fate displayed preferences first for neuronal, then myogenic, and finally osteogenic lineages. In addition, partially differentiated cells, such as neural progenitor cell (NPCs), can be

further directed to more specific phenotypes using substrate modulus. Numerous studies show neuronal selection is favored over glial phenotypes on softer substrates (<1 kPa) [64-67]. Collectively, these discoveries highlight the importance of modulus for directing cell fate, and have transformed how scientists approach scaffold design for tissue regeneration.

Matrix elasticity is an important property of the ECM, and its contribution to directed cell migration and differentiation is vital during embryonic development [7]. Changes in mechanical properties of the ECM are known to occur during aging, and the causal influence of these changes in numerous diseases, such as cancer, are currently under investigation [68-70]. Although a great deal of information has been discovered regarding cellular responses to mechanical stimuli, many details involving downstream signaling, temporal feedback, and dynamic responses remain unclear. In **Chapter 3**, a photolithographic approach to stiffen 3D protein matrices with sub-cellular resolution is presented. Moreover, matrix stiffening can be conducted *in situ* without damaging cells, and on short time scales (~60 s). The innovative platform presented in this dissertation provides a means to evaluate some of the unanswered questions regarding durotaxis and cellular responses to dynamic changes in modulus.

1.2.3 Topographical Cues

In addition to the bulk chemical and mechanical properties, the ECM is filled with nanometer-to-micron-scale landscapes of ridges, pores, and fibers created by biopolymers and the presence of various cell types that can influence cell-matrix interactions. Influences of topography have been directly observed during development, where radial glial cell features guide outgrowth and alignment of axons [71]. Biomaterials have been created to explore effects of topography on cell adhesion, polarization, migration, and

differentiation. The roles of feature sizes, surface roughness, and porosity have been studied since the discovery of contact guidance in the mid-20th century [72, 73]. However, many questions remain regarding the mechanisms involved in the cellular response to topography [74].

Cellular behaviors caused or modified by numerous topographic features, including pillars, grids, and holes, have been studied in detail. In most cases, however, the most effective and widely implemented topographies are variants of fibrillar or grooved substrates. Linear features such as these promote alignment of cytoskeletal filaments, and can be used to control cell morphology and migration persistence. Hoffman-Kim's Lab has extensively studied the alignment and migration of SCs, and have established that bi-directional migration of SCs *in vitro* can be promoted by imparting culture surfaces with ridges and grooves [75]. Axons also respond to the underlying topography of culture surfaces, and have been shown to orient on features as small as a few hundred nanometers [76]. Parameters including groove width, groove depth, and pitch are important aspects of topographical control [77, 78]. For SCs specifically, groove width has a more dominant effect on orientation than depth, but this is not true for all cell types [79].

Fibers are also of particular interests because they are more representative of native ECM than flat, grooved substrates. Fiber orientation can be controlled using electrospinning, magnetic fields, and micropatterning techniques; all approaches are viable for large, 3D scaffold development. Aligned fibers of fibronectin and collagen have been used to promote SC alignment and persistent migration *in vitro* [80, 81]. In addition, aligned collagen scaffolds are currently the best biomaterial-based treatment option for nerve regeneration scaffolds, although they have yet to unseat autologous grafts as preferred materials in treatment of damaged peripheral nerves [82]. Optimal

feature dimensions for topographically based approaches strongly depend on cellular phenotype and the desired response [83].

The rate-limiting step of many engineered regeneration platforms is cell infiltration into biomaterial scaffolds. Absent other cues, gel porosity can have a major influence on cell migration and proliferation. For osteoblasts, pore sizes greater than ~300 μm were shown to be much more supportive of cellular infiltration and proliferation of osteoblasts than were smaller pores [84]. The Rau Group devised a way to tune the porosity of collagen scaffolds without imposing discernible changes on the chemical properties using a novel freeze-drying method [85, 86]. SC infiltration was significantly enhanced after 14 days in gels that contained 20-50 μm pores over gels with smaller and larger average pore sizes [87]. These results are supported by studies conducted on grooved substrates as well that show maximum SC migration and neurite extension on substrates containing feature widths between 20 - 30 μm [78, 88].

Successful efforts to promote unidirectional migration to increase persistence and ultimately, migration speed have been based on presentation of asymmetric topographies. One design employed microposts of variable aspect ratios to increase directional migration [89]. Fibroblasts moved toward higher aspect ratio features 80% of the time, and total cell displacement was biased by ~54 μm over uniform control features. Mahmud and colleagues were able to achieve up to a 68% migration bias in a single direction in response to triangular ratchets [90]. The effectiveness of this approach strongly depended on feature sizes and adsorbed surface coatings, and it also required the presence of non-adhesive domains. Nonetheless, asymmetric topographies provide promise for increasing cell infiltration in 3D scaffolds.

At present, knowledge regarding the role of topography on stem cell differentiation is limited. It is believed that morphology, cytoskeletal arrangement, and

nuclear confinement can all affect gene expression through a variety of intracellular signaling pathways that are independent of other sensing pathways. For example, embryonic stem cells and MSCs have been shown to express neuronal markers when cultured on nano-grooved polydimethylsiloxane (PDMS) substrates, but not on identically stiff but flat PDMS [91, 92]. In a study by Charest *et al.*, myoblast differentiation was not sensitive to underlying topographies [93]; however, a more recent result revealed a slight increase in myogenic expression on patterned relative to smooth substrates [94]. Guvendiren *et al*. imprinted hydrogels with surface wrinkles to tune the ratio of MSCs expressing osteoblasts or adipoblasts markers after 7 days in culture [95]. Topographical effects on differentiation and gene expression also have been observed for neural stem cell lines [96, 97]. Collectively, these results suggest a potentially substantive role for topography during embryogenesis. Further evaluation is needed to determine detailed effects of topographical architectures and dimensions on cell differentiation before implementation in regenerative scaffolds is practical.

Topography, similar to mechanical and chemical cues, also can be used to control a number of vastly different cellular behaviors. As *in vitro* studies move toward 3D environments, the need for better spatial control of microscale topography has never been more essential. The Shear Lab previously established a micro-3D-printing method based on multiphoton lithography (MPL) to 'direct write' protein features within hydrogels [48, 98]. The resultant protein structures can act as 'contact guidance' cues, and they can be fabricated to contain subcellular topographical features that promote cellular behaviors. In **Chapter 3**, a method to modify the topography of protein architectures post-fabrication using site-specific, laser-induced shrinking is presented. Topographical changes can be created *in situ* without altering the apparent substrate moduli. This

technique promises to be a powerful approach for investigating cellular responses to rapid and dynamic changes to the underlying substrate.

1.2.4 Additional Cues

Other strategies to direct cell behavior include electrical cues, geometrical limitations, and degradative capacity, among others. Electrical currents play a key role in wound healing, and are known to promote cell migration toward the cathode for most, but not all, cell types [99]. Schmidt *et al*. encouraged axon extension, nearly doubling the average neurite length, using electrical stimulation [100]. Geometrical cues are chemically restrictive, sub-cellular patterns of adhesive ligands presented in the absence of other cues such as topography. This patterning approach has been used to control cell morphology, multi-cellular organization, and axon extension [101-104]. Matrix reorganization is a term used to describe dynamic changes that occur as cells interact with the surrounding environment. One way a cell moves through the ECM is by secreting proteases to degrade the material, effectively facilitating translocation. Raeber and Lee independently developed methods to chemically modify PEG gels with protease-sensitive linkers, resulting in a significant increase in cell infiltration, proliferation, and survival relative to control gels [105, 106]. These approaches are indeed unique, and could also be revolutionary to the field of tissue engineering.

1.2.5 Combined Effects of Cues

Presenting multiple types of cues within a single *in vitro* environment is more representative of the native ECM than single cue platforms, and could also be a key step toward developing smarter, more responsive, and more effective tissue scaffolds. A number of researchers in this area combine stimuli within a single category, such as multiple chemical cues, and/or incorporate cues from different categories to prompt a

response. The cue combinations can be stimulatory and/or inhibitory of various cellular pathways, and can be arranged in ways that are either competitive or cooperative. In many cases, presentation of multiple cues cannot be dissociated due to limitations associated with their instantiation (e.g. increasing the crosslinking density of collagen hydrogels also increases the concentration of adhesive domains and modulus). However, major advancements in microfluidics, chemistry, and soft lithography have made the design of multi-cue environments less challenging, leading to extraordinary progress in this area of research.

Multiple chemical factors are commonly used to promote differentiation and maintain cell cultures. The effects of combining chemical cues depend on how each signal is transduced, and whether independent or overlapping pathways are involved. Overstimulation of a single receptor by multiple factors may cause desensitization, and could lead to an unanticipated outcome [107]. For instance, directed axonal guidance was achieved when soluble gradients of NGF and neurotrophic factor-3 were presented simultaneously, but combinations of NGF and brain derived neurotrophic factor (BDNF), another chemoattractant, did not yield the same result [108]. Additionally, opposing gradients of immobilized laminin, a chemoattractant, and CSPG, a chemorepellant, have been used to enhance directed axon extension from DRGs [109]. Simultaneous presentation of haptotactic and chemotactic neurotrophic factors can act via cooperative mechanisms as well to reduce the concentrations needed of each species to have an effect. Moore *et al*. revealed that a smaller gradient of NGF provided more directed outgrowth of DRG axons when a soluble neurotrophic factor-3 gradient was present than in its absence [110]. Similar responses of growth cones to combined haptotactic and chemotactic gradients of laminin and BDNF, respectively, were also observed [111].

13

Gomez et al. studied the effects of immobilized NGF and topography on axon polarization and length [112]. No change in polarization was detected when the cues were combined, however, a 25% increase in axon length was observed. The researchers also positioned the cues in a competitive manner, revealing a dominant effect of topography over chemical patterns in neurite outgrowth [113]. This suggests that the mechanism for axonal polarization is controlled primarily by topographical cues, whereas axon length is more responsive to chemical factors. Similarly, fiber alignment overpowered the effect of chemical cues in neurite outgrowth and endothelial cell migration [114, 115].

Stiffness and topography can play a major role in differentiation, and also determine cell fate. Significant combinatory effects on cell polarity, proliferation, and MSC gene expression were discovered when these cues were presented simultaneously [116, 117]. Distinctions between the effect of similar topographies on relatively soft and hard substrates for SC precursors were less encouraging; however, the material stiffness of the soft substrate (1.7 MPa) was orders of magnitude higher than native glial cell tissues [118]. Microposts arrays were generated as an alternative means to combine these two cues, revealing enhanced polarization and alignment of endothelial cells on softer substrates [119]. These results were also obtained on semi-hard PDMS (~MPa) and extremely hard silica (~GPa). When mechanical and chemical gradients were generated in opposite or parallel directions, fibroblasts always migrated toward the higher concentration of collagen regardless of modulus. This result suggests that chemotaxis is superior to durotaxis for directing fibroblast migration [120].

Understanding the interplay of cellular cues in multi-cue environments is an important step toward developing better platforms for tissue regeneration. Despite the significant progress that has been made, many technological challenges persist. Methods to independently modify single cues within 3D scaffolds remain beyond current

capabilities, yet are necessary to truly discern the complexities of the cell-matrix interaction. The techniques presented in this dissertation are designed to provide independent control of such cues to decouple their effects on cell behavior, and eventually provide more effective tissue engineering platforms.

1.3 HYDROGEL FABRICATION FOR CELLULAR MICROENVIRONMENTS

Hydrogels are of widespread interest in the field of tissue regeneration because of structural similarities they share with native ECM. These porous, fibrillar, 3D scaffolds are created from a crosslinked networks of one or more polymer, protein, or polysaccharide, and are aptly named as a significant percentage of their mass is attributable to water. The molecules themselves are only fixed at defined positions, called crosslinks, and the remainder of the molecule is allowed to move freely in solution absent of other restrictions. The viscoelastic properties of hydrogels are a direct result of this molecular mobility. Reducing degrees of freedom by increasing the crosslink densities impacts viscoelastic and structural properties of hydrogels. Hydrogels have become the leading platform for studying cells *in vitro* because of their definable 3D structure. In addition, scientists have engineered ways to control the presentation of topographical, mechanical, and chemical cues within these scaffolds, making them promising materials for translational research.

Physical crosslinking relies on changes in inter- and intramolecular forces to form stable networks. Ionic or thermal manipulations are most commonly used to generate physical crosslinks. In alginate solutions, for example, adjacent molecules are linked through shared interactions with calcium ions to form a thermodynamically favored gel [121, 122]. Since calcium is biocompatible, this process can be used to encapsulate cells within solid alginate hydrogels [123]. Physical crosslinking of some proteins, such as

15

collagen and chitosan, occurs spontaneously at elevated temperatures, making such species primary candidates for the development of injectable hydrogels [124-126].

Chemical crosslinking is a much more diverse process than physical crosslinking, occuring via various reaction mechanisms to form stable, covalent bonds between molecules [127]. Often, chemical crosslinking approaches require use of toxic chemicals and/or organic solvents that are not compatible with living cells. Chemical crosslinking, however, is a popular approach in many applications because it can provide exceptional control of the structural and mechanical properties of hydrogels.

Soft lithography is a technique used to replicate features using elastomeric, deformable molds. This approach, first introduced by Whitesides and colleagues, gained wide adoption in the semiconductor industry because it is cheap, efficient, and reliable [128]. In brief, a master template is created by curing a photoresist film on a silica substrate with ultraviolet (UV) light. Features are created using optically transparent masks to selectively transmit patterns to the photoresist. Alternative techniques to create master templates that are not reliant on photolithography also have been developed [129]. PDMS is poured over the master template, thermally cured, and then separated from the master template. The features from the master are preserved on the surface of the PDMS as negative space with high fidelity, producing a reusable mold. The mold is then filled with a precursor solution and then gelled using one of many possible crosslinking technologies against a rigid substrate, such as glass.

Soft lithographic methods are highly versatile and have been used to fabricate protein and polymeric hydrogels for cell studies [130-132]. Many biological effects, including cellular responses to topography and cell patterning platforms, have progressed because of this technology [133, 134]. Recent work by Fourkas and colleagues has demonstrated that complex, 3D shapes can also be molded using soft lithography [135].

This is an improvement over the layer-by-layer approach originally introduced that requires additional processing and is time intensive [136, 137]. Additionally, soft lithography has tremendous potential for fabricating large-scale arrays for biological applications. Despite recent advances, the technology cannot provide 3D spatial resolution within already existing hydrogel networks.

Photolithographic techniques have undergone extensive development, primarily by the semiconductor industry, and have been useful for generating patterns on a substrate via exposure of a photoresist to high intensity light (typically UV) light. Individual photons provide an appropriate amount of energy to excite electrons to higher energy states from which various reactions can occur. This approach is used commonly to fabricate macromolecular hydrogels for tissue engineering scaffolds. Researchers have incorporated functional groups, such as acrylates, into the backbone of many polymers and proteins in order to promote crosslinking with UV-initiated photosensitizers [138, 139]. When combined with soft lithography, simple 3D features with micrometer resolution can be molded, but this approach does not provide the spatiotemporal advantages of MPL.

Only MPL offers the ability to 'direct-write' the architectural complexity of the ECM with sub-μm feature resolution in all axes. Early work by the Shear Group and others has established MPL as a widely applicable tool for fabrication of proteins and polymers, and MPL is the basis of the work presented in **Chapters 2** and **3** [140]. The theory of multiphoton excitation (MPE) was originally described by Marie Göppert-Mayer in 1931 [141]. She correctly predicted that an electron could be excited to a higher energy state by the simultaneous absorption of two or more photons of lower energy. A representative Jablonkski diagram is shown in **Figure 1.1**. Her theory was not proven experimentally until the invention of lasers 30 years later [142]. Both continuous wave

and pulsed lasers have been used to induce MPE, but pulsed sources are preferred because they dramatically reduce the average laser power required for MPE [143, 144]. For the simultaneous absorption of two or more photons to occur, a high photon flux is required. Regions of high photon flux can be generated via laser beam focusing using a high-numerical aperture (NA) objective. The non-linear dependence of excitation on light intensity limits the excitation to a 3D focal volume that can be on the order of $\sim 1 \ \mu m^3$. Additionally, most proteins and hydrogels are nearly transparent optically at the wavelengths typically used for MPE (near-infrared); therefore, higher depths can be reached without photodamaging out-of-plane molecules.

While early research related to MPE was dedicated to fluorescence, Strickler, Webb and others used MPE for stereolithographic printing of 3D, acrylate resins [145, 146]. Pitts et al. later crosslinked protein hydrogels using a titanium:sapphire (Ti:S) laser to excite a photosensitizer within a dense protein solution [147]. 3D features were created by scanning the laser in a single plane, and axially stitching fabrication planes in a layer-by-layer fashion. The Shear Lab combined this approach with digital masking technology to print free-form, 3D architectures with a library of biocompatible proteins [98, 148, 149]. A simplified schematic of the instrumentation used for this work is described in **Figure 1.2**. Several studies have demonstrated that certain proteins maintain at least a portion of their activity after crosslinking, making MPL a viable approach for printing biomimetic tissue culture platforms [47, 148, 150, 151]. Considering the need for features on various length scales within 3D tissue regeneration scaffolds, a combination of crosslinking platforms is necessary to design microenvironments with the representative complexity of native ECM for tissue engineering.
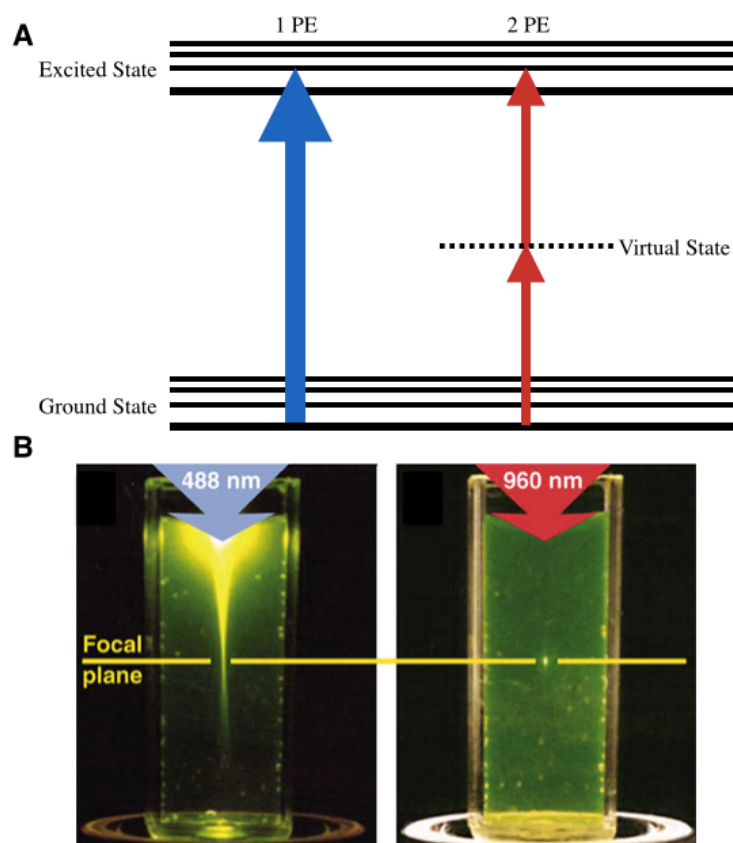
Figure 1.1: Comparison of single- and two-photon excitation (1PE and 2PE, respectively). A) A basic Jablonski diagram to highlight the principle of 1PE and 2PE. B) Fluorescence profiles within a cuvette of fluorescein generated using single (λ = 488 nm) and two-photon (λ = 960 nm) excitation. Emission promoted by 2PE is confined to positions close to the focal plane. Image adapted from [144].
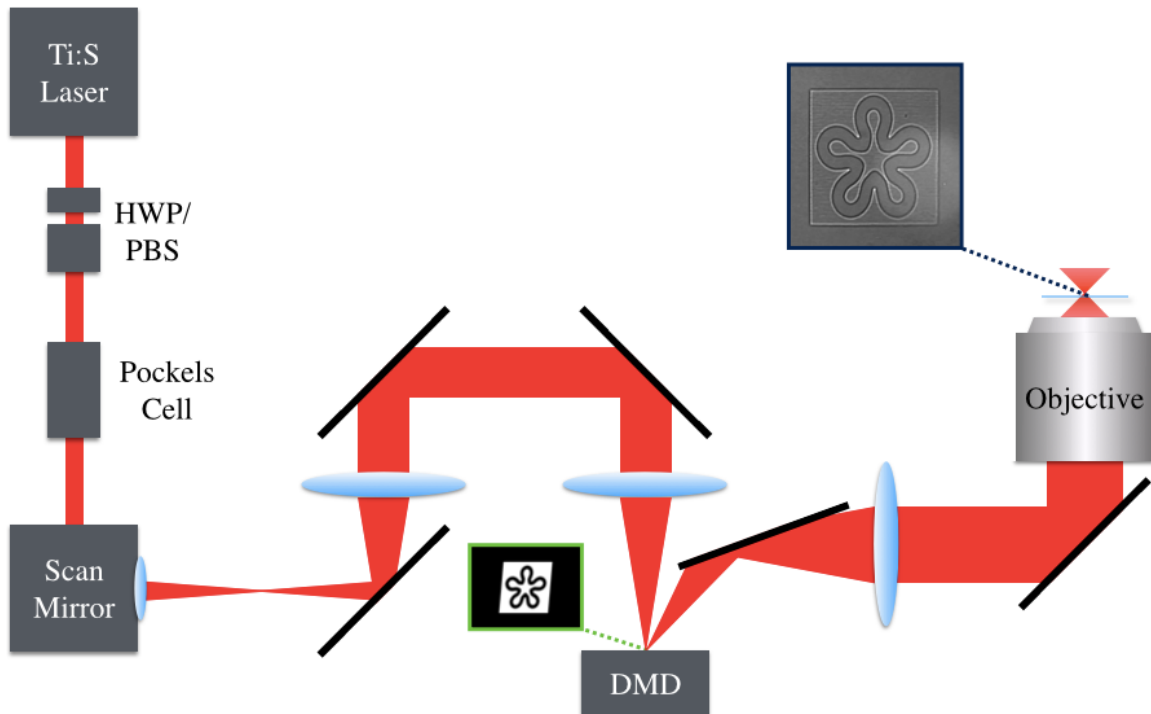
Figure 1.2: Multiphoton lithography instrumentation. The output from a pulsed Ti:S laser is directed through a paired half-wave plate (HWP)/polarizing beam-splitting cube (PBS) for manual laser power attenuation. Automated power attenuation is accomplished by applying voltage to a Pockel's cell using the output from a function generator. A two-axis, galvanometer-driven scan mirror that raster scans the focused laser beam at user-defined waveforms, frequencies, and amplitudes. Using a series of mirrors (black lines) and lenses (blue), the beam is focused on the face of a digital micromirror device (DMD) aligned in a plane that is conjugate to the focal plane of a high-NA objective situated on an inverted microscope. The DMD displays a binary photomask (green inset), where white pixels reflect the laser beam to the back aperture of the objective and result in the fabrication of densely crosslinked structures (navy inset). Image adapted from [152].

1.4 PREVIEW OF CONTENT

As the field of biomaterials progresses, it is clear that the effects of engineered scaffolds are a true integration of all material features including chemical, mechanical, and topographical properties. In order to further advance our understanding of the cell-matrix interaction, new methods must be established that allow for localized and independent control of multiple material properties within a 3D context. Previous work in the labs of Prof. Christine Schmidt and Prof. Jason Shear evaluated the efficacy of 3D-printed protein matrices as tissue engineering scaffolds [48]. The goals of this dissertation were to develop methods to harness more precise control of the chemical, topographical, and mechanical properties of these scaffolds. A strong emphasis has been placed on designing techniques that allow for independent manipulation of single cues, so effects ultimately can be decoupled. **Chapter 2** describes the development of a benzophenone-based immobilization chemistry to functionalize the surface of protein hydrogels for biological studies. **Chapter 3** describes the development of a technique to modify protein hydrogels post-fabrication by either adding topographical features or altering the elastic modulus. **Chapter 4** characterizes the efficacy of fluorescent NO probes for imaging intracellular and extracellular signaling. This work will be foundational in helping to uncover underlying mechanisms of cell-matrix interactions, and could eventually lead to pivotal advances in future designs of biomaterials for targeted treatment and tissue regeneration.

1.5 REFERENCES

1. Harrison, RG, *The outgrowth of the nerve fiber as a mode of protoplasmic movement*. Journal of Experimental Zoology, 1910. **9**(4): p. 787-846.

2. Carrel, AaB, Montrose T., *Cultivation of tissues in vitro and its technique*. Journal of Experimental Medicine, 1911. **13**: p. 387-396.

3. Pampaloni, F, Reynaud, EG, and Stelzer, EHK, *The third dimension bridges the gap between cell culture and live tissue*. Nature Reviews Molecular Cell Biology, 2007. **8**(10): p. 839-845.

4. Wang, X, *et al.*, *Decoupling polymer properties to elucidate mechanisms governing cell behavior*. Tissue Engineering Part B Review, 2012. **18**(5): p. 396-404.

5. Baker, BM and Chen, CS, *Deconstructing the third dimension: How 3d culture microenvironments alter cellular cues*. Journal of Cell Science, 2012. **125**(Pt 13): p. 3015-3024.

6. Frantz, C, Stewart, KM, and Weaver, VM, *The extracellular matrix at a glance*. Journal of Cell Science, 2010. **123**(Pt 24): p. 4195-4200.

7. Goody, MF and Henry, CA, *Dynamic interactions between cells and their extracellular matrix mediate embryonic development*. Molecular Reproduction and Development, 2010. **77**(6): p. 475-488.

8. Hynes, RO, *Integrins: Versatility, modulation, and signaling in cell adhesion*. Cell, 1992. **69**(1): p. 11-25.

9. Akira, S, Uematsu, S, and Takeuchi, O, *Pathogen recognition and innate immunity*. Cell, 2006. **124**(4): p. 783-801.

10. Artavanis-Tsakonas, S, Rand, MD, and Lake, RJ, *Notch signaling: Cell fate control and signal integration in development*. Science, 1999. **284**(5415): p. 770-776.

11. Harburger, DS and Calderwood, DA, *Integrin signalling at a glance*. Journal of Cell Science, 2009. **122**(Pt 2): p. 159-163.

12. Jacobson, MD, Weil, M, and Raff, MC, *Programmed cell death in animal development*. Cell, 1997. **88**(3): p. 347-354.

13. Chao, MV, *Neurotrophins and their receptors: A convergence point for many signalling pathways*. Nature Reviews Neuroscience, 2003. **4**(4): p. 299-309.

14. Reichardt, LF, *Neurotrophin-regulated signalling pathways*. Philosophical Transactions of the Royal Society of London B: Biological Sciences, 2006. **361**(1473): p. 1545-1564.

15. Ide, C, *et al*., *Schwann cell basal lamina and nerve regeneration*. Brain Research, 1983. **288**(1-2): p. 61-75.

16. Tam, SL and Gordon, T, *Mechanisms controlling axonal sprouting at the neuromuscular junction*. Journal of Neurocytology, 2003. **32**(5-8): p. 961-974.

17. Palm, SL and Furcht, LT, *Production of laminin and fibronectin by schwannoma cells: Cell-protein interactions in vitro and protein localization in peripheral nerve in vivo*. Journal of Cell Biology, 1983. **96**(5): p. 1218-1226.

18. Son, YJ, Trachtenberg, JT, and Thompson, WJ, *Schwann cells induce and guide sprouting and reinnervation of neuromuscular junctions*. Trends in Neuroscience, 1996. **19**(7): p. 280-285.

19. Coppola, V, *et al*., *Ablation of trka function in the immune system causes b cell abnormalities*. Development, 2004. **131**(20): p. 5185-5195.

20. Donovan, MJ, *et al*., *Brain derived neurotrophic factor is an endothelial cell survival factor required for intramyocardial vessel stabilization*. Development, 2000. **127**(21): p. 4531-4540.

21. Lindsay, RM, *Role of neurotrophins and trk receptors in the development and maintenance of sensory neurons: An overview*. Philosophical Transactions of the Royal Society of London B: Biological Sciences, 1996. **351**(1338): p. 365-373.

22. Mckerracher, L, Chamoux, M, and Arregui, CO, *Role of laminin and integrin interactions in growth cone guidance*. Molecular Neurobiology, 1996. **12**(2): p. 95-116.

23. Rolls, A, *et al*., *Two faces of chondroitin sulfate proteoglycan in spinal cord repair: A role in microglia/macrophage activation*. PLOS Medicine, 2008. **5**(8): p. e171.

24. Pindzola, RR, Doller, C, and Silver, J, *Putative inhibitory extracellular matrix molecules at the dorsal root entry zone of the spinal cord during development and after root and sciatic nerve lesions*. Developmental Biology, 1993. **156**(1): p. 34-48.

25. Mosna, F, Sensebe, L, and Krampera, M, *Human bone marrow and adipose tissue mesenchymal stem cells: A user's guide*. Stem Cells and Development, 2010. **19**(10): p. 1449-1470.

26. Boote Jones, EN and Mallapragada, SK, *Directed growth and differentiation of stem cells towards neural cell fates using soluble and surface-mediated cues*. Journal of Biomaterials Science Polymer Edition, 2007. **18**(8): p. 999-1015.

27. Tropel, P, *et al*., *Functional neuronal differentiation of bone marrow-derived mesenchymal stem cells*. Stem Cells, 2006. **24**(12): p. 2868-2876.

28. Hu, F, *et al.*, *Effects of epidermal growth factor and basic fibroblast growth factor on the proliferation and osteogenic and neural differentiation of adipose-derived stem cells*. Cell Reprogramming, 2013. **15**(3): p. 224-232.

29. Kosaka, N, *et al.*, *Fgf-4 regulates neural progenitor cell proliferation and neuronal differentiation*. FASEB Journal, 2006. **20**(9): p. 1484-1485.

30. Dimilla, PA, *et al.*, *Maximal migration of human smooth muscle cells on fibronectin and type iv collagen occurs at an intermediate attachment strength*. Journal of Cell Biology, 1993. **122**(3): p. 729-737.

31. Kapur, TA and Shoichet, MS, *Immobilized concentration gradients of nerve growth factor guide neurite outgrowth*. Journal of Biomedical Materials Research A, 2004. **68**(2): p. 235-243.

32. Bonneh-Barkay, D and Wiley, CA, *Brain extracellular matrix in neurodegeneration*. Brain Pathology, 2009. **19**(4): p. 573-585.

33. Suri, S and Schmidt, CE, *Cell-laden hydrogel constructs of hyaluronic acid, collagen, and laminin for neural tissue engineering*. Tissue Engineering Part A, 2010. **16**(5): p. 1703-1716.

34. Deister, C, Aljabari, S, and Schmidt, CE, *Effects of collagen 1, fibronectin, laminin and hyaluronic acid concentration in multi-component gels on neurite extension*. Journal of Biomaterials Science Polymer Edition, 2007. **18**(8): p. 983-997.

35. Dertinger, SKW, *et al.*, *Generation of gradients having complex shapes using microfluidic networks*. Analytical Chemistry, 2001. **73**(6): p. 1240-1246.

36. Gundersen, RW and Barrett, JN, *Characterization of the turning response of dorsal root neurites toward nerve growth factor*. Journal of Cell Biology, 1980. **87**(3 Pt 1): p. 546-554.

37. Zicha, D, Dunn, GA, and Brown, AF, *A new direct-viewing chemotaxis chamber*. Journal of Cell Science, 1991. **99 (Pt 4)**: p. 769-775.

38. Nelson, RD, Quie, PG, and Simmons, RL, *Chemotaxis under agarose: A new and simple method for measuring chemotaxis and spontaneous migration of human polymorphonuclear leukocytes and monocytes*. Journal of Immunology, 1975. **115**(6): p. 1650-1656.

39. Gundersen, RW and Barrett, JN, *Neuronal chemotaxis: Chick dorsal-root axons turn toward high concentrations of nerve growth factor*. Science, 1979. **206**(4422): p. 1079-1080.

40. Letourneau, PC, *Chemotactic response of nerve fiber elongation to nerve growth factor*. Developmental Biology, 1978. **66**(1): p. 183-196.

41.   Mccarthy, JB, Palm, SL, and Furcht, LT, *Migration by haptotaxis of a schwann cell tumor line to the basement membrane glycoprotein laminin*. Journal of Cell Biology, 1983. **97**(3): p. 772-777.

42.   Esch, T, Lemmon, V, and Banker, G, *Local presentation of substrate molecules directs axon specification by cultured hippocampal neurons*. Journal of Neuroscience, 1999. **19**(15): p. 6417-6426.

43.   Yu, LM, Wosnick, JH, and Shoichet, MS, *Miniaturized system of neurotrophin patterning for guided regeneration*. Journal of Neuroscience Methods, 2008. **171**(2): p. 253-263.

44.   Cao, X and Shoichet, MS, *Defining the concentration gradient of nerve growth factor for guided neurite outgrowth*. Neuroscience, 2001. **103**(3): p. 831-840.

45.   Huang, EJ and Reichardt, LF, *Trk receptors: Roles in neuronal signal transduction*. Annual Review Biochemistry, 2003. **72**: p. 609-642.

46.   Alfa, RW, Tuszynski, MH, and Blesch, A, *A novel inducible tyrosine kinase receptor to regulate signal transduction and neurite outgrowth*. Journal of Neuroscience Research, 2009. **87**(12): p. 2624-2631.

47.   Kaehr, B, *et al*., *Guiding neuronal development with in situ microfabrication*. Proceedings of the National Academy of Sciences, 2004. **101**(46): p. 16104-16108.

48.   Seidlits, SK, Schmidt, CE, and Shear, JB, *High-resolution patterning of hydrogels in three dimensions using direct-write photofabrication for cell guidance*. Advanced Functional Materials, 2009. **19**(22): p. 3543-3551.

49.   Basu, S, *et al*., *Multiphoton excited fabrication of collagen matrixes cross-linked by a modified benzophenone dimer: Bioactivity and enzymatic degradation*. Biomacromolecules, 2005. **6**(3): p. 1465-1474.

50.   Basu, S and Campagnola, PJ, *Properties of crosslinked protein matrices for tissue engineering applications synthesized by multiphoton excitation*. Journal of Biomedical Materials Research A, 2004. **71**(2): p. 359-368.

51.   Hoffman, BD, Grashoff, C, and Schwartz, MA, *Dynamic molecular processes mediate cellular mechanotransduction*. Nature, 2011. **475**(7356): p. 316-323.

52.   Schwarz, US and Gardel, ML, *United we stand: Integrating the actin cytoskeleton and cell-matrix adhesions in cellular mechanotransduction*. Journal of Cell Science, 2012. **125**(Pt 13): p. 3051-3060.

53.   Galbraith, CG and Sheetz, MP, *Forces on adhesive contacts affect cell function*. Current Opinion Cell Biology, 1998. **10**(5): p. 566-571.

54.   Miller, K, *et al*., *Mechanical properties of brain tissue in-vivo: Experiment and computer simulation*. Journal of Biomechanics, 2000. **33**(11): p. 1369-1376.

55. Collinsworth, AM, *et al.*, *Apparent elastic modulus and hysteresis of skeletal muscle cells throughout differentiation*. American Journal of Physiology Cell Physiology, 2002. **283**(4): p. C1219-1227.

56. Williams, LN, *et al.*, *The anisotropic compressive mechanical properties of the rabbit patellar tendon*. Biorheology, 2008. **45**(5): p. 577-586.

57. Shepherd, DE and Seedhom, BB, *The 'instantaneous' compressive modulus of human articular cartilage in joints of the lower limb*. Rheumatology, 1999. **38**(2): p. 124-132.

58. Katsamanis, F and Raftopoulos, DD, *Determination of mechanical properties of human femoral cortical bone by the hopkinson bar stress technique*. Journal of Biomechanics, 1990. **23**(11): p. 1173-1184.

59. Pelham, RJ, Jr. and Wang, Y, *Cell locomotion and focal adhesions are regulated by substrate flexibility*. Proceedings of the National Academy of Sciences, 1997. **94**(25): p. 13661-13665.

60. Lo, CM, *et al.*, *Cell movement is guided by the rigidity of the substrate*. Biophysical Journal, 2000. **79**(1): p. 144-152.

61. Gray, DS, Tien, J, and Chen, CS, *Repositioning of cells by mechanotaxis on surfaces with micropatterned young's modulus*. Journal of Biomedical Materials Research A, 2003. **66**(3): p. 605-614.

62. Balgude, AP, *et al.*, *Agarose gel stiffness determines rate of drg neurite extension in 3d cultures*. Biomaterials, 2001. **22**(10): p. 1077-1084.

63. Engler, AJ, *et al.*, *Matrix elasticity directs stem cell lineage specification*. Cell, 2006. **126**(4): p. 677-689.

64. Georges, PC, *et al.*, *Matrices with compliance comparable to that of brain tissue select neuronal over glial growth in mixed cortical cultures*. Biophysical Journal, 2006. **90**(8): p. 3012-3018.

65. Saha, K, *et al.*, *Substrate modulus directs neural stem cell behavior*. Biophysical Journal, 2008. **95**(9): p. 4426-4438.

66. Seidlits, SK, *et al.*, *The effects of hyaluronic acid hydrogels with tunable mechanical properties on neural progenitor cell differentiation*. Biomaterials, 2010. **31**(14): p. 3930-3940.

67. Banerjee, A, *et al.*, *The influence of hydrogel modulus on the proliferation and differentiation of encapsulated neural stem cells*. Biomaterials, 2009. **30**(27): p. 4695-4699.

68. Degroot, J, *The age of the matrix: Chemistry, consequence and cure*. Current Opinion in Pharmacology, 2004. **4**(3): p. 301-305.

69.   Huynh, J, *et al.*, *Age-related intimal stiffening enhances endothelial permeability and leukocyte transmigration*. Science Translational Medicine, 2011. **3**(112): p. 112ra122.

70.   Jaalouk, DE and Lammerding, J, *Mechanotransduction gone awry*. Nature Reviews Molecular Cell Biology, 2009. **10**(1): p. 63-73.

71.   Hatten, ME, *Central nervous system neuronal migration*. Annual Review Neuroscience, 1999. **22**: p. 511-539.

72.   Weiss, P, *The problem of specificity in growth and development*. Yale Journal of Biological Medicine, 1947. **19**(3): p. 235-278.

73.   Curtis, AS and Varde, M, *Control of cell behavior: Topological factors*. Journal of the National Cancer Instititue, 1964. **33**: p. 15-26.

74.   Hoffman-Kim, D, Mitchel, JA, and Bellamkonda, RV, *Topography, cell response, and nerve regeneration*. Annual Review Biomedical Engineering, 2010. **12**: p. 203-231.

75.   Mitchel, JA and Hoffman-Kim, D, *Cellular scale anisotropic topography guides schwann cell motility*. PLOS ONE, 2011. **6**(9): p. e24316.

76.   Johansson, F, *et al.*, *Axonal outgrowth on nano-imprinted patterns*. Biomaterials, 2006. **27**(8): p. 1251-1258.

77.   Li, N and Folch, A, *Integration of topographical and biochemical cues by axons during growth on microfabricated 3-d substrates*. Experimental Cell Research, 2005. **311**(2): p. 307-316.

78.   Mahoney, MJ, *et al.*, *The influence of microchannels on neurite growth and architecture*. Biomaterials, 2005. **26**(7): p. 771-778.

79.   Miller, C, *et al.*, *Oriented schwann cell growth on micropatterned biodegradable polymer substrates*. Biomaterials, 2001. **22**(11): p. 1263-1269.

80.   Ahmed, Z and Brown, RA, *Adhesion, alignment, and migration of cultured schwann cells on ultrathin fibronectin fibres*. Cell Motility and the Cytoskeleton, 1999. **42**(4): p. 331-343.

81.   Eguchi, Y, Ogiue-Ikeda, M, and Ueno, S, *Control of orientation of rat schwann cells using an 8-t static magnetic field*. Neuroscience Letters, 2003. **351**(2): p. 130-132.

82.   Dubey, N, Letourneau, PC, and Tranquillo, RT, *Guided neurite elongation and schwann cell invasion into magnetically aligned collagen in simulated peripheral nerve regeneration*. Experimental Neurology, 1999. **158**(2): p. 338-350.

83.   Clark, P, *et al.*, *Cell guidance by ultrafine topography in vitro*. Journal of Cell Science, 1991. **99 (Pt 1)**: p. 73-77.

84. Murphy, CM, Haugh, MG, and O'brien, FJ, *The effect of mean pore size on cell attachment, proliferation and migration in collagen-glycosaminoglycan scaffolds for bone tissue engineering.* Biomaterials, 2010. **31**(3): p. 461-466.

85. Schoof, H, *et al.*, *Control of pore structure and size in freeze-dried collagen sponges.* Journal of Biomedical Materials Research, 2001. **58**(4): p. 352-357.

86. Kuberka, M, *et al.*, *Magnification of the pore size in biodegradable collagen sponges.* The International Journal of Artificial Organs, 2002. **25**(1): p. 67-73.

87. Bozkurt, A, *et al.*, *In vitro cell alignment obtained with a schwann cell enriched microstructured nerve guide with longitudinal guidance channels.* Biomaterials, 2009. **30**(2): p. 169-179.

88. Goldner, JS, *et al.*, *Neurite bridging across micropatterned grooves.* Biomaterials, 2006. **27**(3): p. 460-472.

89. Sochol, RD, *et al.*, *Unidirectional mechanical cellular stimuli via micropost array gradients.* Soft Matter, 2011. **7**(10): p. 4606-4609.

90. Mahmud, G, *et al.*, *Directing cell motions on micropatterned ratchets.* Nature Physics, 2009. **5**(8): p. 606-612.

91. Yim, EK, Pang, SW, and Leong, KW, *Synthetic nanostructures inducing differentiation of human mesenchymal stem cells into neuronal lineage.* Experimental Cell Research, 2007. **313**(9): p. 1820-1829.

92. Lee, MR, *et al.*, *Direct differentiation of human embryonic stem cells into selective neurons on nanoscale ridge/groove pattern arrays.* Biomaterials, 2010. **31**(15): p. 4360-4366.

93. Charest, JL, Garcia, AJ, and King, WP, *Myoblast alignment and differentiation on cell culture substrates with microscale topography and model chemistries.* Biomaterials, 2007. **28**(13): p. 2202-2210.

94. Wang, PY, Yu, HT, and Tsai, WB, *Modulation of alignment and differentiation of skeletal myoblasts by submicron ridges/grooves surface structure.* Biotechnology and Bioengineering, 2010. **106**(2): p. 285-294.

95. Guvendiren, M and Burdick, JA, *The control of stem cell morphology and differentiation by hydrogel surface wrinkles.* Biomaterials, 2010. **31**(25): p. 6511-6518.

96. Qi, L, *et al.*, *The effects of topographical patterns and sizes on neural stem cell behavior.* PLOS One, 2013. **8**(3): p. e59022.

97. Lim, SH, *et al.*, *The effect of nanofiber-guided cell alignment on the preferential differentiation of neural stem cells.* Biomaterials, 2010. **31**(34): p. 9031-9039.

98.   Nielson, R, Kaehr, B, and Shear, JB, *Microreplication and design of biological architectures using dynamic-mask multiphoton lithography*. Small, 2009. **5**(1): p. 120-125.

99.   Tai, G, *et al.*, *Electrotaxis and wound healing: Experimental methods to study electric fields as a directional signal for cell migration*. Methods in Molecular Biology, 2009. **571**: p. 77-97.

100.   Schmidt, CE, *et al.*, *Stimulation of neurite outgrowth using an electrically conducting polymer*. Proceedings of the National Academy of Sciences, 1997. **94**(17): p. 8948-8953.

101.   Chen, CS, *et al.*, *Geometric control of cell life and death*. Science, 1997. **276**(5317): p. 1425-1428.

102.   Thery, M, *et al.*, *Anisotropy of cell adhesive microenvironment governs cell internal organization and orientation of polarity*. Proceedings of the National Academy of Sciences, 2006. **103**(52): p. 19771-19776.

103.   Scott, MA, Wissner-Gross, ZD, and Yanik, MF, *Ultra-rapid laser protein micropatterning: Screening for directed polarization of single neurons*. Lab on a Chip, 2012. **12**(12): p. 2265-2276.

104.   Jiang, X, *et al.*, *Directing cell migration with asymmetric micropatterns*. Proceedings of the National Academy of Sciences, 2005. **102**(4): p. 975-978.

105.   Lee, SH, *et al.*, *Proteolytically degradable hydrogels with a fluorogenic substrate for studies of cellular proteolytic activity and migration*. Biotechnology Progress, 2005. **21**(6): p. 1736-1741.

106.   Raeber, GP, Lutolf, MP, and Hubbell, JA, *Molecularly engineered peg hydrogels: A novel model system for proteolytically mediated cell migration*. Biophysical Journal, 2005. **89**(2): p. 1374-1388.

107.   Freedman, NJ and Lefkowitz, RJ, *Desensitization of g protein-coupled receptors*. Recent Progress in Hormonal Research, 1996. **51**: p. 319-351; discussion 352-313.

108.   Cao, X and Shoichet, MS, *Investigating the synergistic effect of combined neurotrophic factor concentration gradients to guide axonal growth*. Neuroscience, 2003. **122**(2): p. 381-389.

109.   Li, GN, Liu, J, and Hoffman-Kim, D, *Multi-molecular gradients of permissive and inhibitory cues direct neurite outgrowth*. Annals of Biomedical Engineering, 2008. **36**(6): p. 889-904.

110.   Moore, K, Macsween, M, and Shoichet, M, *Immobilized concentration gradients of neurotrophic factors guide neurite outgrowth of primary neurons in macroporous scaffolds*. Tissue Engineering, 2006. **12**(2): p. 267-278.

111. Wang, CJ, *et al*., *A microfluidics-based turning assay reveals complex growth cone responses to integrated gradients of substrate-bound ecm molecules and diffusible guidance cues*. Lab on a Chip, 2008. **8**(2): p. 227-237.

112. Gomez, N, *et al*., *Immobilized nerve growth factor and microtopography have distinct effects on polarization versus axon elongation in hippocampal cells in culture*. Biomaterials, 2007. **28**(2): p. 271-284.

113. Gomez, N, Chen, SC, and Schmidt, CE, *Polarization of hippocampal neurons with competitive surface stimuli: Contact guidance cues are preferred over chemical ligands*. Journal of the Royal Society Interface, 2007. **4**(13): p. 223-233.

114. Sundararaghavan, HG, *et al*., *Fiber alignment directs cell motility over chemotactic gradients*. Biotechnology and Bioengineering, 2013. **110**(4): p. 1249-1254.

115. Zander, NE and Beebe, TP, Jr., *Immobilized laminin concentration gradients on electrospun fiber scaffolds for controlled neurite outgrowth*. Biointerphases, 2014. **9**(1): p. 011003.

116. Li, Z, *et al*., *Differential regulation of stiffness, topography, and dimension of substrates in rat mesenchymal stem cells*. Biomaterials, 2013. **34**(31): p. 7616-7625.

117. Lu, D, *et al*., *Differential regulation of morphology and stemness of mouse embryonic stem cells by substrate stiffness and topography*. Biomaterials, 2014. **35**(13): p. 3945-3955.

118. Cai, L, *et al*., *Photocured biodegradable polymer substrates of varying stiffness and microgroove dimensions for promoting nerve cell guidance and differentiation*. Langmuir, 2012. **28**(34): p. 12557-12568.

119. Dickinson, LE, *et al*., *Endothelial cell responses to micropillar substrates of varying dimensions and stiffness*. Journal of Biomedical Materials Research A, 2012. **100**(6): p. 1457-1466.

120. Hale, NA, Yang, Y, and Rajagopalan, P, *Cell migration at the interface of a dual chemical-mechanical gradient*. Applied Materials & Interfaces, 2010. **2**(8): p. 2317-2324.

121. Gacesa, P, *Alginates*. Carbohydrate Polymers, 1988. **8**(3): p. 161-182.

122. Kuo, CK and Ma, PX, *Ionically crosslinked alginate hydrogels as scaffolds for tissue engineering: Part 1. Structure, gelation rate and mechanical properties*. Biomaterials, 2001. **22**(6): p. 511-521.

123. Lee, KY and Mooney, DJ, *Alginate: Properties and biomedical applications*. Progress in Polymer Science, 2012. **37**(1): p. 106-126.

124. Rosenblatt, J, Devereux, B, and Wallace, DG, *Injectable collagen as a ph-sensitive hydrogel*. Biomaterials, 1994. **15**(12): p. 985-995.

125. Tan, H and Marra, KG, *Injectable, biodegradable hydrogels for tissue engineering applications*. Materials, 2010. **3**(3): p. 1746-1767.

126. Ta, HT, Dass, CR, and Dunstan, DE, *Injectable chitosan hydrogels for localised cancer therapy*. Journal of Controlled Release, 2008. **126**(3): p. 205-216.

127. Hennink, WE and Van Nostrum, CF, *Novel crosslinking methods to design hydrogels*. Advanced Drug Delivery Reviews, 2012. **64, Supplement**(0): p. 223-236.

128. Zhao, X-M, Xia, Y, and Whitesides, GM, *Soft lithographic methods for nano-fabrication*. Journal of Materials Chemistry, 1997. **7**(7): p. 1069-1074.

129. Xia, Y, *et al.*, *Unconventional methods for fabricating and patterning nanostructures*. Chemical Reviews, 1999. **99**(7): p. 1823-1848.

130. Suh, KY, *et al.*, *A simple soft lithographic route to fabrication of poly(ethylene glycol) microstructures for protein and cell patterning*. Biomaterials, 2004. **25**(3): p. 557-563.

131. Paguirigan, AL and Beebe, DJ, *Protocol for the fabrication of enzymatically crosslinked gelatin microchannels for microfluidic cell culture*. Nature Protocols, 2007. **2**(7): p. 1782-1788.

132. Tang, MD, Golden, AP, and Tien, J, *Molding of three-dimensional microstructures of gels*. Journal of the American Chemical Society, 2003. **125**(43): p. 12988-12989.

133. Qin, D, Xia, Y, and Whitesides, GM, *Soft lithography for micro- and nanoscale patterning*. Nature Protocols, 2010. **5**(3): p. 491-502.

134. Whitesides, GM, *et al.*, *Soft lithography in biology and biochemistry*. Annual Review Biomedical Engineering, 2001. **3**: p. 335-373.

135. Lafratta, CN, Li, L, and Fourkas, JT, *Soft-lithographic replication of 3d microstructures with closed loops*. Proceedings of the National Academy of Sciences, 2006. **103**(23): p. 8589-8594.

136. Unger, MA, *et al.*, *Monolithic microfabricated valves and pumps by multilayer soft lithography*. Science, 2000. **288**(5463): p. 113-116.

137. Leung, WY, *et al.*, *Fabrication of photonic band gap crystal using microtransfer molded templates*. Journal of Applied Physics, 2003. **93**(10): p. 5866-5870.

138. Ifkovits, JL and Burdick, JA, *Review: Photopolymerizable and degradable biomaterials for tissue engineering applications*. Tissue Engineering, 2007. **13**(10): p. 2369-2385.

139. Davis, KA, Burdick, JA, and Anseth, KS, *Photoinitiated crosslinked degradable copolymer networks for tissue engineering applications*. Biomaterials, 2003. **24**(14): p. 2485-2495.

140. Lafratta, CN, *et al.*, *Multiphoton fabrication*. Angewandte Chemie International Edition, 2007. **46**(33): p. 6238-6258.

141. Göppert-Mayer, M, *Elementary processes with two quantum transitions*. Annalen der Physik, 1931. **18**(7-8): p. 466-479.

142. Kaiser, W and Garrett, CGB, *Two-photon excitation in ca*. Physical Review Letters, 1961. **7**(6): p. 229-231.

143. Hell, SW, *et al.*, *Two-photon near- and far-field fluorescence microscopy with continuous-wave excitation*. Optical Letters, 1998. **23**(15): p. 1238-1240.

144. Zipfel, WR, Williams, RM, and Webb, WW, *Nonlinear magic: Multiphoton microscopy in the biosciences*. Nature Biotechnology, 2003. **21**(11): p. 1369-1377.

145. Maruo, S, Nakamura, O, and Kawata, S, *Three-dimensional microfabrication with two-photon-absorbed photopolymerization*. Optical Letters, 1997. **22**(2): p. 132-134.

146. Strickler, JH and Webb, WW, *Three-dimensional optical data storage in refractive media by two-photon point excitation*. Optical Letters, 1991. **16**(22): p. 1780-1782.

147. Pitts, JD, *et al.*, *Submicron multiphoton free-form fabrication of proteins and polymers: Studies of reaction efficiencies and applications in sustained release*. Macromolecules, 2000. **33**(5): p. 1514-1523.

148. Kaehr, B and Shear, JB, *Mask-directed multiphoton lithography*. Journal of the American Chemical Society, 2007. **129**(7): p. 1904-1905.

149. Kaehr, B and Shear, JB, *Multiphoton fabrication of chemically responsive protein hydrogels for microactuation*. Proceedings of the National Academy of Sciences, 2008. **105**(26): p. 8850-8854.

150. Hill, RT, *et al.*, *Microfabrication of three-dimensional bioelectronic architectures*. Journal of the American Chemical Society, 2005. **127**(30): p. 10707-10711.

151. Pins, GD, *et al.*, *Multiphoton excited fabricated nano and micro patterned extracellular matrix proteins direct cellular morphology*. Journal of Biomedical Materials Research A, 2006. **78**(1): p. 194-204.

152. Connell, JL, *Characterization and microfabrication of environmentally sensitive materials for studying bacterial group behaviors*. 2012, The University of Texas at Austin.

Chapter 2: Developing a benzophenone-based immobilization method for patterning cells on three-dimensional (3D) protein architectures

2.1 CHAPTER SUMMARY

Inter-cellular communication occurs through a milieu of sensory pathways that can process chemical, mechanical, topographical, and electrical inputs. Various proteins, peptides, ions, and synthetic molecules have been used to study how cells detect and interpret specific signals. Sensory molecules used have been isolated and presented to cells as soluble or immobilized cues to promote specific cellular behaviors such as differentiation, adhesion, and migration. This chapter introduces a novel method to immobilize chemical cues to micro-3D-printed (μ-3DP) protein architectures. Benzophenone-biotin (BP-b) is photochemically activated via multiphoton excitation to promote a non-specific, 3D-localized reaction with the protein matrix. The relative extent of biotin immobilization is quantified using a fluorophore-conjugated neutravidin (NA) molecule that binds to biotin in a 1:4 ratio. Experimental parameters, including laser power, grayscale masking, BP-b concentration, and the number of immobilization scans are used to generate step and continuous gradients of biomolecules. Immobilization is achieved within and on the surface of 3D architectures with microscale resolution in all axes. Additionally, chemical modifications are made without altering the elastic modulus or topographical properties of the substrate. Surfaces were rendered bioadhesive by incorporating biotinylated, universally adhesive peptides, RGD (Arg-Gly-Asp) and IKVAV (Ile-Lys-Val-Ala-Val), to promote Schwann cell (SC) adhesion and polarization. This capability is demonstrated on both planar and 3D structures. Scan parameters needed to immobilize sufficient concentrations for efficient cell patterning create sub-micron topographical changes simultaneously; however, ~200 nm deep indentations alone do not promote cell adhesion or polarization. Further optimization is needed to

increase cell adhesion at reduced scan powers, thus avoiding both mechanical and topographical changes to these protein matrices. This technique introduces an additional degree of chemical specificity that can be used to elucidate cell-matrix interactions and direct cell behavior. Ultimately, the work improves the capacity of micro-3D (μ-3D) protein scaffolds to be used as biocompatible, contact guidance cues for investigating or directing cell behavior on 3D biomaterial scaffolds.

2.2 BACKGROUND AND MOTIVATION

The extracellular matrix (ECM) is a dynamic, 3D environment that contains a plethora of physical and chemical cues that control cell function. Native ECM is described as an interpenetrating network of structural proteins such as collagen, laminin, and fibronectin that are secreted by cells. The protein composition of the ECM, as well as the structure of the proteins themselves is tissue specific. Within a single tissue containing many cell types, heterogeneity abounds in the form of localized domains of proteins and other chemical cues necessary for proper tissue function [1]. The chemical composition underlies other important topographical and mechanical properties that can also contribute to form and function [2-4]. In the field of tissue regeneration, a strong emphasis has been placed on identifying what signals direct cells during embryonic development, and researchers have made countless attempts to recreate these signals *in vitro*. Each discovery leads to a better understanding of the cell-matrix interaction, and reveals a reality that all chemical and biophysical properties must be considered when designing biomaterials for tissue engineering, including chemical, mechanical, and topographical cues that all have independent and combinatorial effects on cell differentiation, migration, proliferation, and death [5]. Differential, independent, and localized control of these properties in 3D scaffolds is crucial to advancing our

34

understanding of the cellular response, and will inform the design of future tissue engineering platforms.

The primary focus of Christine Schmidt's research is to design materials that target the regeneration of peripheral and central nervous tissue. Previous collaborative work with Jason Shear's Group has combined μ-3DP protein structures, composed of bovine serum albumin (BSA), with hyaluronic acid (HA) based hydrogel constructs to promote and guide the migration of dorsal root ganglia (DRGs) and neural progenitor cells (NPCs) [6]. Interaction efficiency of the cells with unmodified protein hydrogels was less than 30%. However, when 5% (w/w) biotinylated-BSA was incorporated into the protein matrix via fabrication and laminin-derived, IKVAV peptides were attached to the structures, the interaction efficiency increased to ~70%. Unfortunately, the method to produce chemically functionalized protein hydrogels restricted the user to a homogenous distribution of biotin throughout the matrix.

To tailor the surface chemistry these scaffolds exhibit in localized, 3D space, a photolithographic method is developed to immobilize BP-b to protein hydrogels after fabrication. The effect of the immobilization on the mechanical and topographical properties is also characterized. Differential (gradients), localized (sub-micron resolution), and independent control of immobilization on 3D surfaces is displayed. To demonstrate the utility of this technique for biomaterial applications, adhesive peptides are immobilized to promote the adhesion of Schwann cells (SCs). Additionally, user-defined regions of immobilized peptides promote SC alignment and patterning.

2.2.1 Neural development and nerve regeneration

Peripheral nerve tissue is composed of a unique orientation of neurons, glial cells, and extracellular matrix proteins. The axons are organized into fascicles, which are larger

tube-like structures surrounded by a dense, protective layer of myofibroblasts known as the perineurium. Within each fascicle are a number of myelinated axons separated by tough, connective tissue known as the endonerium. A single nerve fiber is wrapped in epineurium, the outermost layer, and usually contains many nerve fascicles. The epineurium contains the vasculature that supplies the nerve with nutrients and removes wastes, as well as acts as an additional protective layer [7]. In the case of injury, severity of nerve damage depends on the extent to which internal tissue structures are damaged. Typically damage to the outer layers of the nerve is quickly repaired and does not affect functionality. Even complete transections of the nerve are capable of regenerating naturally if the gap between the nerve ends is smaller than 1 mm. The most serious injury is a complete transection of the nerve that results in a large gap between the nerve ends, and these require other treatment methods to ensure functional recovery.

The requirements for nerve development and post-injury regeneration are vaguely understood. Recommended characteristics for an ideal regenerative scaffold include degradability, porosity, chemical functionality, topographical signals, and incorporation of support cells; however, it is unclear what role each of these variables play and which ones are critical [8]. Son and Thomspon showed that SCs migrate first and provide chemical and topographical support for axon extension [9]. SCs, along with macrophages, also aid in clearing debris in the nerve gap, allowing for new axon formation extending from the proximal end of the nerve to the distal end. The extension rate can range from 2-5 mm per day [10]. Functional recovery is achieved once the axons reconnect with their distal targets.

The most successful treatments for large peripheral nerve gaps to date are autologous and decellularized nerve grafts. Many researchers are attempting to recapitulate these environments using synthetic and natural biomaterials to treat injured

nerves, but these endeavors have fallen short of improving upon the current treatment standards [8]. A major reason for the shortcoming of biomaterials to treat nerve regeneration is that the majority of researchers focus on therapies for directing and increasing axon extension. In this chapter, SCs are the primary focus for adhesion and cell patterning, as their infiltration into nerve regeneration scaffolds is believed to be a rate-limiting step in functional recovery [11]. Combining the immobilization technology with the previously described platform in HA hydrogels will enhance our ability to test the effect of chemical cue presentation on SC migration and infiltration. The immobilization platform is not limited to investigating SCs, and instead presents a versatile, 3D approach for chemical patterning with the potential to direct multiple cellular responses such as differentiation, migration, and organization.

2.2.2 Cell Patterning *In Vitro*

Dictating the exact position or orientation of cells within a matrix using immobilized chemical cues is paramount to gain a better understanding of cellular signaling. An archaic method to position cells within culture systems uses a pipette to physically suction and move a cell to the desired location. This method is not ideal for 3D or *in vivo* applications, and has been supplanted by the recent invention of biological 3D printing [12]. Traditional two-dimensional approaches, single-photon photolithography and microcontact printing (μCP), have been used extensively to pattern biomolecules capable of promoting selective adhesion [13, 14]. These biomolecules include families of ECM proteins such as collagen, laminin, and fibronectin and specific peptide sequences such as RGD and IKVAV [15-18]. Additionally, organization of cues into geometric patterns can coordinate cell morphology, which can have substantial effects on cell proliferation, differentiation, and function [19, 20]. Ideally, spontaneous organization of

cells within hydrogels is key for translational studies to promote proper tissue regeneration. This endeavor requires immobilization of multiple cues at defined positions within a 3D matrix to direct cell migration, morphology, and gene expression. Currently a limited number of methods exist to direct-write complex immobilization patterns within 3D hydrogels, and more approachable technologies need to be developed to probe cellular dynamics in 3D environments.

2.2.3 Chemical Patterning Technologies

Scientists have sought for decades to control the interaction of cells with biomaterials by tailoring the surface chemistry presented to cells. A plethora of influential techniques have been invented to achieve these modifications [14, 21, 22]. These approaches have revealed important details regarding the underlying mechanisms that govern cell-matrix interactions, and have led to significant advances in the field of tissue engineering. Below, a number of the most prominent approaches used for *in vitro* cell studies, as well as their respective advantages and disadvantages are highlighted. A summary of this information is provided in **Table 2.1**.

Bioconjugation

Dozens of chemical reaction mechanisms are employed to conjugate biomolecules to various substrates or molecules to improve cell-material interactions. Proteins, polysaccharides, nanoparticles, and lipids are common substrates that have been modified using potential bioconjugation chemistries [23, 24]. To remain within the scope of this document, only a few reactions related to proteins and polymers will be presented.

One established method to prime carboxyl functional groups for reaction with primary amines requires a carbodiimide in combination with N-hydroxysulfosuccinimide (NHS) to form stable amides [25]. This approach has been used extensively to

38

fluorescently label proteins to aid in visualization, and modify polymer backbones with acrylate groups for photocrosslinking [26-28]. It also has been used to render many bulk hydrogels, including alginate and HA cell adhesive [29, 30].

The idea of "click" chemistry was first introduced by Sharpless *et al*. to refer to a series of modular reactions used to construct larger compounds [31]. "Click" reactions are highly selective and exothermic (>20 kcal/ml). They display high percent yields and form stable products. A number of reaction schemes fit the profile of a "click" reaction, such as Diels-Alder reactions, Michael Additions, ring-opening epoxides, and cycloadditions [32, 33]. These reactions have been exhausted to selectively couple proteins to surfaces, and more recently were combined with photoexcitation to pattern materials in 3D [34, 35]. As development of bioconjugation chemistries continues, the primary focus for tissue engineering applications needs to be on establishing spatially and temporally resolved mechanisms capable of providing multiple cues within a 3D construct.

Self-assembled monolayers (SAMs), discovered in 1983 by Nuzzo and Allara, are formed from spontaneous adsorption of alkanethiols on metal surfaces [36]. The deposition can be performed in either gas or liquid phases. The monolayer thickness is tunable, as heights as low as 1 nm have been achieved. Tethering long chain polymers or other functional groups can be used to promote further adsorption of biomolecules and proteins that promote or prevent cell adhesion. Although SAMs are stable under ambient conditions, they can also be desorbed easily from a metal surface by applying electric potential, acid/base etching, or exposure to ultraviolet (UV) radiation. Microfluidics have been designed to pattern cell adhesive regions through the selective desorption and re-adsorption of SAMs [37]. SAM density has also been controlled using variable UV exposure to create gradients of biomolecules [38]. These techniques rely on the fragile

nature of SAMs, a feature that can also lead to defects. Another significant drawback is that SAMs can only be applied to metal surfaces.

Soft Lithography

Soft lithography uses elastomeric polymers, such as polydimethylsiloxane (PDMS), as molds or stamps to replicate features on a surface. Kumar and Whitesides introduced the concept of μCP in 1994 and revolutionized how SAMs were applied [39, 40]. First, a master template of photoresist was etched on silica using traditional photolithographic methods. PDMS was poured over the master, heat cured, then separated from the master. The features from the master were preserved on the PDMS as negative space, producing a reusable stamp. The stamp was then coated in "ink," an ethanolic solution containing gold-reactive thiols, capable of diffusing into the PDMS. When the stamp was applied to a gold-coated substrate, only positive features on the PDMS contacted the surface and resulted in chemical adsorption. As a result, physical features on the PDMS were effectively converted into a chemical pattern on the substrate.

This technique is advantageous because large arrays can be created and replicated quickly using a single mold, highly resolved (~50 nm) features are attainable, and the materials and equipment costs are relatively cheap compared to photolithography. However, μCP also has many limitations. Organic solvents, excluding ethanol, induce swelling of the PDMS, altering the features and decreasing the pattern resolution. PDMS is also hydrophobic, restricting the application of aqueous-based solutions. Additionally, features may be distorted due to the force exerted during the stamping procedure. Ink diffusion can also lead to the creation of edge effects. Soft substrates, such as hydrogels, are also difficult to pattern because of substrate deformation caused by the application of

the stamp. Many of these challenges have been addressed in the last 20 years through the development of better instrumentation, materials, and methods.

Chou and colleagues invented nanoimprint lithography, a process using thermoplastic polymers, to achieve feature sizes approaching 25 nm [41]. Colloids have also been used to form masks for selective etching of SAMs [42]. The size and organization of the colloids can be controlled in 3D space using electric fields, but the geometries are limited to simple designs (e.g. circles or triangles). Another technique, dip-pen nanolithography (DPN), uses the tip of an atomic force probe as the stamp instead of PDMS [43]. This approach allows for simultaneous deposition of multiple molecules, and can be used to pattern soft substrates such as hydrogels [44-46]. Recent improvements to DPN allow for control of protein deposition down to a single protein molecule [47]. Layer-by-layer deposition has also been demonstrated for the production of 3D arrays using DPN, but is impractical for large volumes [48]. Despite advances and increased interests in this technology, soft lithography has not usurped photolithographic techniques as the primary option for chemically patterning 3D scaffolds.

Photolithography

Single-photon lithography is the most widely used technique to chemically modify biomaterials. It can be used in combination with μCP or microfluidics to create complex patterns and gradients with sub-cellular resolution on a variety of substrates. An inspirational study conducted by Adams *et al*. used a laser-based approach to immobilize gradients of benzophenone-conjugated, IKVAV on etched plastic [49]. When DRGs were plated on the substrates, axons preferentially extended towards the higher concentration of the peptide. Photolithography has also been used to chemically pattern soft hydrogels and elastomers to control cellular organization [50, 51]. UV lasers provide quasi-3D

41

spatial resolution and have been used to promote cell migration into hydrogels [52, 53]. Since high doses of radiation are required for photolithography, it is generally not recommended for *in situ* studies. Moreover, many proteins are photodamaged by UV light, thus presenting a challenge for patterning in the presence of other biomolecules [54, 55]. By limiting exposure time, researchers have modified substrates in the presence of cells to control cell adhesion [56-59]. Despite the limitations associated with traditional photolithography, it will continue to be influential for large-scale biomaterial modification because it is well established and easily accessible.

In contrast to single-photon lithography, multiphoton lithography (MPL) provides 3D-localized control of patterning because it requires the near-simultaneous absorption of two or more photons. The non-linear dependence of photoexcitation on light intensity provides a distinct advantage over traditional photolithography, because the excitation voxel is confined to regions of high photon flux, such as the focal plane of a microscope objective. This technique provides a diffraction-limited resolution approaching ~1 μm in 3D, and offers control over both the distribution and concentration of chemical cues within 3D constructs.

The West Group first demonstrated the ability to selectively pattern biomolecules and cells within optically transparent hydrogels using multiphoton excitation (MPE) [50]. Since the same functional groups were used for fabrication and MPE excitation, hydrogel deformation was apparent as an increase in crosslinking density resulted from the immobilization scan. Other mechanisms including coumarin-uncaging and "click" reactions have been developed to reduce cytotoxicity and avoid structural changes to the matrix. However, these approaches require chemical modifications to the polymer backbone prior to fabrication to achieve functionalization [34, 60]. Promising results show control over cell migration and cellular orientation within 3D hydrogels using

MPE-induced immobilization strategies [34, 61]. Many of these approaches have also been used to pattern multiple biomolecules within 3D constructs [34, 62, 63]. MPE is an exceptional tool for small volume and single cell investigations because of the spatial resolution provided, but is impractical for macroscopic studies because of optical limitations and time constraints.

Herein, a novel approach to tailor the surface presentation of μ-3D printed protein hydrogels through direct and localized immobilization of BP-b using MPE is presented. An ability to tune the degree of immobilization using a range of possible variables including BP-b concentration, average laser power, and the number of immobilization laser scans is demonstrated. Continuous and step gradients of immobilized chemicals are created using both a Pockels cell and grayscale mask to modulate laser power during immobilization scans. Topography and stiffness are evaluated using atomic force microscopy (AFM) to identify scan conditions that prevent structural changes to the protein hydrogel. In addition, the scaffolds are rendered bioadhesive by immobilizing RGD to increase SC interaction. Sub-cellular patterns of RGD are effective for promoting selective adhesion and cell polarization on planar and 3D scaffolds. This technique provides significant advantages over other MPE-induced immobilization platforms including: 1) insertion of photoactivated BP-b is non-selective, thus a number of hydrogel constructs can be functionalized without need for polymer modification. 2) BP-b can be immobilized without altering the structural properties of a matrix. 3) Finally, *in situ* modifications are possible without damaging nearby cells, as other researchers have shown using more destructive wavelengths [56]. This immobilization technology will be instrumental for investigating cell-matrix interactions as it provides more precise and independent control of cue presentation within 3D culture environments.

Patterning Technique	Achievable Resolution (nm)	Advantages	Limitations
Bioconjugation	N/A	Robust, bulk immobilization	Site specificity, toxicity
Traditional Photolithography	30	Large arrays, bulk immobilization	3D spatial resolution, high energy wavelengths
Soft Lithography (μCP)	50	Cost, high-throughput, reproducible	3D patterning
Multiphoton Lithography (MPL)	200	3D, direct-write, rapid prototyping	Optically limited, time intensive

Table 2.1: Summary of chemical patterning methods.

2.3 MATERIALS AND METHODS

2.3.1 Reagents

Bovine serum albumin (BSA, BAH64) was obtained from Equitech-Bio (Kerrvile, TX) and rose bengal (RB, 33000) was purchased from Sigma Aldrich (St. Louis, MO). Sterile, phosphate buffered saline (PBS, SH3026401) solution was purchased from Thermo Scientific (Waltham, MA). Dimethyl sulfoxide (DMSO, BP-231) was obtained from Fisher Scientific (Fairlawn, NJ). Benzophenone-biotin (10267) was obtained from Quanta Biodesign (Powell, Ohio). Neutravidin-TMR (A-6373), Alexafluor 594 phallodin (A12381), and 4',6-diamidino-2-phenylindole (DAPI, D1306) were purchased from Life Technologies (Carlsbad, CA). Biotinylated-RGD was provided by American Peptide (Sunnyvale, CA). Cell culture mediums including Dulbecco's modified eagles medium (DMEM, high glucose, SH30022) and Leibovitz L-15 (SH30525) were purchased from Fisher Scientific. Mitogenic factors used to maintain SC cultures including bovine pituitary extract (BPE, P1476) and forskolin (F6886) were acquired from Sigma Aldrich. Fetal bovine serum (FBS, SH3008803) and trypsin (SH3004201) were purchased from Fisher Scientific. Penicillin streptomycin (PSA, 1507-063, Life Technologies) was used as a general antibiotic in experimental media. All reagents were stored in a manner consistent with the supplier's recommendations.

2.3.2 μ-3D Protein Hydrogel Fabrication

The instrumentation used to fabricate protein hydrogels is depicted in **Figure 1.2** and the digital micromirror device (DMD)-directed MPL technique has been described in **Chapter 1** and in other previously published work [64-68]. Briefly, a mode-locked Ti:S oscillator (Coherent, Mira 900F) was pumped by a 532 nm frequency doubled laser (Coherent, Verdi, 10 W). The Ti:S output wavelength was tuned to 740 nm and directed

via a sequence of mirrors and lenses into the back aperture of a microscope objective (40X/1.3 NA, Zeiss Fluar). A half-wave plate and polarizing beamsplitter were used to manually attenuate the power so that the average laser power was 22 mW at the back aperture of the objective. A dual-axis, galvanometer-driven scan mirror (Leica, TCS-4D) was used to raster scan the beam at user defined waveforms, frequencies, and amplitudes. For large structure fabrication, the scan mirror was set to scan in a single x-axis (the fast axis), and an automated stage (model 562, Newport Corporation) was used to translate the sample relative to the focal plane in the orthogonal axis at a velocity of 20 μm/s [69]. Prior to the objective, the beam was focused on the face of a DMD projector (BenQ, MP510) with individually addressable, reflective mirrors located in a plane conjugate to the focal plane of the objective. By displaying a binary digital mask, the mirrors were positioned to reflect the beam toward or away from the objective. Binary images were created in Photoshop (Adobe, San Jose, CA), ImageJ (National Institutes of Health, Bethesda, MD), and PowerPoint (Microsoft Corporation, Santa Rosa, CA). The beam was re-collimated using a tube lens and reflected into the objective on a Zeiss Axiovert 135 microscope via a dichroic mirror.

BSA hydrogels were crosslinked to the surface of No. 1 coverslips (Fisher Scientific) or No. 1.5 welled-coverslips (Fisher Scientific) for cell experiments. A fabrication solution of 400 mg/mL BSA and 10 mM RB was used to fabricate all structures. The beam was focused into the solution and raster scanned to crosslink BSA layers. 3D features were created using a layer-by-layer approach, synchronizing the presentation of digital masks with incremental stage translation in the optical axis. All communication between equipment was coordinated using Labview software (National Instruments, Austin, TX). Axial step sizes were maintained at 1 μm for all structures. Residual fabrication solution was removed through a series of PBS washes. When

specified, structures were re-scanned with the beam using a protocol identical to fabrication for laser shrinking. Structures were then photobleached using a 30-minute exposure to the "full" output of a tungsten-halogen arc lamp reflected onto the sample via a 99/1 mirror. This step was required to minimize structural deformation and eliminate competitive photon absorption. The Shear Group has studied the impact of photobleaching on the swelling properties of protein structures extensively [70]. Further discussion on the impact of photobleaching pertaining to structure modulus, swelling, and cell adhesion is in **sections 2.4.2** - **2.4.4**.

2.3.3 Benzophenone Immobilization

A stock solution of 10 mg/mL BP-b in DMSO was made and stored in the dark. The stock was diluted with an equal volume of PBS prior to immersing the protein structures to create a 50/50 (v/v) solution of DMSO/PBS with a 5 mg/mL BP-b concentration. When different concentrations were used, the stock concentration was adjusted to maintain a 50/50 (v/v) DMSO:PBS ratio. The laser beam was manually focused on the glass and an automated stage was stepped a set distance to the desired starting plane. The scanning procedure used for MPE of BP-b was identical to fabrication. For 3D immobilization, the galvanometer-driven mirror was used to raster the beam in both axes. The laser was raster scanned between 1 and 12 times in a single plane. When immobilization was performed in multiple planes, the stage was translated 1 μm in the optical axis using the automated stage, and the process was repeated until the beam reflection from the structure was no longer visible. To create gradients, the beam power was electrooptically attenuated using a synthesized function generator (Model DS345, Stanford Research Systems, Sunnyvale, CA) to deliver user-defined waveforms of voltage to a Pockels cell (350-50, Conoptics, Danbury, CT). Triggering of the Pockels

cell and function generator was synchronized with the immobilization scan using Labview software. After the BP-b immobilization, the structures were thoroughly rinsed with large volumes (~500 μL) of PBS prior to incubation in a 2 μM NA-TMR solution. After rinsing, a 5 μM solution of b-RGD was used to prepare the protein scaffolds for cell studies. Care was taken to minimize light exposure throughout this process.

2.3.4 Fluorescence Imaging

Fluorescence images were acquired using a 10X/0.5 NA (Fluar, Zeiss) or 10X/0.3 NA objective (UPlanFl, Olympus) on an inverted Zeiss Axiovert microscope. A Cy3/TRITC filter set [Ex/Em: 545(25)/605(70), 49004, Chroma] was used with an attached Zeiss HBO-100 mercury arc lamp to illuminate the NA-TMR. One of two digital cameras was used: a 14 bit digital camera (C4742-98, Hamamatsu) or an Orca Flash 2.8 (C11440-10C, Hamamatsu), with Metamorph (Universal Imaging Corporation) and HCImage (Hamamatsu) acquisition software, respectively. All files were saved as tagged image files (.tif). Brightness and contrast levels were adjusted using ImageJ, and a lookup table ('gem') was sometimes applied to aid in visualization. Background images were acquired prior to NA-TMR immobilization for appropriate corrections.

3D image stacks were acquired using a Leica SP2 AOBS confocal microscope (Leica Microsystems). A 40X/1.25 NA, oil immersion objective was used for all acquisitions. Excitation and emission wavelengths were optimized for each fluorophore. Spacing between image planes was set to approximately 500 nm for all acquisitions. 3D reconstructions were created in ImageJ and Imaris (Bitplane) software. Levels were adjusted to aid in visualization.

2.3.5 Structural Characterization

An atomic force microscope (AFM, MFP-3D-BIO, Asylum Research) was used to acquire all force curves and topographical images. Protein hydrogels were submerged in PBS for the duration of data acquisition. For modulus measurements, a gold-coated cantilever (silicon, k = 3.8 N/m, PT.GS.AU, Novascan) with an attached 10 μm-diameter borosilicate bead was used to generate deflection versus displacement curves. Code was written in Matlab to automate the data analysis, except for the selection of the contact point. The program implemented a while loop to fit the Hertz model to the experimental data until a maximum R-squared value was obtained. A 5% strain limitation was imposed, equivalent to an indentation depth of approximately 300 nm. A total of four force curves were taken per structure then averaged to approximate the structure modulus. The average values from a minimum of three BSA pads were averaged again to obtain final values. Protein hydrogels were fabricated at a nominal height of 11 microns and photobleached with the arc lamp. Height measurements were obtained by taking the difference between the position of hydrogel contact and an adjacent glass measurement.

Topographical images were acquired in 'contact mode' using a triangular shaped cantilever (silicon nitride, k = 0.17 N/m, MSCT, Veeco) with a pyramidal tip (2.5 – 8 μm tall, 40 nm-radius). A setpoint of 0.3 deflection volts was used to maintain contact. Imaging frequency (0.25 – 0.5 Hz) was optimized for each sample. The scan area, 65 μm, and pixel resolution, 256 x 256, were consistent for all images. The z-position channel was saved as a tab-delimited text file, and then imported into Matlab to generate surface plots.

2.3.6 Cell Culture

Schwann cells (SCs, S16, CRL-2941) harvested from rat sciatic nerve were purchased from the American Type Culture Collection (ATCC). SCs were maintained

using previously published protocols [71]. In brief, SCs were kept in DMEM, high glucose media containing 10% (v/v) FBS, 2 μM forskolin, and 30 μM BPE. Cells were passaged using 0.25% trypsin (1X) every 4 – 7 days. Cells were not used after the 11th passage. A phosphate buffered experimental media (L-15, 1% FBS, 1% PSA) was used during time-lapse image acquisition because carbon dioxide was not available. Cells were fixed using a 4% formaldehyde solution (C001D76, Thomas Scientific, Swedesboro, NJ) after imaging, then permeated using a 0.1% Triton X-100 solution (T8532, Sigma Aldrich). Supplier recommended DAPI and phalloidin staining protocols were followed to immunostain all cells.

2.3.7 Time-lapse Acquisition

An environmental chamber was constructed out of plexiglass and an aluminum floor to fit on the stage of an inverted Zeiss Axiovert microscope. The temperature in the chamber was controlled using a heat gun (4HWK1, Westward) and heated stage (Brook Industries). The heat gun was modified to connect to a PID controller (T1620000, Red Lion) that monitored and maintained the inlet air temperature at a user-defined set point. Polyethylene tubing was used to connect the heat gun to the environmental chamber. For more information on chamber construction, see [72]. Images were acquired in 5-minute intervals using Metamorph software. A 5X/0.12 NA (Apochromat, Zeiss) or 10X/0.5 NA objective (Fluar, Zeiss) was used to acquire all images. All images were exported as tagged image file (.tif) stacks, and videos were created in ImageJ.

2.4 RESULTS AND DISCUSSION

2.4.1 Two-Photon Immobilization of Benzophenone

Galardy *et al.* first identified BP as a photoreactive species in 1974 and used it as a labeling agent for proteins [73]. Upon absorption of UV radiation (λ = ~260 nm) BP is

excited into a triplet state, generating a highly reactive, free radical. The radical inserts into available, weak carbon-hydrogen σ-bonds or relaxes to the ground state if a reaction does not occur [74]. Stability and reactivity of BP in aqueous solvents provide significant advantages over other photoreactive species. It was not until 1997 that Hypolite *et al*. demonstrated the versatility of BP to be used as a patterning agent for the immobilization of protein gradients [75]. In a motivational study for neural tissue engineering and this work, Adams and colleagues used a UV laser to produce immobilized gradients of BP-conjugated, IKVAV to direct axonal outgrowth from DRGs [49].

Furthermore, multiphoton activation of BP and its dimer using much longer wavelengths has been reported in the literature [76, 77]. A plot of the log-log power dependence collected at a wavelength of 780 nm for the dimer had a slope of 2.54, suggesting a combination of two- and three-photon events. The observed absorption was primarily attributed to excitation of the benzophenone monomer [76]. A Ti:S laser tuned to a wavelength of 740 nm was used to excite BP-b in all experiments presented in this document. Alternative wavelengths were tested, but produced significant structural deformation of the protein matrix, believed to be caused by three-photon absorption by the proteins, and were not evaluated further. Using this technique, localized immobilization of BP-b within protein constructs is confirmed with immaterial levels of non-specific binding. This work is the first reported use of benzophenone as a reagent to pattern substrates chemically using MPE.

The concentration dependence of BP-b immobilization is evaluated at concentrations between 2 and 15 mg/mL, 3 to 22 mM respectively. BP-b precipitation occurrs in pure aqueous solvents at concentrations approaching 2 mg/mL. Cell adhesion studies tested at this concentration were minimally effective; therefore, DMSO was incorporated into the solution to increase the solubility. A 1:1 (v/v) ratio of DMSO and

PBS is used to avoid an irreversible deformation that occurs to protein hydrogels in pure (100%) DMSO. This improves the maximum solubility of BP-b to 15 mg/mL, and does not have noticeable effects on the excitation of BP-b or the protein structures. To study the effects of concentration, a single plane within a protein structure was scanned six times using average laser powers measured at the back aperture of the objective between 11 and 17 mW. For comparison, 22 mW is used for fabrication of BSA hydrogels with identical instrumentation. For all experiments within this chapter, immobilized BP-b is labeled using NA-TMR for visualization and quantification.

Specific to this experiment, the fluorescence intensity within each scan region of a background-subtracted image is averaged. **Figure 2.1** shows the results of variable concentrations at numerous powers. While an inverse relationship between BP excitation efficiency and concentration at concentrations above 1 mM has been reported, these studies show a consistent increase in fluorescence intensity with concentration [76]. Additionally, a net positive effect on immobilization from the addition of DMSO is observed at 2 mg/mL, most likely as a result of improved solubility. An optimum BP-b concentration of 5 mg/mL is selected to provide adequate levels of immobilization for cell studies while minimizing structural deformation. This concentration is used for all remaining experiments within this chapter, unless otherwise noted.

To study the impact of laser power on BP-b immobilization, μ3DP BSA pads were scanned with the laser six times in a single plane at various powers (**Figure 2.2**). An eight-fold change in the resulting fluorescence intensity of NA-TMR is achieved at power ranges from 5 – 22 mW. Higher fluorescence signal in these studies may, in part, be due to shrinking of the protein matrix and an increase in voxel size at higher laser powers. However, when topographical changes were avoided using a combination of laser

shrinking and photobleaching steps prior to BP-b immobilization, similar results are obtained.

The probability of a two-photon absorption event is proportional to the square of the light intensity, and a three-photon event is proportional to the light intensity cubed. When a linear regression is applied to a log-log plot of intensity versus emission, the linear slope indicates the number of photons absorbed in the process. Previous studies classify the MPE of benzophenone at wavelengths between 780 – 840 nm as a combination of two and three photon events [76]. The log-log plot of NA-TMR fluorescence versus laser power between powers of 9 and 17 mW has a slope of 2.06, indicating a two-photon absorption is occurring. Over the entire power range tested, the slope decreased to 1.65. Deviation from two-photon behavior is most likely the result of a convolution of factors. First, NA-TMR fluorescence obtained via widefield fluorescence is not a direct measure of BP excitation. A single NA molecule can bind up to four biotins. According to the specification sheet, each NA-TMR molecule has between 5 - 8 fluorophores conjugated to it (Life Technologies). In addition, the quantum yield of a similar conjugate, streptavidin-TMR, has been measured to be only 0.19 [78]. Upon excitation, BP could potentially react with itself to form a dimer instead of the protein structure, and not all excitation events have to lead to a reaction. Despite these observed deviations from non-linear behavior, the results indicate that power provides excellent control of the extent of immobilization.

An additional strategy to increase the extent of immobilization is to increase the laser fluence by increasing the number of times a spatial region is scanned. Protein pads were scanned 1, 2, 4, 6, or 12 times in a single plane at average powers - 11 and 22 mW. The results shown in **Figure 2.3** reveal an additive effect of fluorescence with an increase in number of scans. The benefit generated from additional scanning is diminished at

higher values of scan number. This non-linear behavior could be due to the occupation of available reactive sites within the protein matrix. As expected, the effect of increasing the number of scans is much lower than an equivalent increase in power. In fact, four scans at 11 mW are needed to obtain the same fluorescence of a single scan conducted at 22 mW.

One advantage to using scan number is that step gradients can be created with relative ease using digital masking to control the number of times a region is scanned. The lateral distance between steps can be tuned using a DMD to achieve sub-cellular resolution. To maximize the range of immobilization a combination of power, BP-b concentration, and immobilization scans can be used. Additional variables that are known to affect MPE but were not tested rigorously include objective magnification, numerical aperture, and scan speed. Future studies should evaluate the impact of these factors, as they could potentially provide more pathways to tune the extent of immobilization.

Inherent variability associated with the fabrication and immobilization scans contribute to the heterogeneity of BP-b immobilization between structures, as well as a lack of reproducibility. An uneven distribution of protein density within the hydrogel matrix results from the layer-by-layer approach used for fabrication. As subsequent layers are stitched together, axial attenuation of the laser power from light scattering can conceivably contribute to axial variability in the crosslinked protein density. In addition, changes within the fabrication solution occur over the time course of an experiment. Based on visual observation of the color retained within the matrix, fabricated structures exhibit different optical densities and retain less photosensitizer as the time between scans increases. Since the position for the immobilization scan is derived using manual focusing, the focal plane for adjacent pads could vary up to 1 μm.

To assess the reproducibility between structures within a single sample, three structures were fabricated and scanned using identical parameters. Care was taken to

fabricate quickly (tens of minutes) and the focal plane for the immobilization scan was measured relative to the glass using an automated stage. An approximate standard deviation of 15% of the average intensity is achieved for each set of powers tested as shown in **Figure 2.4**. This value is significantly higher than the ~4% deviation in fluorescence intensity on a single structure. Comparable variability is obtained from experiments conducted on different days. To minimize variability from external factors, single structure immobilization protocols are implemented.
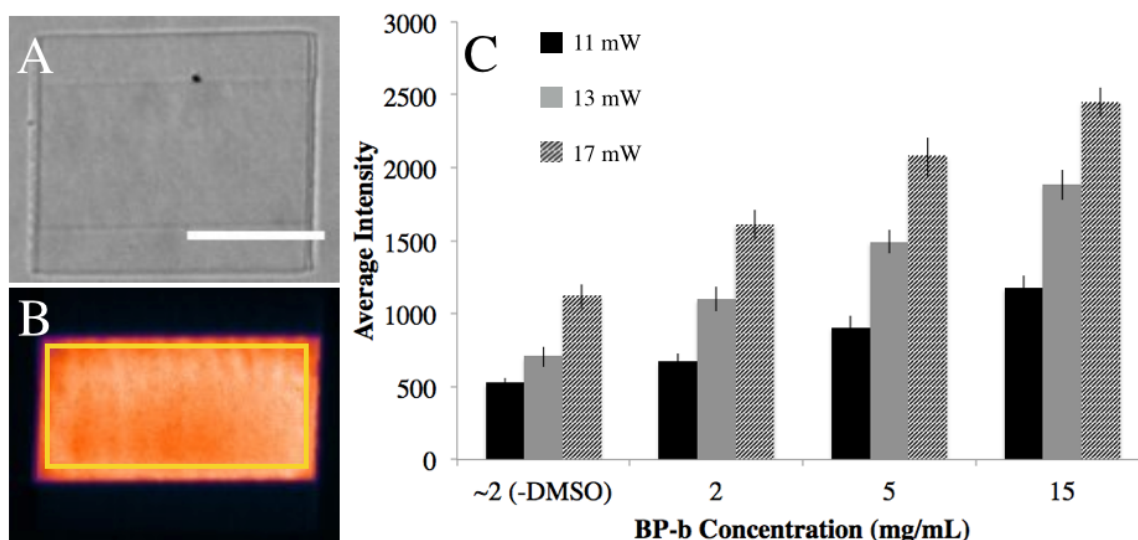
Figure 2.1: Effect of concentration on BP-b immobilization. A) A brightfield image of a 100 x 80 x 8 μm BSA pad that is scanned in a 15 mg/mL BP-b solution using an average laser power of 17 mW. The structure was scanned 6 times in a single optical plane at approximately one-half of its height. A difference in optical density is apparent between scanned and unscanned regions, and is indicative of structural deformation (scale bar = 50 μm). B) The corresponding fluorescence image was acquired using a TRITC filter set. The fluorescence intensity is averaged within the yellow box and the results are plotted in (C). Each bar represents the average pixel intensity of a single ~5000 μm² area. The addition of DMSO did not have a negative effect on immobilization. Intensity scales with both concentration and power. The error bars are the +/- standard deviation of the pixel intensity within each region.
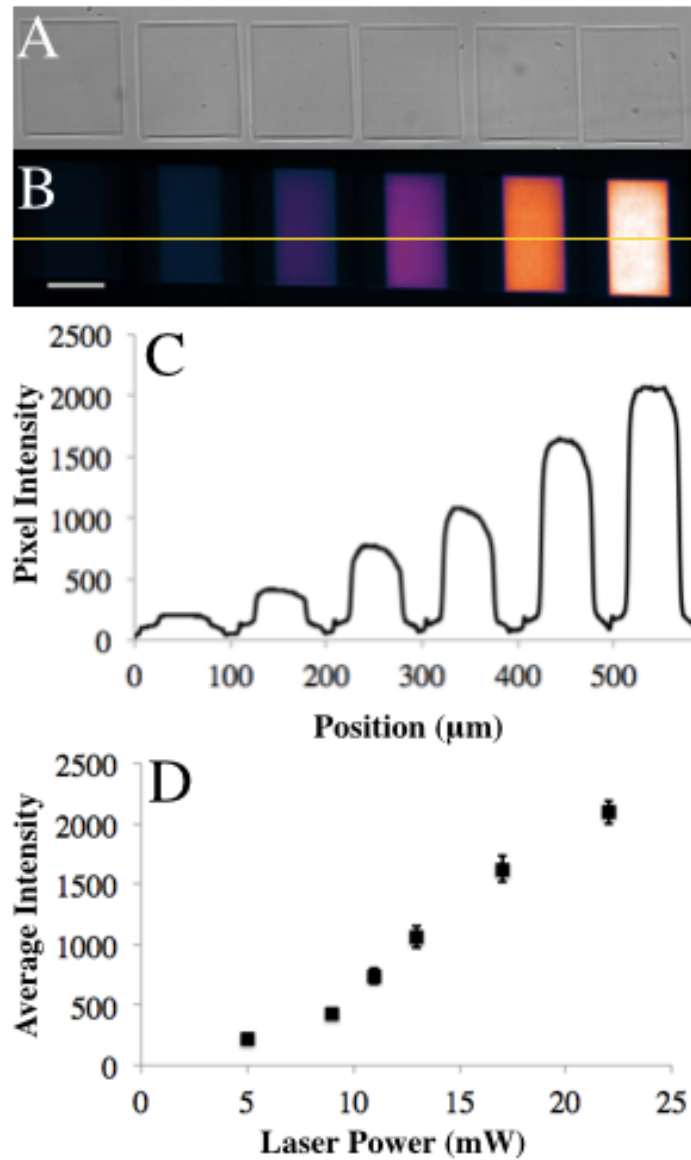
Figure 2.2: Effect of laser power on BP-b immobilization. A) A brightfield image of BSA pads that are scanned in a 5 mg/mL BP-b solution using variable laser power. The structures are scanned 6 times in a single plane at approximately one-half of their height. B) The corresponding fluorescence image was acquired using a TRITC filter set (scale bar = 50 μm). A linescan, represented by the yellow line, of the fluorescence intensity across the image is plotted in (C). D) A plot of the average fluorescence intensity of NA-TMR within a single scan region versus laser power. Changing power produces the largest absolute range of immobilization. The error bars represent the +/- standard deviation within each region.
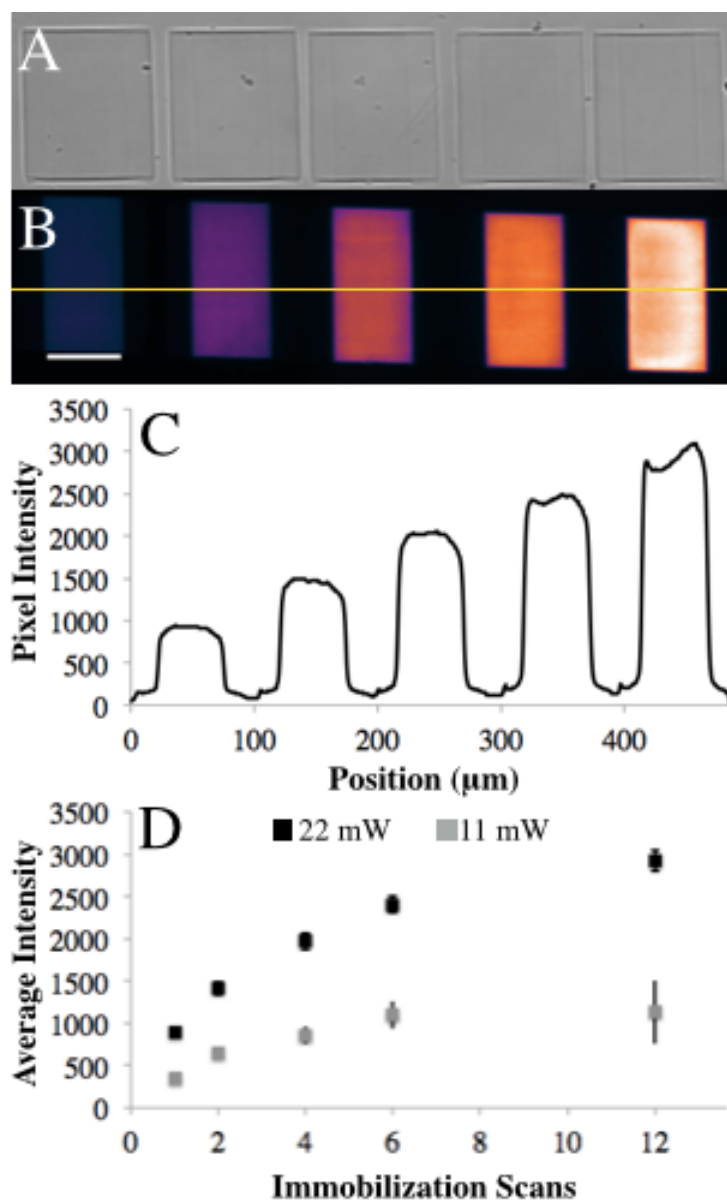
Figure 2.3: Effect of the number of immobilization scans on BP-b immobilization. A) A brightfield image of BSA pads that have been scanned in the presence of 5 mg/mL BP-b using an average laser power of 22 mW. Each structure was scanned between 1 and 12 (increasing from left to right) times in a single plane at approximately half its height. B) The corresponding fluorescence image was acquired using a TRITC filter set (scale bar = 50 μm). The fluorescence intensity profile of a linescan, shown in yellow, across the image is plotted in (C). A graph representing the average fluorescence intensity versus the number of scans for average laser powers of 11 (gray) and 22 (black) mW is shown in (D).
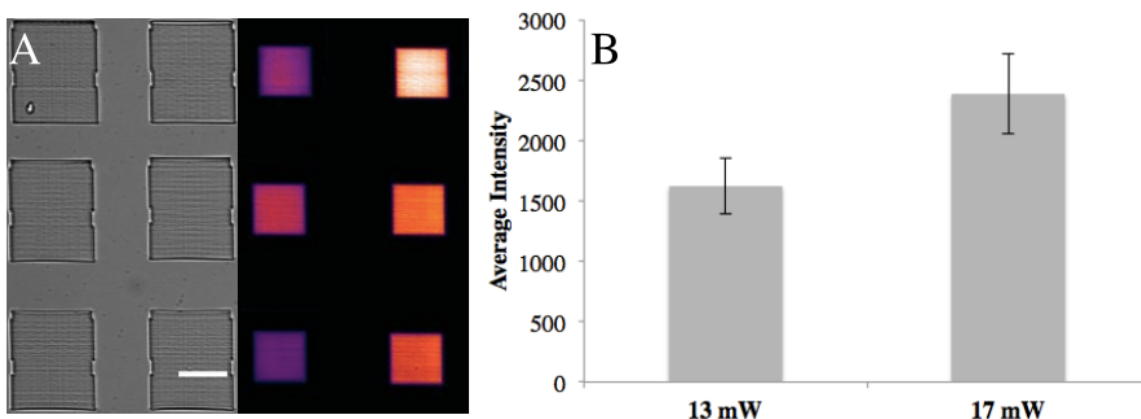
Figure 2.4: Reproducibility of BP-b immobilization. A) The brightfield and corresponding fluorescence image of a set of 6 BSA pads (scale bar = 50 μm). Three pads were scanned using a laser power of 13 mW (left column) and 17 mW (right column). These pads were laser-reduced with 2 scans prior to photobleaching. A bar graph representing the average fluorescence intensity of each set is shown in (B). The error bars represent the +/- standard deviation of the average values. A standard deviation of ~15% of the intensity was calculated (p-value = 0.125, paired t-test).

2.4.2 Microscale Compressive Modulus Measurements

The BP-b-based conjugation is designed to provide independent control over the extent of immobilization without impacting the crosslinking density of the protein hydrogel. In this study, two material properties are evaluated using an AFM to characterize structural changes, Young's modulus and topography. All measurements are acquired in PBS solution (pH = 7.4), as a true representation of the material properties is desired.

The well-established Hertz model relationship is used to calculate the microscale compressive modulus of the protein structures [79]. Assuming a spherical object contacts a flat, homogenous surface, the force (F) applied to the cantilever is described by the following relationship:

$$F = \frac{4}{3}\left(\frac{E}{1-v^2}\right)\sqrt{R\delta^3}$$
Equation 2.1

where E represents the elastic modulus of the substrate, v is Poisson's ratio, R is the bead radius, and δ is the indentation. Poisson's ratio is a ratio of transverse to axial strain, and the accepted value for incompressible materials deformed at low indentations is 0.5. The force applied to the cantilever can also be calculated using Hooke's law:

$$F = -kx$$
Equation 2.2

where k is defined as the spring constant of the cantilever and x is the linear displacement. We calculated the elastic modulus by combining and rearranging these equations. Most hydrogels have been reported to exhibit linear stress-strain behavior under macroscale compression at indentation depths up to 20% of its height [80]. For

AFM measurements, a 10% strain maximum is suggested [81]. A strain limitation of 5%, equivalent to an indentation depth of approximately 300 nm, was imposed for all experiments in these studies. Structure heights are maintained above 7 μm, an experimentally determined threshold to avoid interference from the glass as shown in **Figure 2.5**.

The structures were photobleached prior to immobilization to minimize the reactivity of residual photosensitizer partitioned within the BSA structure from the fabrication. Complete photobleaching, qualitatively defined as the loss of pink color attributable to RB, is achieved with a 30-minute exposure to the "full" output of a halogen arc lamp. Light exposure has been shown to cause significant swelling of BSA structures, and AFM measurements to measure the structure height confirm these results [70]. The structures in **Figure 2.6** were nominally fabricated to stand 11 μm tall and swelled to 14 μm after photobleaching (~30%). The photobleaching also resulted in a 50% reduction of the elastic modulus (~20 kPa to ~10 kPa). More specific data regarding the effects of photobleaching on modulus will be discussed in **Chapter 3**.

To evaluate the effect of BP-b immobilization on Young's modulus of protein hydrogels, BP-b immobilization was conducted using three scan conditions. Structures were fabricated to have a nominal height of 11 μm. The initial scan plane was set to approximately 80% of the nominal height (9 μm above the glass), and the stage was sequentially stepped in 1-μm increments to ensure the surface of the structure was scanned. No distinguishable difference in the measured height or modulus between scanned structures and a control group are observed, even at powers typically used for fabrication.
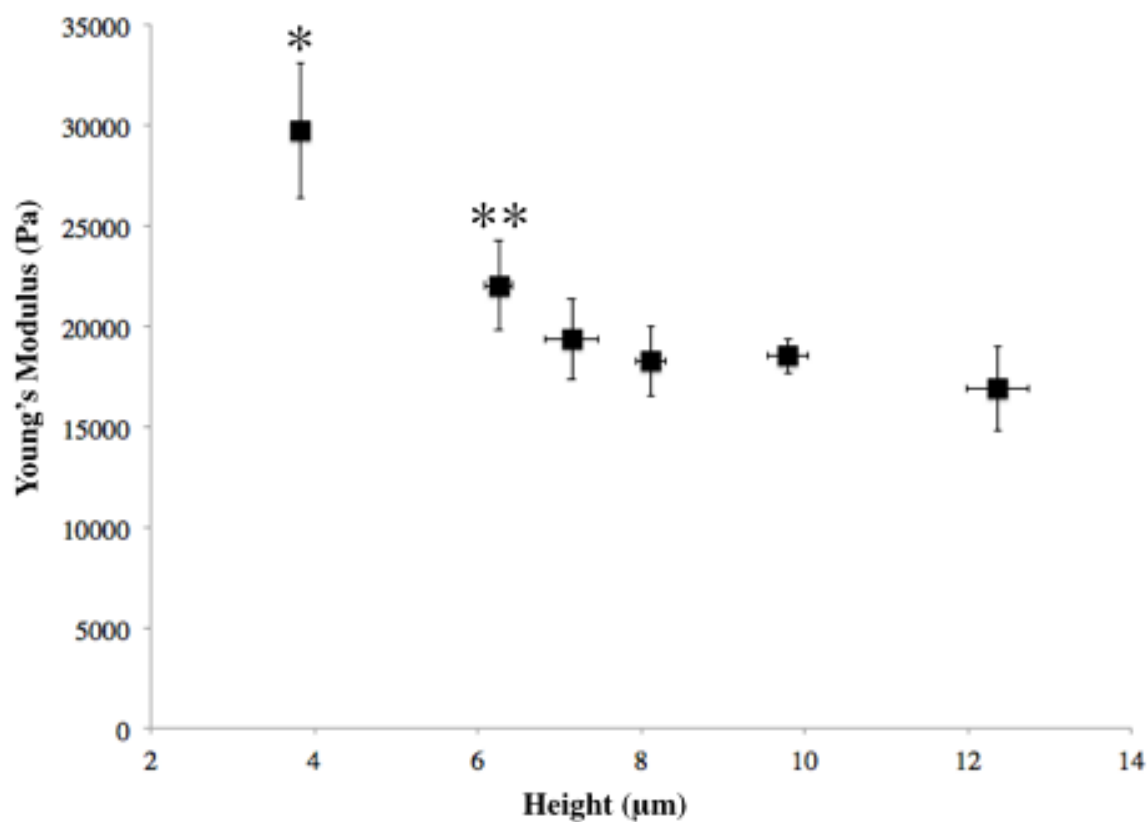
Figure 2.5: Effect of structure height on measured modulus. BSA hydrogels are fabricated using an identical protocol except for number of axial steps to vary the hydrogel height. Hydrogels less than 7 μm appear stiffer due of the underlying glass substrate (* - p-value < 0.05 when measured against all other data sets, ** - p-value < 0.05 when compared to the modulus for 10- and 12-μm-tall hydrogels). There is no difference in the measured modulus for structure heights greater than 7 μm. (n = 4 for each data point).
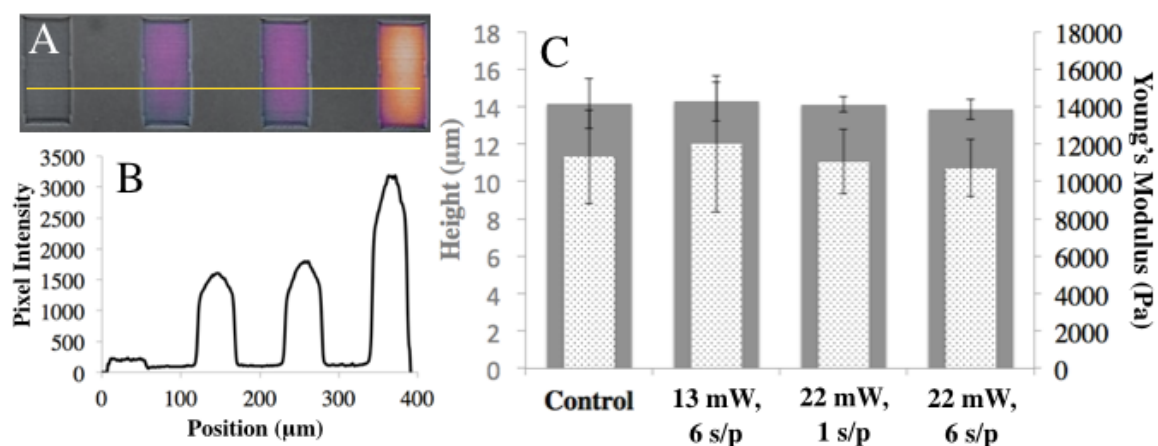
Figure 2.6: Effect of BP-biotin immobilization on elastic modulus. A) A brightfield image with the corresponding NA-TMR fluorescence image overlayed. A representative linescan (yellow line) of the fluorescence intensity across the image is plotted in (B). C) A combined bar graph plotting the measured height on the left axis (gray bars) and elastic modulus on the right axis (patterned bars, inset). The error bars represent the standard deviation of measurements taken on independent pads (n = 3). Significant changes are not seen in the height or elastic modulus as a result of the BP-b immobilization.

2.4.3 Surface Topography Characterization

In addition to conserving the modulus of the hydrogel, topographical changes must also be avoided as they too can affect cell adhesion and migration. Simultaneous imprinting of topographical features was considerable for photobleached pads at all powers tested (**Figure 2.7**). Laser-induced shrinking was used as an additional post-fabrication modification to completely avoid effects on hydrogel topography from the BP-b immobilization scan. Relying on residual photosensitizer trapped within the structure after fabrication and rinsing, a laser beam is scanned through the structure consistent with fabrication protocols to promote further crosslinking and effectively condense the protein matrix. The amount of photosensitizer within a hydrogel is reduced with each subsequent laser scan, and crosslinking density of the protein matrix increases, making it more resistant to further deformation. By limiting the photosensitizer prior to photobleaching, structural swelling is also eliminated. Laser-induced shrinking is the basis for the work presented in **Chapter 3**, and its impact on structural properties will be discussed in greater detail.

The effect of shrinking can be qualitatively assessed based on changes in the optical density of the pad. However, optical density is not calibrated to provide quantitative values. Scanning electron microscopy (SEM) is also not suited for these measurements because it requires the substrate to be fixed and dehydrated during preparation. Instead, an AFM is used to acquire topographical maps of the BSA structures in PBS. To ascertain whether simultaneous topography is being generated during BP-b immobilization, linear patterns with defined widths of 10 μm are scanned. Structures are scanned 6 times in a single plane positioned at one-half of the nominal height.

As shown in **Figure 2.7(C)**, the BP-b immobilization scans imprint features of nearly 500 nm in photobleached only structures at the lowest powers tested. Structures that are laser reduced with two scans prior to photobleaching are more resistant to changes. For these structures, imprinted features are avoided altogether at the lowest power tested, and 500 nm features are created at near fabrication powers. Increasing the number of laser shrinking scans to four further reduces changes as a result of the BP-b immobilization (**Figure 2.7(D)**). Specific to this experiment, structures are scanned through multiple planes to simulate sample preparation used for cell adhesion studies. An upper threshold of 11 mW and 12 scans avoid structural changes to the hydrogel. These conditions are used for cell adhesion studies discussed in **section 2.4.6**.

Additional comparisons of the topography between BP-immobilized and non-functionalized regions do not reveal a discernible difference in surface roughness (data not shown). Furthermore, protein hydrogels scanned in the absence of BP-b undergo an identical change in surface topography (data not shown). This suggests the imprinting is due to the absorption of light by residual photosensitizer or the BSA, and not the excitation of BP-b. If structures are fabricated using alternative photosensitizers or via a non-photolithographic fabrication method, the effects of the BP-b immobilization scan could potentially be eliminated. Ultimately, the concurrent creation of topography on the protein hydrogels is avoided when additional post-fabrication modifications and the appropriate scan conditions are used. Therefore, this technique can be useful to investigate and decouple the effects of chemical cues from other material properties on cell behavior.
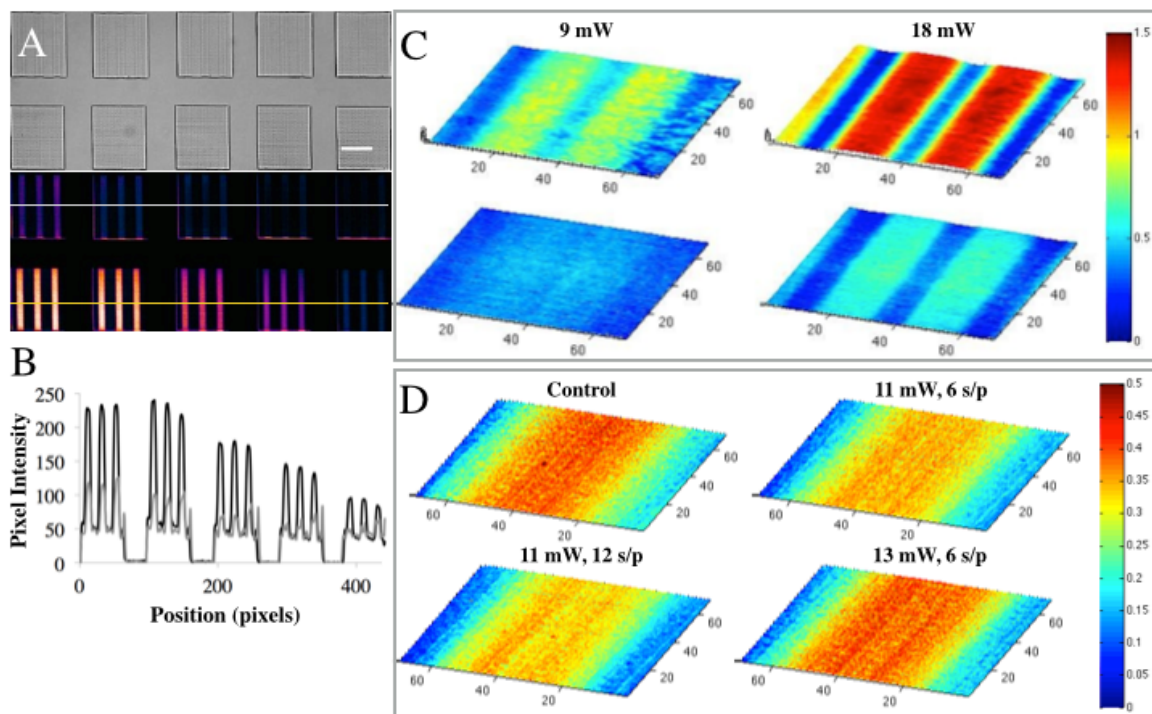
Figure 2.7: Effect of BP-biotin immobilization on topography. A) Brightfield and corresponding fluorescence images of BP-b functionalized BSA pads (scale bar = 50 μm). The top row of pads were photobleached, and the bottom row were laser-reduced with 2 scans prior to photobleaching. The laser power or number of scans used for immobilization increases from right to left. All pads are scanned in a single plane at approximately half of the nominal height. Higher fluorescence intensity is observed for laser-reduced pads (black) versus non-reduced structures (gray) as shown by the linescans, represented by a yellow and gray line, respectively, plotted in (B). This difference is most likely due to the increased density of available reactive sites within the voxel as a result of the shrinking step. C) Topographical maps of bleached (top) and laser-reduced (bottom) pads after BP-b immobilization (colorbar = 1.5 μm). The laser power for the immobilization scan is indicated at the top of each column. A significant indentation is created at both powers for non-reduced structures. Less shrinking of the matrix occurrs for laser-reduced hydrogels, and the presence of features is eliminated at a 9 mW scan power. D) Increasing the number of photoreduction scans to 4, further minimizes the structural changes created by the BP-b immobilization scan (colorbar = 0.5 μm). A maximum of 12 scans/plane using an average laser power of 11 mW does not noticeably change the substrate topography relative to a control. All axes for (C) and (D) are in units of μm.

66

2.4.4 Production of Immobilized Chemical Gradients

Immobilized chemical gradients have been widely used to influence cell migration and polarization and play key roles during development and tissue regeneration [82]. A significant problem associated with many of the techniques used to generate chemical gradients is that other properties of the material are also affected; therefore, effects on cell behavior cannot be attributed only to the chemical presentation. In addition, most techniques are restricted to simple patterns (e.g. linear) that can only be changed along a single axis. However, BP-b immobilization can be achieved without adverse affects on the material properties as shown in **sections 2.4.2 and 2.4.3**. In addition, the extent of immobilization can be controlled using an array of variables including laser power, the number of laser scans, and BP-b concentration as demonstrated in **section 2.4.1**. In this section, immobilized chemical gradients are produced using two distinct methods to modulate the laser power during immobilization: a Pockels cell and a grayscale mask.

A Pockels cell applies an electric field across an optical medium to alter the refractive index and produce birefringence, an effect first studied by Friedrich Carl Alwin Pockels in 1893. The percent of light refracted can be controlled by the magnitude of the applied voltage. This device can be used in connection with a polarizing beam-splitter to effectively modulate the output power of a laser. In these studies, a function generator is used to apply a voltage input function to the Pockels cell at user-defined amplitudes and frequencies to produce an output power range from 9 – 18 mW. The triggering of the Pockels cell is synchronized with the BP-b immobilization scan using Labview software. Each scan is performed 6 times in a single plane at approximately one-half of the nominal height of a BSA pad. Three regions are immobilized sequentially on a single pad using a variety of waveforms (sine, triangle, constant) or frequencies (0.1 Hz to 10 Hz) in **Figure**

2.8. Fidelity between input functions and corresponding NA-TMR fluorescence is observed. Approximately a three-fold increase in fluorescence intensity over a distance of 50 μm is achieved with very low noise using power modulation. The slope and distance of the gradient are adjustable by altering the input frequency and/or amplitude of the function generator.

An additional technique to produce gradients is via presentation of grayscale photomasks using a DMD. Typically, binary masks are used to signal reflective mirrors on the DMD to be in the "on" or "off" position. Mirrors in the "on" position direct the laser beam to the back aperture of the objective, and "off" mirrors send the laser beam to a beam block. Gray values cause the mirrors to switch between positions rapidly, with the respective time in either position determined by the magnitude of the value. This approach has been used with other photolithographic systems to generate complex images and patterns of immobilized proteins [83]. Here, grayscale photomasks are used to control the extent of BP-b immobilization. A simple, linear gradient is created in **Figure 2.8** using a photomask with gray values varying linearly from 0 - 255. A six-fold intensity change over 20 μm is achieved, indicating this technique has a very small working range of gray values. Identifying and isolating the effective range of gray values could offer much more control of the slope and distance of immobilized gradients. In addition to creating more complex patterns than a Pockels cell, a higher lateral resolution can also be achieved using the DMD.
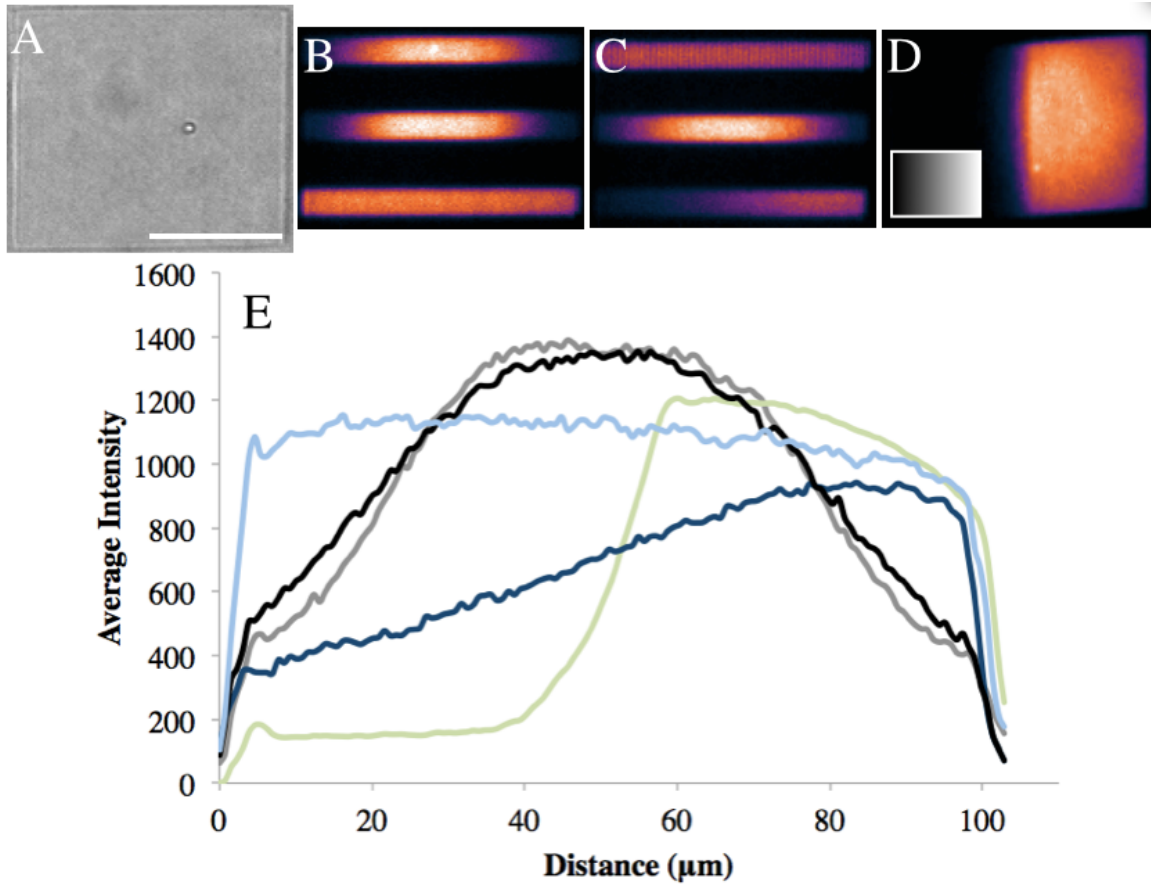
Figure 2.8: Immobilized chemical gradients. A) A representative brightfield image of a BSA pad (scale bare = 50 μm). (B - C) Three 10 μm stripes are immobilized on a single pad using a Pockels cell to modulate the laser power. The waveform and frequency are altered to generate a collection of gradient profiles. D) A gradient is produced using a grayscale photomask (inset). E) Representative linescans of NA-TMR fluorescence for a triangle function at 0.2 Hz (black, C: middle), sine function at 0.2 Hz (gray, B: middle), triangle function at 0.1 Hz (dark blue, C: bottom), constant voltage (light blue, B: bottom), and grayscale mask (green, D).

2.4.5 3D Immobilization

3D resolution is imperative to developing biomaterials that can spatially orient and direct cells within engineered tissue constructs. To demonstrate 3D capabilities of this technique, a sequence of masks is displayed to immobilize BP-b in a spiral pattern presented on the surface or within conical and cylindrical hydrogels. To tune the extent of immobilization, laser power is modulated using a Pockels cell as described in **section 2.4.4**. High resolution in all axes is achieved, and pattern fidelity is maintained. The primary use of BP-b immobilization in this dissertation is as surface immobilization technique to promote cell adhesion, but its application for the immobilization of biomolecules within protein scaffolds is also demonstrated.

The cones in **Figure 2.9(A, B)** and **(D)** were fabricated using a layer-by-layer approach to a total height of 20 um. After rinsing, the structures were reduced using two and four additional laser scans, respectively, prior to photobleaching. The BP-b immobilization was conducted using 4 and 6 scans in a single plane, respectively, beginning at the base of the cones and axially stepping through the entire structure in 1 μm increments. The increase in crosslinking density of the protein matrix and short NA-TMR incubation times (3 hours) restrict the NA-TMR labeling to the surface of the hydrogel only. The average fluorescence intensity for the spiral (**Figure 2.9A**) is 93 with a standard deviation of 11% in an 8-bit image. The deviation is most likely caused by an increase in scatter and beam attenuation during image acquisition as the structure thickness increases. A decrease in signal with axial height is consistent for all confocal acquisitions. Since a calibration was not established to correct for beam attenuation, gray values of NA-TMR patterns are only compared relative to each other. Beam attenuation may also occur during BP-b immobilization, and further experimentation is required to establish proper correction protocols.

In **Figure 2.9(C)** a spiral pattern extending 5 μm from the base into a 10 μm-tall cone is shown to demonstrate the ability to immobilize BP-b within 3D protein hydrogels as well. The fabrication and immobilization scans for this structure were performed using a 100X, 1.3 NA objective. The structure was not laser reduced or photobleached prior to immobilization. A longer incubation time (12 hours) allowed for the diffusion of NA-TMR into the construct. Axial resolution of ~1 μm is demonstrated, proving this technique allows for immobilization of biomolecules with highly resolved, 3D spatial distribution.

In addition to the organization of immobilized biomolecules, immobilized concentration can also play a role in cellular guidance. Creation of planar gradients using a Pockels cell and grayscale mask was discussed in **section 2.4.4**. To produce 3D gradients, a Pockels cell was used to modulate the laser power in the optical axis during the immobilization of BP-b spiral patterns on cones (**Figure 2.10**) and cylindrical posts (**Figure 2.11**). The frequency was set to span the entire power range over the time required for a single immobilization scan through a hydrogel (triangle function, 0.05 Hz, 100 second immobilization scan). For certain scans, the frequency was doubled to immobilize the full triangle function, or the phase was shifted 180 degrees to change the direction of the gradient. The process was then repeated either two or four times to amplify the extent of immobilization for improved visualization. All fluorescence profiles generated along spiral patterns of the cones are plotted in **Figure 2.10D**. A steady decrease in fluorescence intensity at increasing z-axis planes is observed for constant immobilization powers; therefore, profiles are only assessed relative to one another. Although specific concentrations of immobilized NA-TMR is not determined for these studies, a variety of fluorescence intensity profiles are produced in 3D via laser power attenuation.
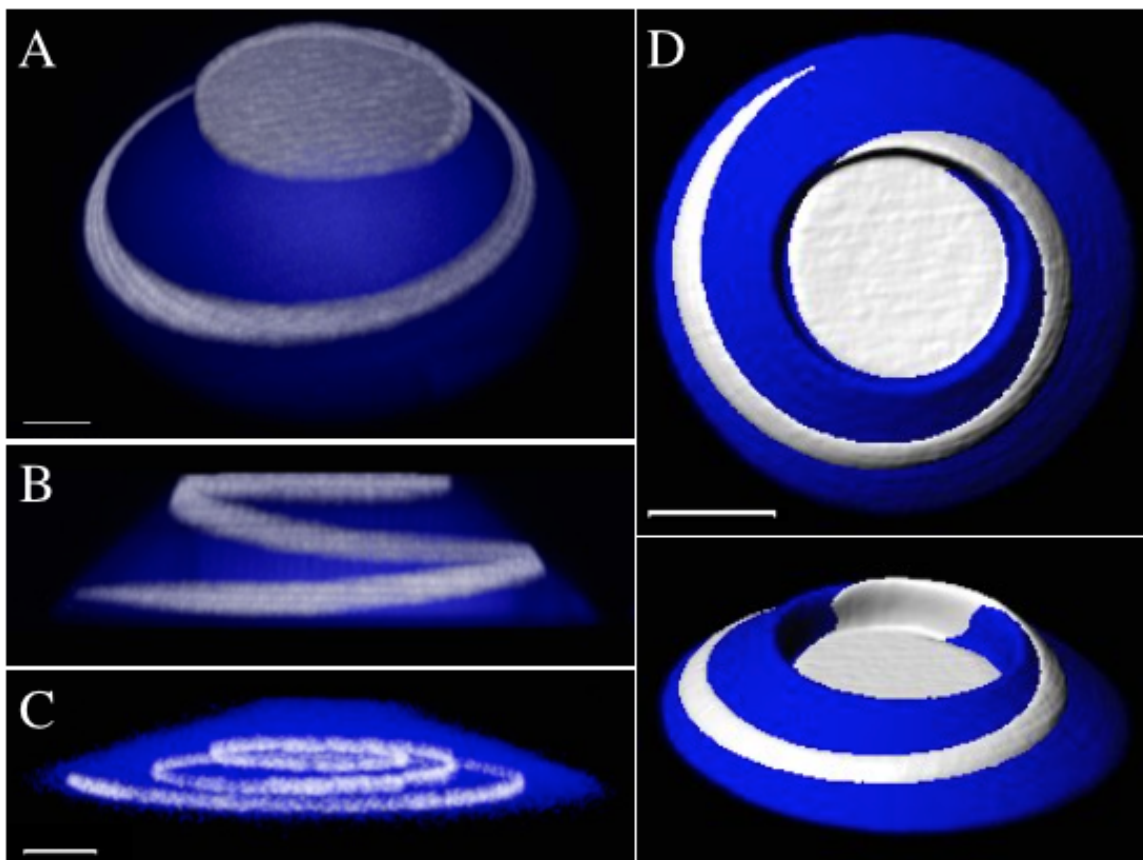
Figure 2.9: Confocal reconstructions of 3D patterned conical protein hydrogels. (A – B) Confocal projections of a BSA cone (blue) with an immobilized spiral pattern of NA-TMR (white). Labeling is restricted to the surface of the cone by limiting the NA-TMR incubation time (scale bar = 10 μm). C) Reconstruction of sub-surface immobilization of NA-TMR within a 10 μm tall BSA cone. A 1.3 NA, 100X objective is used for fabrication and immobilization (scale bar = 5 μm). D) A top-down view (top) and angled view (bottom) of a surface recreation representing a conical structure with an inset top. A spiral of NA-TMR is immobilized around the cone and the inset feature is also patterned (scale bar = 20 μm). All images were created using Imaris software.
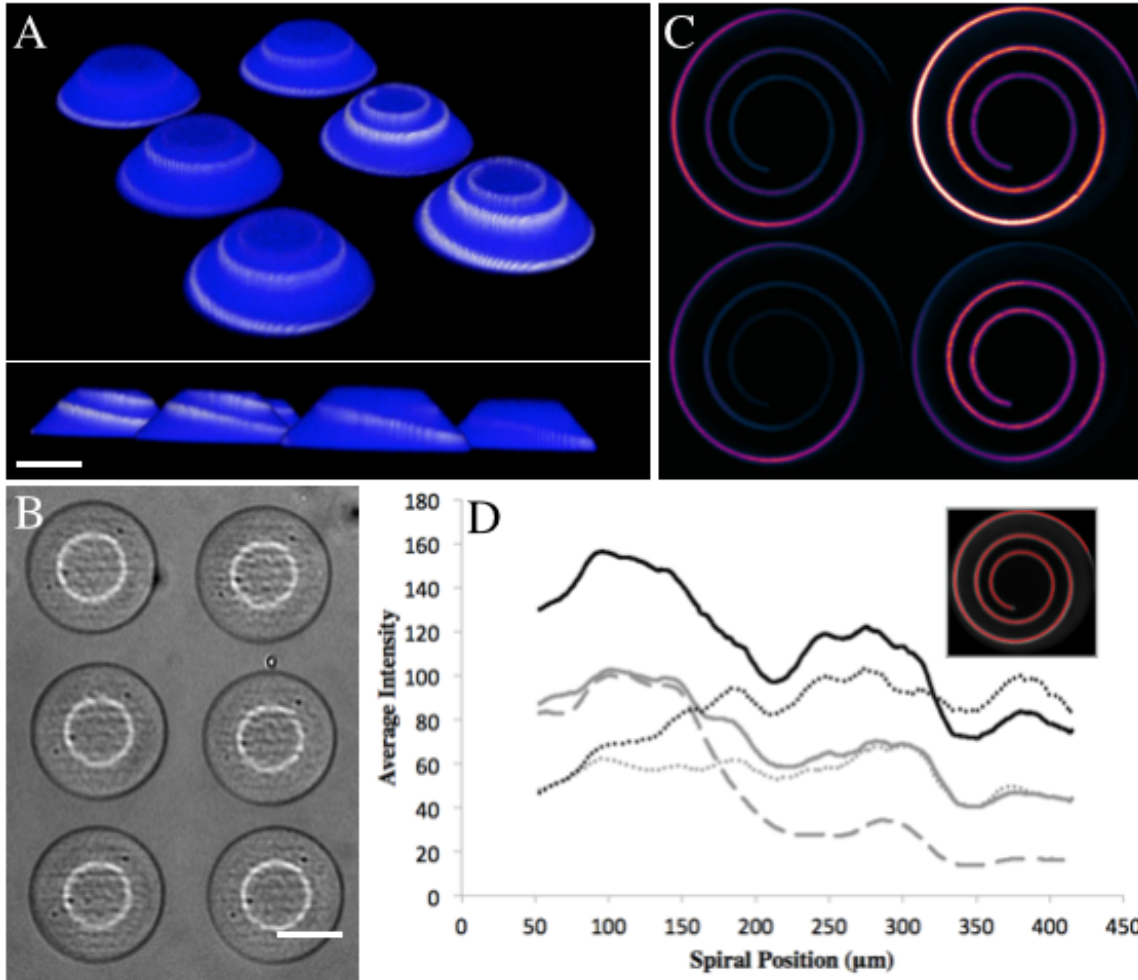
Figure 2.10: Immobilized 3D gradients on conical protein hydrogels. A) Confocal reconstruction of conical BSA structures with immobilized NA-TMR (white) spirals that exhibit different intensity profiles. An angled view (top) and side view (bottom) from opposite perspectives are shown (scale bar = 25 μm). B) Brightfield image of the cones (scale bar = 50 μm). C) Z-axis projections of confocal stacks for the NA-TMR channel only. The extent of immobilization is altered by adjusting the number of immobilization scans/plane at a constant laser power (2 scans, top left; 4 scans, top right). Continuous gradients both increasing (bottom right) and decreasing (bottom left) with z-position are also produced (power range: 9 – 18 mW). D) A 20 μm moving average of numerous spiral traces (example of trace inset as red line) is plotted. Patterns created using 4 scans/plane are in black (constant power – solid line, increasing gradient – dotted line), while patterns created using 2 scans/plane are in gray (constant power – solid line, increasing gradient – dotted line, decreasing gradient – dashed line). All images were created in ImageJ. Acquisition parameters and brightness and contrast adjustments were consistent.
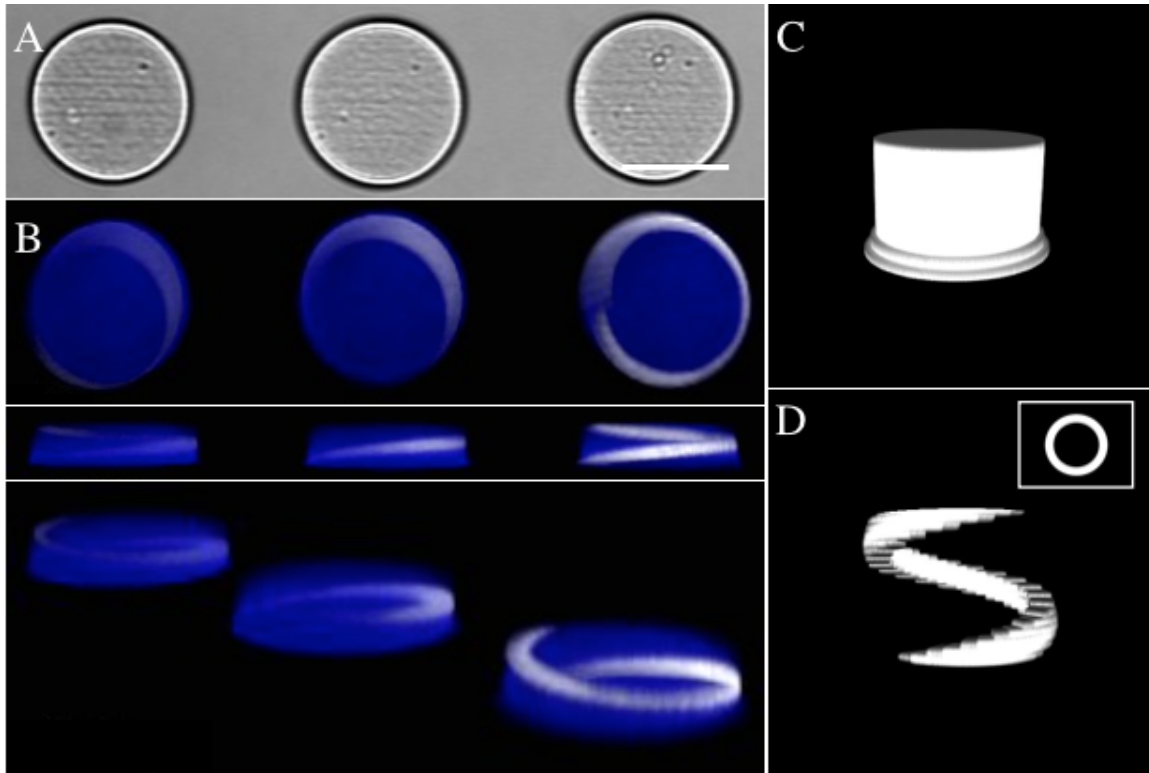
Figure 2.11: Immobilized 3D gradients on cylindrical posts. A brightfield image of 20 μm tall BSA posts (scale bar = 50 μm). B) A sequence of confocal reconstructions of the posts showing the protein structure (blue) and NA-TMR (white) immobilization wrapping 360° around the post. A top-down (top), side (middle), and angled view (bottom) are shown. A different immobilization protocol was used for each post to produce various intensity profiles in 3D space (constant power: right, triangle function: middle, increasing gradient: left). Mask projections used for post fabrication (C) and BP-b immobilization (D) are provided to show pattern fidelity is maintained. The view in (D) most closely resembles the side view projection in (B). The inset in (D) provides a top-down view of the spiral pattern.

2.4.6 Schwann Cell (SC) Adhesion and Patterning

Previous results have demonstrated that μ-3D printed protein hydrogels are suitable for cell culture, and that incorporation of IKVAV peptides into BSA hydrogels increased cell adhesion [6]. SCs are the primary focus of this work, as their slow infiltration speed into nerve gaps post-injury is believed to be a rate-limiting step preventing successful regeneration [84, 85]. In an effort to control SC adhesion and promote polarization on μ-3D printed scaffolds, BP-b immobilization is used to functionalize protein hydrogels with biotinylated-RGD (b-RGD), a cell adhesive peptide [15]. Peptide functionalized structures display a significant increase in cell adhesion relative to unmodified equivalents, and the ability to precisely control adhesion sites and promote cell polarization is demonstrated.

To study cell adhesion, planar BSA pads are modified with b-RGD using immobilization conditions that prevent structural modifications as shown in **sections 2.4.2** - **2.4.3**. SC adhesion to the structures was monitored using time-lapse microscopy (**Figure 2.12**). Two hours after the introduction of SCs, the cell density is much higher on an RGD-functionalized region of a BSA pad. SCs flatten and remain on the RGD-functionalized region for up to 12 hours, indicative of strong cell-matrix interactions. Fewer cells (2 versus 7 for RGD regions) are on the unmodified pads after two hours, and migrated to the modified areas over the time course of the experiment. Better adhesion is observed when the laser power used for immobilization is increased beyond the threshold to avoid structural deformation (**Figure 2.12B**). Extended cell adhesion on unmodified pads is rarely observed, except at structure edges. Linear features on the order of 1 μm are created at edges that may provide topographical signals to promote cell adhesion. Other differences at the edges, including crosslinking density and photosensitizer concentration, may also contribute to a differential response to photobleaching.

Particularly, cells exhibit a higher affinity for BSA pads that are not laser-reduced prior to photobleaching. Based on previous experiments from the Shear Group, the effect of photobleaching on cell adhesion to BSA structures is possibly due to a change in the effective charge of the structure [70]. Laser-induced shrinking reduces the photosensitizer content and minimizes changes to the structure during photobleaching; therefore, BSA hydrogels maintain their commonly observed non-adhesive properties. The effect of photobleaching on cell adhesionto hydrogels is not studied in more detail in this work, but could offer a simple route for patterning cells in the future.

Methods to localize cell adhesion have been used to dictate the distribution of cellular co-cultures for *in vitro* tissue models [14, 21, 51, 86, 87]. Additionally, cell morphology has primary effects on cell function, and it has been controlled using arrays of geometrical adhesive patterns [19, 88, 89]. Specific to SCs, polarization has been identified as a prerequisite for myelination, and may play significant roles in demyelinating diseases such as Charcot-Marie-Tooth disease [90]. To demonstrate the capability of this technique to pattern SCs, 10 μm wide, linear patterns of b-RGD are immobilized on the surface of planar protein pads as shown in **Figure 2.13**. Cell adhesion and elongation is primarily restricted to the patterned regions during 12 hours of imaging. SC extension over 100 μm was consistently observed within RGD-patterned regions. The laser power used for BP-b immobilization in this study was 22 mW; therefore, simultaneous imprinting of ~200 nm features did occur. The 200 nm features alone, created by scanning in the absence of BP-b, did not promote cell adhesion or alignment.

Cells were also patterned on 3D structures as shown in **Figure 2.14 and 2.15**. Similar to planar adhesion studies, cells only interacted with b-RGD functionalized surfaces. A phalloidin stain was used to visualize the f-actin filaments within the cell. These fibers are anchored by focal adhesions, which are strong integrin-mediated cell-

surface attachments [91]. Expression of f-actin was co-localized with b-RGD patterns, demonstrating that functionalization promotes strong cell-substrate interactions.
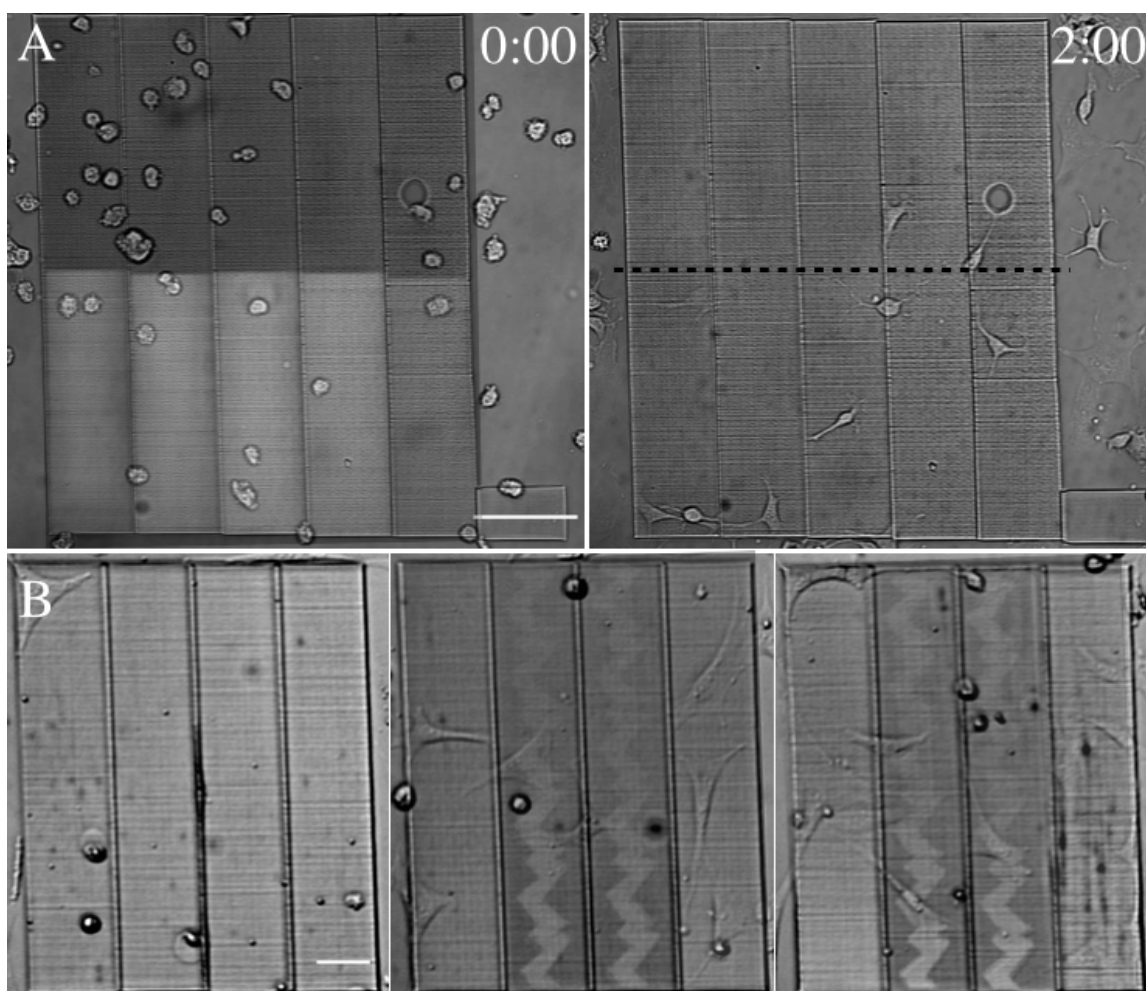
Figure 2.12: Promoting Schwann cell adhesion via b-RGD functionalized BSA pads. A) Time-lapse sequence of SCs on partially, b-RGD functionalized BSA pads (scale bar = 100 μm). Images were acquired at 5-minute intervals for 12 hours, and frame 1 and 24 are shown (time stamps, in hours, located at the top right of each image) to highlight cell adhesion. The NA-TMR fluorescence image is overlayed in the t = 0 image to show the bottom half of the pad is functionalized. This division is recreated using a dotted line in the 2 hour image. The cell density after two hours in culture is significantly higher on the RGD-functionalized region. B) SCs after 14 hours in culture on BSA pads that are unmodified (left) or functionalized with b-RGD using immobilization powers of 11 mW (middle) and 22 mW (right). Scale bar = 50 μm.
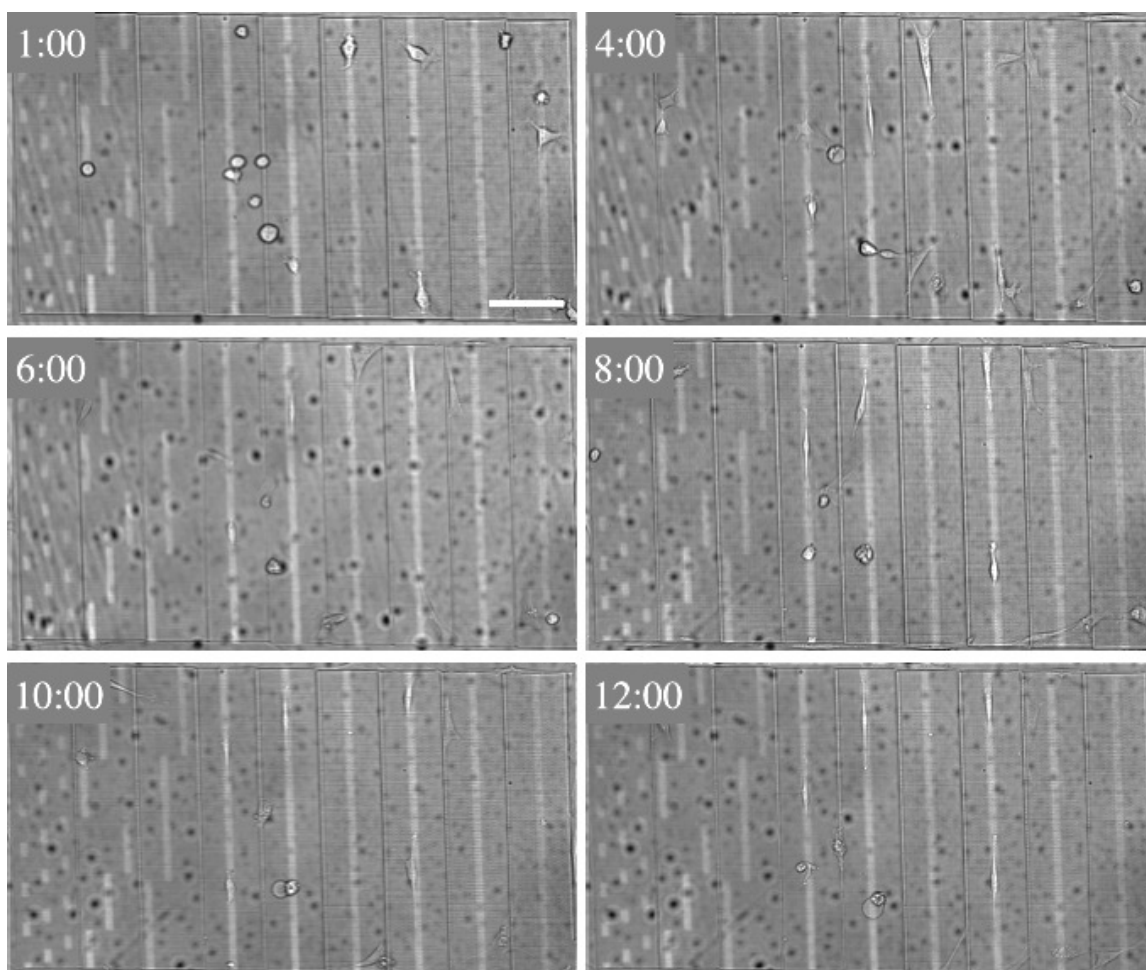
Figure 2.13: SC patterning on immobilized regions of b-RGD. A time-lapse sequence of SC adhesion and migration on b-RGD patterned BSA pads. The NA-TMR fluorescence image is displayed as an overlay to show b-RGD patterned regions. SCs adhere to and align primarily within the patterned regions. A time stamp, in hours, is located at the top left of each image. The out of plane dark spots are from accumulated condensation on the bottom of the coverslip. Scale bar = 100 μm.
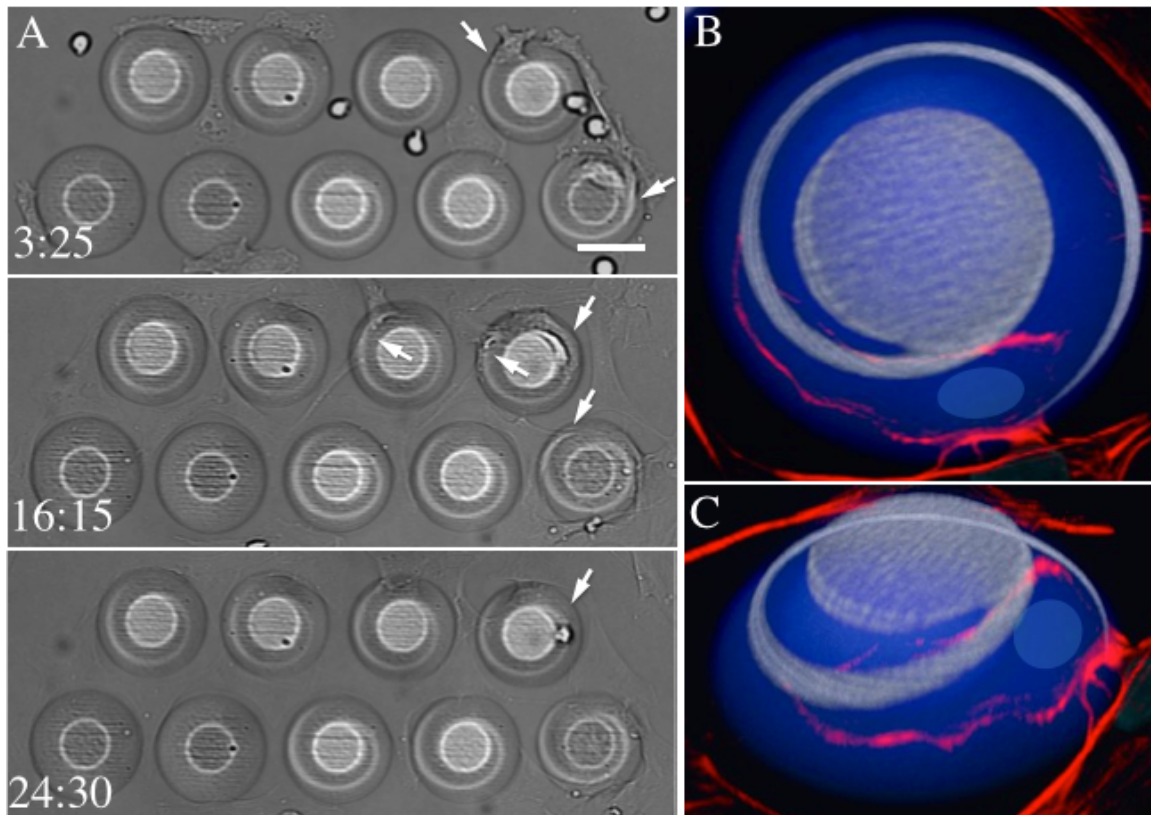
Figure 2.14: SC patterning on immobilized spirals of b-RGD on BSA cones. A) Time-lapse sequence of SCs interacting with b-RGD functionalized cones (scale bar = 50 μm). Time stamps, in hours, are located at the bottom left of each frame. The spiral immobilization, represented by NA-TMR fluorescence, is overlayed on the brightfield images to aid in visualization. White arrows denote regions where cell extensions are interacting with the b-RGD functionalized spirals. Extended cell adhesion is not observed on cones without immobilized b-RGD spirals. (B-C) Cells were fixed with paraformaldehyde then stained with phalloidin-Alexa fluor 594 and DAPI before confocal imaging. The BSA (blue), NA-TMR (white), F-actin (red), and DAPI (cyan, drawn in to aid in visualization) channels were acquired, and 3D reconstructions were generated using Imaris software. Actin expression is co-localized with the b-RGD spiral on a cone.
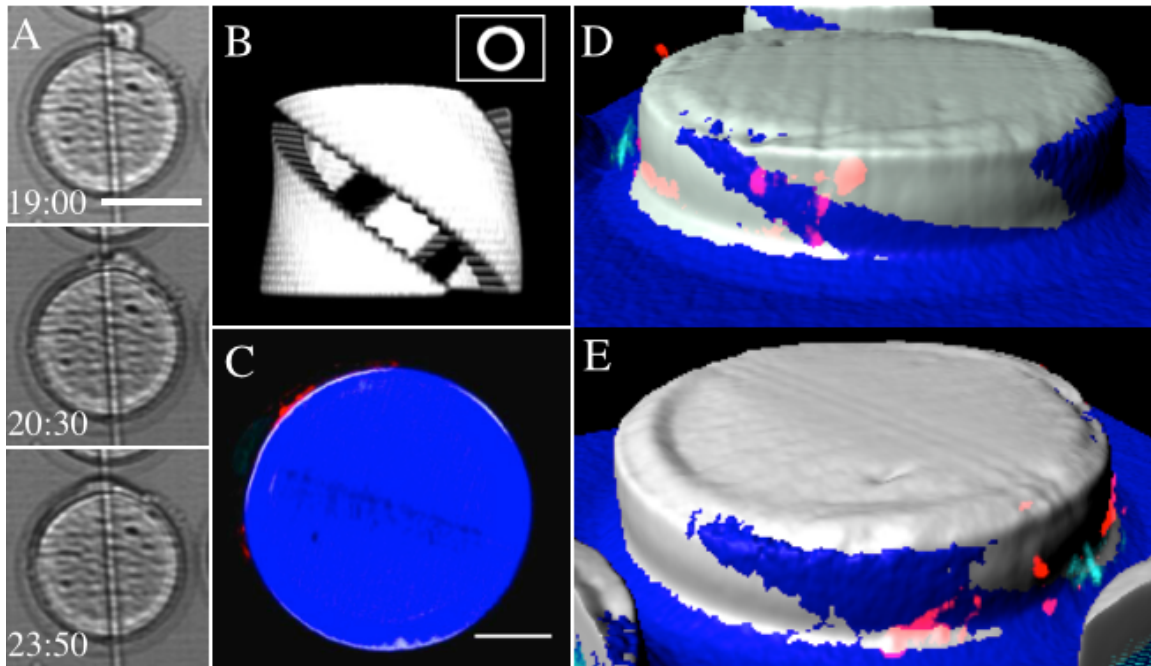
Figure 2.15: SC adhesion on immobilized spirals of b-RGD around a cylindrical BSA post. A) Time-lapse sequence of a SC interacting with a b-RGD functionalized post (scale bar = 50 μm). Time stamps, in hours, are located at the bottom left of each frame. B) A 3D reconstruction of the spiral immobilization mask used with a top-down view inset within the image. (C-E) The cell was fixed and stained with phalloidin-Alexa fluor 594 and DAPI, then imaged using confocal microscopy. The BSA (blue), NA-TMR (white), F-actin (red), and DAPI (cyan) channels were acquired. 3D reconstructions were generated using Imaris software. A single slice 10 μm above the base of the cone is provided in (C). Two side views rotated slightly are shown with the structure and pattern represented as surfaces (D-E). Actin expression is co-localized with b-RGD functionalized regions on the post.

2.5 CONCLUSIONS

This chapter demonstrates the potential of an MPE-induced BP-b immobilization to render μ-3D printed protein scaffolds biofunctional. Precise control over the 3D spatial organization and the extent of BP-b immobilization both on and within protein scaffolds is exhibited. Conditions are identified that allow for tunability of the chemical presentation without altering the mechanical or topographical properties of the substrate. This technique could be used to investigate the response of cells to chemical, mechanical, and topographical signals independent of each other in 3D tissue scaffolds. Ultimately, BP-b immobilization using MPE provides a versatile platform for the chemical modification of various proteins and polymers that could be applied to any cell culture system.

To improve upon the results presented here, future work should focus on synthesizing water-soluble BP-conjugates. Direct conjugation of biomolecules to the BP could also be valuable to avoid the requirement of NA-biotin binding chemistry. These modifications would allow for dynamic chemical changes to be made *in situ* to the underlying substrate of cells. Additional studies could investigate the cellular response to immobilized chemical gradients. Preliminary efforts to promote directional migration were unsuccessful, but only a limited number of cell phenotypes and biomolecules were evaluated.

2.6 REFERENCES

1. Frantz, C, Stewart, KM, and Weaver, VM, The extracellular matrix at a glance. Journal of Cell Science, 2010. 123(Pt 24): p. 4195-4200.

2. Curtis, A and Wilkinson, C, Topographical control of cells. Biomaterials, 1997. 18(24): p. 1573-1583.

3. Wells, RG, The role of matrix stiffness in regulating cell behavior. Hepatology, 2008. 47(4): p. 1394-1400.

4. Discher, DE, Janmey, P, and Wang, Y-L, Tissue cells feel and respond to the stiffness of their substrate. Science, 2005. 310(5751): p. 1139-1143.

5. Wong, JY, Leach, JB, and Brown, XQ, Balance of chemistry, topography, and mechanics at the cell–biomaterial interface: Issues and challenges for assessing the role of substrate mechanics on cell response. Surface Science, 2004. 570(1–2): p. 119-133.

6. Seidlits, SK, Schmidt, CE, and Shear, JB, High-resolution patterning of hydrogels in three dimensions using direct-write photofabrication for cell guidance. Advanced Functional Materials, 2009. 19(22): p. 3543-3551.

7. Schmidt, CE and Leach, JB, Neural tissue engineering: Strategies for repair and regeneration. Annual Review of Biomedical Engineering, 2003. 5: p. 293-347.

8. Li, GN and Hoffman-Kim, D, Tissue-engineered platforms of axon guidance. Tissue Engineering Part B Review, 2008. 14(1): p. 33-51.

9. Son, YJ and Thompson, WJ, Nerve sprouting in muscle is induced and guided by processes extended by schwann cells. Neuron, 1995. 14(1): p. 133-141.

10. Fugleholm, K, Schmalbruch, H, and Krarup, C, Early peripheral nerve regeneration after crushing, sectioning, and freeze studied by implanted electrodes in the cat. Journal of Neuroscience, 1994. 14(5 Pt 1): p. 2659-2673.

11. Son, YJ, Trachtenberg, JT, and Thompson, WJ, Schwann cells induce and guide sprouting and reinnervation of neuromuscular junctions. Trends in Neuroscience, 1996. 19(7): p. 280-285.

12. Roth, EA, et al., Inkjet printing for high-throughput cell patterning. Biomaterials, 2004. 25(17): p. 3707-3715.

13. Zheng, W, Zhang, W, and Jiang, X, Precise control of cell adhesion by combination of surface chemistry and soft lithography. Advanced Healthcare Materials, 2013. 2(1): p. 95-108.

14. Falconnet, D, et al., Surface engineering approaches to micropattern surfaces for cell-based assays. Biomaterials, 2006. 27(16): p. 3044-3063.

15. Ruoslahti, E, Rgd and other recognition sequences for integrins. Annual Review of Cell and Developmental Biology, 1996. 12(1): p. 697-715.

16. Martin, GR and Timpl, R, Laminin and other basement membrane components. Annual Review of Cell Biology, 1987. 3(1): p. 57-85.

17. Mcdonald, JA, Extracellular matrix assembly. Annual Review of Cell Biology, 1988. 4: p. 183-207.

18. Tashiro, K, et al., A synthetic peptide containing the ikvav sequence from the a chain of laminin mediates cell attachment, migration, and neurite outgrowth. Journal of Biological Chemistry, 1989. 264(27): p. 16174-16182.

19. Chen, CS, et al., Geometric control of cell life and death. Science, 1997. 276(5317): p. 1425-1428.

20. Mcbeath, R, et al., Cell shape, cytoskeletal tension, and rhoa regulate stem cell lineage commitment. Developmental Cell, 2004. 6(4): p. 483-495.

21. Ross, AM and Lahann, J, Surface engineering the cellular microenvironment via patterning and gradients. Journal of Polymer Science Part B: Polymer Physics, 2013. 51(10): p. 775-794.

22. Ogaki, R, Alexander, M, and Kingshott, P, Chemical patterning in biointerface science. Materials Today, 2010. 13(4): p. 22-35.

23. Kalia, J and Raines, RT, Advances in bioconjugation. Current Organic Chemistry, 2010. 14(2): p. 138-147.

24. Hermanson, GT, Bioconjugate techniques. 2013: Elsevier Science & Technology Books.

25. Fischer, ME, Amine coupling through edc/nhs: A practical approach, in Surface plasmon resonance, N.J. Mol and M.J.E. Fischer, Editors. 2010, Humana Press. p. 55-73.

26. Lundblad, RL, Chemical reagents for protein modification. Third ed. 2005: Taylor & Francis.

27. Leach, JB, et al., Development of photocrosslinkable hyaluronic acid-polyethylene glycol-peptide composite hydrogels for soft tissue engineering. Journal of Biomedical Materials Research A, 2004. 70(1): p. 74-82.

28. Jeon, O, et al., Photocrosslinked alginate hydrogels with tunable biodegradation rates and mechanical properties. Biomaterials, 2009. 30(14): p. 2724-2734.

29. Dhoot, NO, et al., Peptide-modified alginate surfaces as a growth permissive substrate for neurite outgrowth. Journal of Biomedical Materials Research A, 2004. 71(2): p. 191-200.

30. Camci-Unal, G, et al., Hydrogel surfaces to promote attachment and spreading of endothelial progenitor cells. Journal of Tissue Engineering Regenerative Medicine, 2013. 7(5): p. 337-347.

31. Kolb, HC, Finn, MG, and Sharpless, KB, Click chemistry: Diverse chemical function from a few good reactions. Angew Chemie International Edition, 2001. 40(11): p. 2004-2021.

32. Binder, WH and Sachsenhofer, R, 'Click' chemistry in polymer and materials science. Macromolecular Rapid Communications, 2007. 28(1): p. 15-54.

33. Moses, JE and Moorhouse, AD, The growing applications of click chemistry. Chemical Society Review, 2007. 36(8): p. 1249-1262.

34. Deforest, CA, Polizzotti, BD, and Anseth, KS, Sequential click reactions for synthesizing and patterning three-dimensional cell microenvironments. Nature Materials, 2009. 8(8): p. 659-664.

35. Lutz, J-F and Zarafshani, Z, Efficient construction of therapeutics, bioconjugates, biomaterials and bioactive surfaces using azide–alkyne "click" chemistry. Advanced Drug Delivery Reviews, 2008. 60(9): p. 958-970.

36. Nuzzo, RG and Allara, DL, Adsorption of bifunctional organic disulfides on gold surfaces. Journal of the American Chemical Society, 1983. 105(13): p. 4481-4483.

37. Koepsel, JT and Murphy, WL, Patterning discrete stem cell culture environments via localized self-assembled monolayer replacement. Langmuir, 2009. 25(21): p. 12825-12834.

38. Moore, NM, et al., The use of immobilized osteogenic growth peptide on gradient substrates synthesized via click chemistry to enhance mc3t3-e1 osteoblast proliferation. Biomaterials, 2010. 31(7): p. 1604-1611.

39. Kumar, A, Biebuyck, HA, and Whitesides, GM, Patterning self-assembled monolayers: Applications in materials science. Langmuir, 1994. 10(5): p. 1498-1511.

40. Kumar, A and Whitesides, G, Features of gold having micrometer to centimeter dimensions can be formed through a combination of stamping with an elastomeric stamp and an alkanethiol "ink" followed by chemical etching. Applied Physics Letters, 1993. 63(14): p. 2002-2004.

41. Chou, SY, Krauss, PR, and Renstrom, PJ, Imprint of sub-25 nm vias and trenches in polymers. Applied Physics Letters, 1995. 67(21): p. 3114-3116.

42. Choi, D-G, et al., Particle arrays with patterned pores by nanomachining with colloidal masks. Journal of the American Chemical Society, 2005. 127(6): p. 1636-1637.

43. Piner, RD, et al., "Dip-pen" nanolithography. Science, 1999. 283(5402): p. 661-663.

44. Jang, JW, Smetana, A, and Stiles, P, Multi-ink pattern generation by dip-pen nanolithography. Scanning, 2010. 32(1): p. 24-29.

45. Rakickas, T, et al., Functional hydrogel density patterns fabricated by dip-pen nanolithography and photografting. Small, 2011. 7(15): p. 2153-2157.

46. Sekula, S, et al., Multiplexed lipid dip-pen nanolithography on subcellular scales for the templating of functional proteins and cell culture. Small, 2008. 4(10): p. 1785-1793.

47. Bellido, E, et al., Controlling the number of proteins with dip-pen nanolithography. Advanced Materials, 2010. 22(3): p. 352-355.

48. Wu, C-C, et al., Porous multilayer-coated afm tips for dip-pen nanolithography of proteins. Journal of the American Chemical Society, 2009. 131(22): p. 7526-7527.

49. Adams, DN, et al., Growth cones turn and migrate up an immobilized gradient of the laminin ikvav peptide. Journal of Neurobiology, 2005. 62(1): p. 134-147.

50. Hahn, MS, et al., Photolithographic patterning of polyethylene glycol hydrogels. Biomaterials, 2006. 27(12): p. 2519-2524.

51. Sugiura, S, et al., Surface modification of polydimethylsiloxane with photo-grafted poly(ethylene glycol) for micropatterned protein adsorption and cell adhesion. Colloids and Surfaces B: Biointerfaces, 2008. 63(2): p. 301-305.

52. Luo, Y and Shoichet, MS, A photolabile hydrogel for guided three-dimensional cell growth and migration. Nature Materials, 2004. 3(4): p. 249-253.

53. Musoke-Zawedde, P and Shoichet, MS, Anisotropic three-dimensional peptide channels guide neurite outgrowth within a biodegradable hydrogel matrix. Biomedical Materials, 2006. 1(3): p. 162-169.

54. Becker, MM and Wang, Z, Origin of ultraviolet damage in DNA. Journal of Molecular Biology, 1989. 210(3): p. 429-438.

55. Hu, ML and Tappel, AL, Potentiation of oxidative damage to proteins by ultraviolet-a and protection by antioxidants. Photochemistry and Photobiology, 1992. 56(3): p. 357-363.

56. Sasaki, N, et al., Photochemical immobilization of cells onto a glass substrate for in situ DNA analysis. Analytical Sciences, 2012. 28(6): p. 537-539.

57. Edahiro, J-I, et al., In situ control of cell adhesion using photoresponsive culture surface. Biomacromolecules, 2005. 6(2): p. 970-974.

58. Bryant, SJ, Nuttelman, CR, and Anseth, KS, Cytocompatibility of uv and visible light photoinitiating systems on cultured nih/3t3 fibroblasts in vitro. Journal of Biomaterials Science Polymer Edition, 2000. 11(5): p. 439-457.

59. Kloxin, AM, et al., Photodegradable hydrogels for dynamic tuning of physical and chemical properties. Science, 2009. 324(5923): p. 59-63.

60. Wylie, RG and Shoichet, MS, Two-photon micropatterning of amines within an agarose hydrogel. Journal of Materials Chemistry, 2008. 18(23): p. 2716-2721.

61. Lee, S-H, Moon, JJ, and West, JL, Three-dimensional micropatterning of bioactive hydrogels via two-photon laser scanning photolithography for guided 3d cell migration. Biomaterials, 2008. 29(20): p. 2962-2968.

62. Wylie, RG, et al., Spatially controlled simultaneous patterning of multiple growth factors in three-dimensional hydrogels. Nature Materials, 2011. 10(10): p. 799-806.

63. Hoffmann, JC and West, JL, Three-dimensional photolithographic patterning of multiple bioactive ligands in poly(ethylene glycol) hydrogels. Soft Matter, 2010. 6(20): p. 5056-5063.

64. Spivey, EC, et al., Multiphoton lithography of unconstrained three-dimensional protein microstructures. Advanced Functional Materials, 2013. 23(3): p. 333-339.

65. Ritschdorff, ET, Nielson, R, and Shear, JB, Multi-focal multiphoton lithography. Lab on a Chip, 2012. 12(5): p. 867-871.

66. Ritschdorff, ET and Shear, JB, Multiphoton lithography using a high-repetition rate microchip laser. Analytical Chemistry, 2010. 82(20): p. 8733-8737.

67. Nielson, R, Kaehr, B, and Shear, JB, Microreplication and design of biological architectures using dynamic-mask multiphoton lithography. Small, 2009. 5(1): p. 120-125.

68. Kaehr, B and Shear, JB, Mask-directed multiphoton lithography. Journal of the American Chemical Society, 2007. 129(7): p. 1904-1905.

69. Spivey, EC, Multiphoton lithography of mechanically and functionally tunable hydrogels. 2012, The University of Texas at Austin.

70. Connell, JL, Characterization and microfabrication of environmentally sensitive materials for studying bacterial group behaviors. 2012, The University of Texas at Austin.

71. Forciniti, L, et al., Schwann cell response on polypyrrole substrates upon electrical stimulation. Acta Biomaterialia, 2014. 10(6): p. 2423-2433.

72.   Hoppe, TJ, Laser-based techniques for manipulating the single-cell environment. 2013, The University of Texas at Austin.

73.   Galardy, RE, et al., Photoaffinity labeling of peptide hormone binding sites. Journal of Biological Chemistry, 1974. 249(11): p. 3510-3518.

74.   Dorman, G and Prestwich, GD, Benzophenone photophores in biochemistry. Biochemistry, 1994. 33(19): p. 5661-5673.

75.   Hypolite, CL, et al., Formation of microscale gradients of protein using heterobifunctional photolinkers. Bioconjugate Chemistry, 1997. 8(5): p. 658-663.

76.   Pitts, JD, et al., New photoactivators for multiphoton excited three-dimensional submicron cross-linking of proteins: Bovine serum albumin and type 1 collagen. Photochemistry and Photobiology, 2002. 76(2): p. 135-144.

77.   Li, H, et al., Two-photon optical properties of novel branched conjugated derivatives carrying benzophenone moiety with various electron donor-acceptor substituent groups. Journal of Fluorescence, 2011. 21(1): p. 393-407.

78.   Panchuk-Voloshina, N, et al., Alexa dyes, a series of new fluorescent dyes that yield exceptionally bright, photostable conjugates. Journal of Histochemistry and Cytochemistry, 1999. 47(9): p. 1179-1188.

79.   Hertz, H, Über die berührung fester elastischer körper (on the contact of elastic solids). Journal fur die Reine Angewandte Mathematik, 1881. 92: p. 156-171.

80.   Burdick, JA, et al., Controlled degradation and mechanical behavior of photopolymerized hyaluronic acid networks. Biomacromolecules, 2005. 6(1): p. 386-391.

81.   Dimitriadis, EK, et al., Determination of elastic moduli of thin layers of soft material using the atomic force microscope. Biophysical Journal. 82(5): p. 2798-2810.

82.   Keenan, TM and Folch, A, Biomolecular gradients in cell culture systems. Lab on a Chip, 2008. 8(1): p. 34-57.

83.   Waldbaur, A, et al., Maskless projection lithography for the fast and flexible generation of grayscale protein patterns. Small, 2012. 8(10): p. 1570-1578.

84.   Feneley, MR, Fawcett, JW, and Keynes, RJ, The role of schwann cells in the regeneration of peripheral nerve axons through muscle basal lamina grafts. Experimental Neurololgy, 1991. 114(3): p. 275-285.

85.   Gulati, AK, Evaluation of acellular and cellular nerve grafts in repair of rat peripheral nerve. Journal of Neurosurgery, 1988. 68(1): p. 117-123.

86.   Sugiura, S, et al., Dynamic three-dimensional micropatterned cell co-cultures within photocurable and chemically degradable hydrogels. Journal of Tissue Engineering and Regenerative Medicine, 2013: p. n/a-n/a.

87.	Yamato, M, et al., Thermally responsive polymer-grafted surfaces facilitate patterned cell seeding and co-culture. Biomaterials, 2002. 23(2): p. 561-567.

88.	Chen, B, et al., Geometric control of cell migration. Scientific Reports, 2013. 3: p. 2827.

89.	Wan, LQ, et al., Geometric control of human stem cell morphology and differentiation. Integrated Biology, 2010. 2(7-8): p. 346-353.

90.	Masaki, T, Polarization and myelination in myelinating glia. ISRN Neurology, 2012. 2012: p. 28.

91.	Geiger, B, Spatz, JP, and Bershadsky, AD, Environmental sensing through focal adhesions. Nature Reviews Molecular Cell Biology, 2009. 10(1): p. 21-33.

Chapter 3: Real-time topographical and mechanical manipulation of three-dimensional (3D) protein hydrogels

3.1 CHAPTER SUMMARY

Structural properties of the extracellular matrix (ECM), including topography and stiffness, have profound effects on cell behaviors such as differentiation, migration, and morphology [1, 2]. While ample details regarding cellular probing using mechanotransduction are understood, many questions remain unanswered regarding the underlying mechanisms of cellular interpretations to these cues, and what roles they play in development, regeneration, and disease [3-5]. Cellular studies are commonly performed within static culture environments that lack the highly dynamic, cell-matrix interactions that occur *in vivo* [6]. Cells are constantly remodeling their surroundings by secreting ECM proteins/proteases, and by applying traction forces to the environment through integrin-mediated adhesions [7, 8]. A limited number of cell culture systems can provide dynamic and spatiotemporal control capable of mimicking these conditions *in vitro*.

This chapter describes a novel method to rapidly remodel the topographical and mechanical features of micro-three dimensionally printed (μ-3DP) protein hydrogels. Previous work in the Shear Group has demonstrated the viability of μ-3DP protein hydrogels as substrates for cell culture [9-11]. Here, a multiphoton excitation (MPE)-based shrinking technique is introduced to manipulate two substrate properties essential for tissue engineering scaffolds: topography and stiffness. Residual photosensitizer partitioned in the hydrogel after fabrication is exploited to promote additional crosslinking when exposed to a tightly focused, near-infrared mode-locked laser beam. Additional crosslinking condenses the protein matrix at a localized, 3D voxel positioned within a hydrogel, which translates to imprinted topographical features on the hydrogel

surface. The size and geometry of the imprinted features are defined using a combination of digital photomasks and laser scanning parameters, including laser power, location of scan planes, and the number of scan repetitions to achieve up to a five-fold reduction in volume. Imprinted features that result in a 30% reduction in structure height, equivalent to 3 – 5 μm, are created without altering the mechanical or chemical properties of the surface. When optical planes closer to the hydrogel surface are selectively scanned, the elastic modulus of the hydrogel increases approximately six-fold, from 15 to 90 kPa. This response is characterized, and then used to imprint substrates with indistinguishable topographies and dramatically different moduli. Gradients of substrate stiffness are generated by temporally attenuating the laser scan power used for imprinting that could be used to study durotactic migration. Since the laser beam is confined to a small voxel ($\sim$ 1 μm^3) within the structure, *in situ*, real-time modifications are made without noticeable effects on the health of adherent cells. This proof-of-concept study opens the door for future investigations of cellular responses to dynamic and spatiotemporal modifications of topography and modulus on biologically relevant, *in vitro* culture systems. Additionally, this technique can be used to decouple cellular responses to mechanical and topographical presentations in biologically relevant stiffness domains.

3.2 BACKGROUND AND MOTIVATION

The cell-matrix interaction is a constantly evolving, two-way dialogue that is continuously remodeled via degradation, assembly, and tensile processes [12]. The specific properties of native ECM are critical in maintaining tissue homeostasis and regulating cell behaviors such as proliferation, differentiation, migration, and death [13]. Dynamic changes to the ECM occur most notably during development, regeneration, and disease [7, 12]. The static culture environments that are primarily used to study cells *in*

vitro do not provide a means to study cellular responses to spatiotemporal manipulations. Although various mechanisms for cellular probing of ECM properties have been discovered, little is understood regarding how dynamic changes to the ECM affect cell behavior [4]. In recent years, responsive and trigger-sensitive platforms have been developed to study some dynamic aspects of cell-matrix interactions. These platforms have revealed previously undetectable relationships between matrix stiffening and gene expression for example, and could eventually lead to a better understanding of embryonic development and disease progression [6].

3.2.1 Dynamic Topographical Presentations

Sub-cellular surface topographies have broad applications for a variety of tissue engineering paradigms [1, 14]. Effects of grooved topography on the alignment and migration of many cell types on planar surfaces are well documented [14-16]. Extensive studies have also explored the roles of feature depth, pitch, and geometry [17-20]. It is believed that topography guides cell migration/growth by directing the distribution of cytoskeletal proteins, integrins, and focal adhesion complexes [21-25]. Another potentially important driving force is nuclear distortion, which is known to have significant effects on gene expression [26, 27]. A combination of these two effects most likely contributes to topographical control of cell behavior. Platforms capable of delivering dynamic topographical control will provide more insight into the underlying mechanisms that govern cell behavior.

Direct observations of dynamic topographical guidance *in vivo* are limited. One example was discovered in the cortex of brain, where neurons extend axons along tracks of radial glial cell protrusions [28-30]. In this specific case, the glial cells may provide additional trophic support in addition to topographical cues. Ono *et al.* also observed

neuronal migration along parallel ECM fibers in the medulla oblongata, and provided sufficient evidence to ensure development of fibers preceded cell migration [31]. Despite limited evidence implicating topography directly during embryonic development in other systems, the importance of cell polarization for tissue morphogenesis is well established [32-34]. Additionally, a loss of cell polarity is a contributing factor in the progression of diseases, such as fibrosis and cancer [34-37]. Technologies capable of altering the topography rapidly and *in situ* are necessary to clarify the specific roles of ECM topography relating to these phenomena.

3.2.2 Relevance of Dynamic Mechanical Properties

Cells interact with surrounding environments via integrin-mediated adhesions to probe matrix properties such as ligand density and viscoelasticity [38]. Matrix mechanics, and more specifically stiffness, can dictate cell behaviors such as migration, morphology, and differentiation through mechanotransduction signaling pathways [2]. Additionally, patterns of matrix stiffness are capable of promoting cell adhesion, polarization, and migration in the absence of additional cues [39, 40]. Sub-cellular variations in stiffness have also shown great promise for elucidating intracellular mechanisms and promoting localized intracellular responses [41, 42].

Dynamic changes in ECM mechanics are critical for many developmental and regenerative outcomes. Localized degradation by cell-secreted proteolytic enzymes precedes 3D cell translocation [43]. Upregulation of enzyme secretion is observed during inflammation and tissue repair to enhance infiltration of fibroblasts and macrophages to the affected site [44]. Conversely, matrix stiffening is also a physiologically relevant phenomenon that results from increased protein deposition and crosslinking [45]. Increases in matrix mechanics usually accompany aging, injury, and disease states,

including cancer and artherosclerosis [46-50]. Matrix stiffening has classically been considered an outcome of disease, but was recently identified as a primary contributor to disease progression in numerous studies [51-54]. In cancer metastasis specifically, cell proliferation and migration are enhanced due to stiffer matrix properties [55, 56]. Deciphering the spatiotemporal response to matrix mechanics could lead to better treatments for these diseases; however, a dearth of culture systems exist to evaluate these interactions.

3.2.3 Dynamic Culture Systems for *In Situ* Studies

Stimuli-responsive culture systems are required to recapitulate dynamic cell-matrix interactions *in vitro*. Hydrogels that react to biomolecular cues, such as protease sensitive polymers, are valuable for translational studies; however, user-defined triggers are preferred to evaluate cellular responses to stimuli with high temporal resolution [57-59]. To evaluate cell-matrix interactions, technologies must provide spatiotemporal and independent control of chemical, mechanical, and topographical signals. Despite the potential impact, platforms that are capable of modulating stiffness and/or topography in the presence of cells in real-time are limited. These transitions can be activated via externally applied forces, light, or environmental stimuli such as pH and temperature.

Physical triggers are procedurally simple, and do not require expensive equipment. External forces (e.g. compression) have been applied to soft materials, such as polydimethylsiloxane (PDMS), to create reversible grooves for studying the temporal nature of cell alignment [60, 61]. These studies revealed that stem cell alignment decreased slightly with culture time and at higher cell densities, but the ability of cells to align is generally preserved and reversible for many cycles. PDMS however, is not an ideal substrate for most physiological systems because of its stiffness (~1 MPa), and the

compression only produces pre-defined topographies created via plasma oxidation. To simulate matrix stiffening, Riveline and colleagues inserted a needle beneath the surface of filopodia to stimulate mechanosensing pathways [62]. In a similar study, optically manipulated glass beads also increased focal adhesion expression at cell binding sites when an external force was applied [63]. These were the first studies to successfully evaluate cellular responses to dynamic changes in the apparent stiffness of the surrounding microenvironment, and motivated the development of less invasive platforms.

Hydrogel systems triggered by chemical stimuli have also been evaluated as dynamic culture systems. Collagen-and-alginate-based composite hydrogels stiffen with the introduction of calcium ions due to physical crosslinking between the alginate chains [64]. Mean cell area, a common assessment of cell adhesion, increased during periods of gel stiffening. This effect was negated when calcium chelators, such as citrate, were introduced to soften the matrix. Unfortunately matrix stiffening is not isolated within this system, as calcium is also a signaling molecule that is associated with a multitude of intracellular signaling cascades [65]. Other self-assembling hydrogels that function via DNA and thiol-based chemistries also have been used to simulate matrix stiffening [66, 67]. Each of these approaches however, is hindered by slow reaction kinetics (> 4 hours), increase the crosslinking density, and is irreversible. Many materials also swell or contract in response to pH, as changes to charges within the polymeric network redistribute intra- and intermolecular forces. The Shear Group has studied the response of various protein hydrogels to pH changes extensively, but has not yet applied this work to mammalian cell culture [11]. Yoshikawa *et al*. developed tri-block copolymers that exhibit a 40-fold change in stiffness between a pH transition from 7 - 8 [68]. Projected cell area was tuned using sequential step changes in stiffness; however, possible

contributions from pH, hydrophobic interactions, and porosity cannot be neglected. At present, no established chemically responsive system offers 3D-spatial control on a sub-cellular scale.

Temperature-responsive platforms have been investigated primarily as injectable drug and cell delivery scaffolds. However, interest in dynamic culture systems has propelled the use of thermally responsive polymers, including N-isopropylacylamide and pluronic, to modulate surface topography and mechanical properties [69-72]. Numerous shape memory polymers (SMPs) have also been designed to present topographical changes with temperature transitions [73, 74]. However, SMPs can only cycle through a maximum of four confirmations, and the topography cannot be adjusted after the initial design is established [75]. Most temperature transitions of SMPs are designed to occur between 20°C and 50°C, which is a concern for temperature stimulated transitions because even short deviations from physiological temperatures could induce a stress response in the cells [76]. In addition, improvements are needed to provide spatial and real-time control over substrate properties.

Light-activated systems offer both temporal and spatial control of hydrogel properties. The Anseth Group developed the first photolabile polyethylene glycol (PEG) hydrogel by incorporating nitrobenzyl monomers that degrade when exposed to ultraviolet (UV) or two-photon wavelengths [77]. They demonstrated the ability to dynamically tune the mechanical and topographical features of the hydrogel *in situ* to control cell differentiation, migration, and alignment [78-81]. However, photo-erosion completely destabilizes existing cell-matrix adhesions, preventing the evaluation of adherent cellular responses to dynamic changes on short time scales. A decrease in matrix mechanics is also not as significant of a factor as matrix stiffening in tissue morphogenesis and disease progression. Hydrogels that stiffen with light exposure

usually involve sequential crosslinking steps, such as methacrylated-hyaluronic acid gels used by Burdick and colleagues [82, 83]. Stiffening from 3 to 30 kPa was prompted via additional UV exposure at various time points over 14 days to control the phenotypic populations of MSCs. Noticeable changes in cell area and motility were also reported within 4 hours of stiffening. Other light responsive systems based on synthetic polymers and peptides have potential, but have not been used in the presence of cells [40, 84].

Light-responsive systems are advantageous because they provide spatial control and rapid reaction times. Unfortunately, most of these systems also require toxic photosensitizers and/or induce simultaneous changes to multiple structural and mechanical properties. Overall, these dynamic platforms are beginning to gain traction and results that recreate some aspects of complex cell-matrix interactions *in vitro* are encouraging. A major challenge that still lies ahead is conceiving methods that can decouple many of the material properties known to influence cells. Systems activated using MPE, such as the work presented here, may provide control and resolution necessary to answer lingering questions regarding dynamic cell-matrix interactions.

3.3 MATERIALS AND METHODS

3.3.1 Reagents

Bovine serum albumin (BSA, BAH64) was obtained from Equitech-Bio (Kerrvile, TX), and rose bengal (RB, 33000) was purchased from Sigma Aldrich (St. Louis, MO). To promote cell adhesion gelatin (G2500, Sigma Aldrich) was included in fabrication solutions. Sterile, phosphate buffered saline (PBS, SH3026401) solution was purchased from Thermo Scientific (Waltham, MA). Alexafluor-488 phalloidin (A12381) was purchased from Life Technologies (Carlsbad, CA). Cell culture mediums including Dulbecco's modified eagles medium (DMEM, high glucose, SH30022) and Leibovitz L-

15 (SH30525) were purchased from Fisher Scientific. Mitogenic factors used to maintain SC cultures including bovine pituitary extract (BPE, P1476) and forskolin (F6886) were acquired from Sigma Aldrich. Fetal bovine serum (FBS, SH3008803), bovine calf serum (SH3007203), and trypsin (SH3004201) were purchased from Fisher Scientific. Penicillin streptomycin (PSA, 1507-063, Life Technologies) was used as a general antibiotic in experimental media. Ethanol (04-355-451) used for sterilization was purchased from Fisher Scientific. Type I Collagen (354249, BD Biosciences) was used to coat BSA hydrogels for cell adhesion. All reagents were stored in a manner consistent with the supplier's recommendations.

3.3.2 Fabrication of Protein Hydrogels

The instrumentation used to fabricate protein hydrogels is depicted in **Figure 1.2**, and the digital micromirror devide (DMD)-directed multiphoton lithography (MPL) technique has been described in **Chapter 1** and other previously published work [9, 85-88]. Briefly, a mode-locked Ti:S oscillator (Coherent, Mira 900F) was pumped by a 532-nm frequency doubled diode laser (Coherent, Verdi, 10 W). The output wavelength was tuned to 740 nm and directed through a sequence of optics into the back aperture of a microscope objective (40X/1.3 NA, Zeiss Fluar). A half-wave plate and polarizing beamsplitter were used to attenuate the laser power manually so that the average laser power measured at the back aperture of the objective was between 18 - 22 mW. A dual-axis, galvanometer-driven scan mirror obtained from a dismantled confocal microscope (Leica, TCS-4D) was used to raster-scan the laser beam at user defined waveforms, frequencies, and amplitudes. For large structure fabrication, the scan mirror was set to scan only in a single axis (the fast axis), and an automated stage (model 562, Newport Corporation) was used to translate the sample relative to the focal plane in the orthogonal

axis at a velocity of 20 μm/s [89]. Prior to reaching the objective, the beam was focused on the face of a DMD (BenQ, MP510) with individually addressable mirrors located in a plane conjugate to the focal plane of the objective. By displaying a binary digital photomask, the mirrors were positioned to reflect the beam toward or away from the objective. Binary images were created in Photoshop (Adobe, San Jose, CA), ImageJ (National Institutes of Health, Bethesda, MD), and PowerPoint (Microsoft Corporation, Santa Rosa, CA). The beam was re-collimated using a tube lens and reflected into the objective on a Zeiss Axiovert 135 microscope via a dichroic mirror.

Protein hydrogels were crosslinked to No. 1 coverslips (Fisher Scientific) or No. 1.5 welled-coverslips (Fisher Scientific) for cell experiments. A fabrication solution of 400 mg/mL BSA and 10 mM RB was used to fabricate BSA hydrogels. For some studies, specifically when cell adhesion was desired, a fabrication solution composed of 300 mg/mL BSA, 100 mg/mL gelatin, and 15 mM RB was used. The beam was focused into the fabrication solution and raster-scanned to crosslink protein layers. 3D features were created using a layer-by-layer approach, synchronizing the presentation of digital masks with incremental stage translation in the optical axis. All communication between equipment was coordinated using Labview software (National Instruments, Austin, TX). Axial step sizes were set between 1.0 – 1.5 μm for all structures. Residual fabrication solution was removed using a series of PBS washes, elevated temperatures (50°C) were used for gelatin removal, and hydrogels were stored in PBS at room temperature.

3.3.3 Laser Shrinking

After rinsing, protein hydrogels were re-scanned with the laser beam used for fabrication. The average laser power used for laser shrinking was 22 mW, measured at the back aperture of the objective, unless otherwise stated. The initial scan plane was

manually focused on the base of the hydrogel then scanned layer-by-layer through the entire height of the structure. Axial step sizes of 1 μm were used for all scans. This procedure was repeated up to 4 times to maximize the extent of contraction. An alternative protocol was used for matrix stiffening, where the initial scan plane was established relative to the base by translating the automatic stage a user-defined axial distance. The hydrogels were scanned up to 4 times in a single plane at a stage velocity of 20 μm/s. The stage was then translated an additional distance of 1 μm axially, and the laser scanning procedure was repeated. Independent of the protocol used, shrinking of a single hydrogel required less than 10 minutes to complete. When stated, the hydrogels were photobleached using a 30 minute exposure to the "full" output of a tungsten-halogen arc lamp reflected onto the sample via a 99/1 mirror.

3.3.4 Atomic Force Microscopy

An atomic force microscope (AFM, MFP-3D-BIO, Asylum Research) was used to acquire all force curves and topographical images. Protein hydrogels were submerged in PBS for the duration of data acquisition. For modulus measurements, a gold-coated cantilever (silicon, k = 3.8 N/m, PT.GS.AU, Novascan) with an attached 10-μm-diameter borosilicate bead was used to generate deflection versus displacement curves. Matlab was used to automate the data analysis, except for the selection of the contact point. The program implemented a while loop to fit the Hertz model to the experimental data until a maximum R-squared value was obtained. A 5% strain limitation was imposed, equivalent to an indentation depth of approximately 300 nm. Height values were obtained by taking the difference between the z-position of hydrogel contact and an adjacent glass measurement. All hydrogels measured were taller than 7 μm, the experimentally determined value to avoid sensing the underlying substrate, unless otherwise noted.

Topographical images were acquired in 'contact mode' using a triangular-shaped cantilever (silicon nitride, k = .17 N/m, MSCT, Veeco) with a pyramidal tip (2.5 – 8 μm tall, 40-nm-radius). A setpoint between 0.3 – 0.5 deflection volts was used to maintain contact. Imaging frequency (0.20 – 0.5 Hz), scan area, and pixel resolution were optimized for each sample. The z-position channel was saved as a tab-delimited text file, and then imported into Matlab to generate surface plots.

3.3.5 Cell studies

NIH-3T3 fibroblasts (CRL-1658) and Schwann cells (SCs, S16, CRL-2941) harvested from rat sciatic nerve were purchased from the American Type Culture Collection (ATCC). Fibroblasts were cultured in high glucose, DMEM with 10% (v/v) BCS. SCs were maintained using previously published protocols [90]. In brief, SCs were kept in DMEM, high glucose media containing 10% (v/v) FBS, 2 μM forskolin, and 30 μM BPE. Cells were passaged using 0.25% trypsin (1X) every 4 – 7 days. A phosphate buffered experimental media (L-15, 1% serum, 1% PSA) was used during time-lapse image acquisition. The environmental chamber is described in detail in **section 2.5.7**. All hydrogels were sterilized using a 30 second exposure to ethanol. For BSA hydrogels, a collagen coating was applied to promote cell adhesion. Collagen was diluted to a concentration of 0.1 mg/mL in a 30% ethanol solution, and incubated a minimum of 4 hours at room temperature. Cells were incubated between 30 minutes and 4 hours after plating to allow for cell adhesion prior to imprinting. Care was taken to minimize ambient light exposure and time outside of an incubator during scanning. Cells were then placed back in the environmental chamber for continued time-lapse acquisition.

3.4 RESULTS AND DISCUSSION

Protein hydrogels can be μ-3DP to exhibit desirable chemical and mechanical properties for cell culture by altering the protein composition or fabrication parameters. Many protein and polymer hydrogels have been made using MPL to create dense hydrogel networks with preserved biological activity [9, 11, 91]. Biotinylated proteins or the benzophenone-biotin immobilization described in **Chapter 2** can also be used to tailor the chemical presentation of the hydrogels [10]. In addition to hydrogel composition, fabrication solution concentrations (protein and photosensitizer), fabrication laser power, and objective selection are some that can be used to tune the hydrogel modulus during fabrication. Ranges of moduli from 1 kPa to 1 MPa for protein hydrogels have been reported [89, 92]. Here, protein hydrogels used to demonstrate topographical manipulation, matrix stiffening, and modulus studies (**sections 3.4.1, 3.4.4 – 3.4.6**) are composed of BSA. For cell studies, BSA/gelatin composite hydrogels are used to promote cell adhesion (**sections 3.4.2 – 3.4.3**). The nominal stiffness of these hydrogels ranges from 7 – 15 kPa. Additional tuning of protein composition or hydrogel modulus was not within the scope of this proof-of-concept study.

3.4.1 Laser-Induced Shrinking

In this section, protein hydrogels are manipulated post-fabrication using an MPE-based approach. The same laser source used for fabrication is focused within the hydrogel after fabrication and rinsing to promote localized excitation of residual photosensitizer. Rose bengal is retained with the protein hydrogel because it partitions within hydrophobic pockets of the BSA and can be trapped within the densely crosslinked matrix via intermolecular interactions. The photosensitizer forms highly reactive, singlet oxygen species that further crosslink the protein matrix, leading to matrix contraction. The contraction can be uniformly distributed throughout the matrix or spatially confined

using dynamic masking to imprint sub-cellular surface topographies, as shown in **Figure 3.1**. Gradient photomasks are also displayed on a DMD to modulate the laser fluence for imprinting multifaceted, 3D topographies as shown in **Figure 3.1D**. In **Figure 3.1C**, a nearly five-fold reduction in hydrogel volume is achieved when the laser is scanned through the entire hydrogel. Reducing the crosslinking during fabrication or maximizing the laser power and number of laser scan repetitions used for imprinting can further increase the extent of contraction.

In **Figure 3.2,** the creation, then elimination, and finally reversal of a feature is achieved using sequential laser scans. First, a flat BSA pad was fabricated to have a nominal height of 10 μm. For the initial imprint, a digital photomask of a 40 x 40 μm white square with a centered 20 x 20 μm black square overlay is used to form a 2-μm tall elevation. This elevation is subsequently reduced to a few hundred nanometers by imprinting while displaying the inverse of the initial photomask. Further imprinting using the same photomask resulted in the creation of an approximately 1-μm depression. This strategy of creating and eliminating features could be useful for studying cell cycling between grooved and flat substrates. Although hydrogels are stable for months in buffer, future studies should assess how storage might impact the shrinking potential of hydrogels after many days in cell culture. Further exploration of fabrication parameters, photosensitizer loading, and shrinking methods are also needed to optimize the effects of laser shrinking.
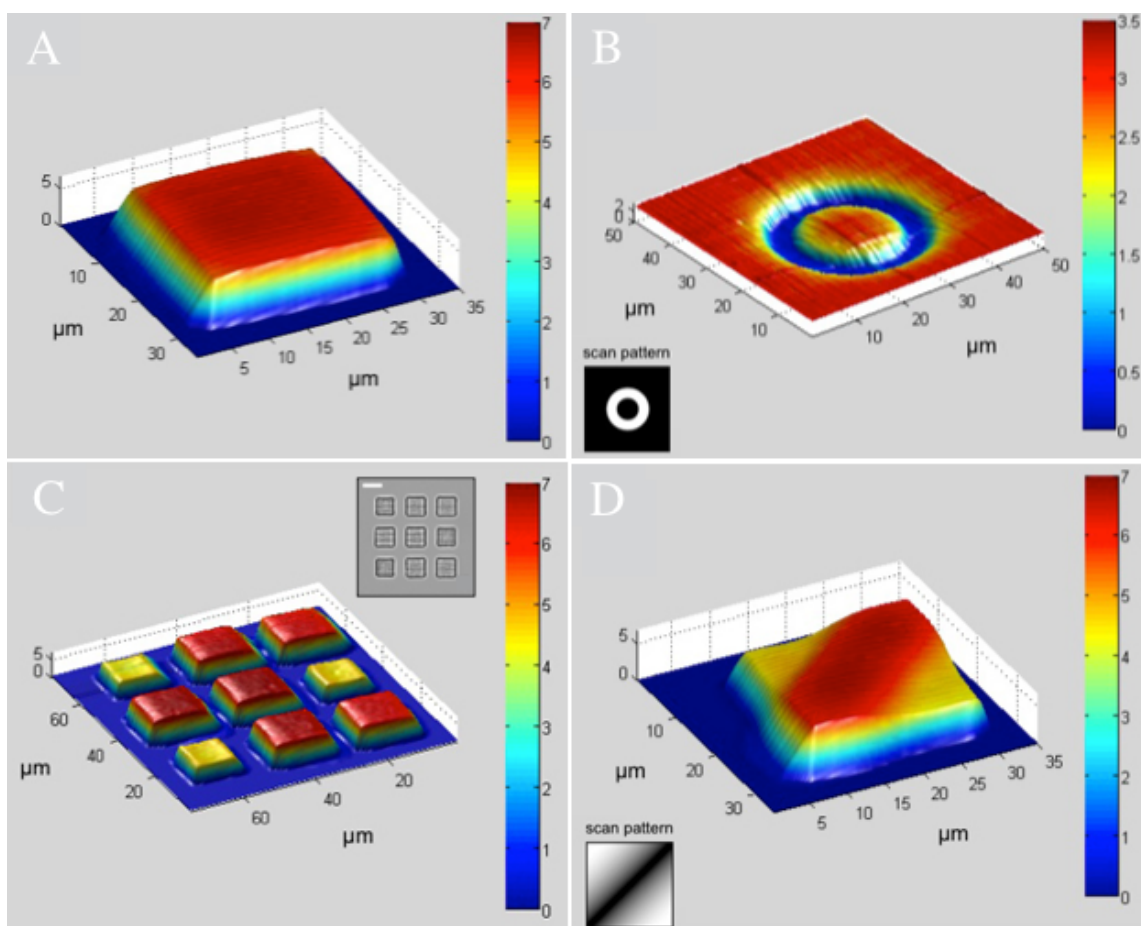
Figure 3.1: AFM surface representations of imprinted protein substrates. A) An unmodified protein pad. B) An "island" imprinted on the pad by scanning an annular binary mask (inset) through the entirety of the structure. C) A 3 x 3 array of protein pads that were originally fabricated to stand 7-μm-tall. Three of the structures were uniformly imprinted to reduce the volume five-fold. A brightfield image of the array is provided in the inset (scale bar = 10 μm). D) A grayscale gradient mask (inset) was used to imprint an originally flat pad (as in A) to create a complex topography with rounded edges. All axes, including the colorbars, are in units of μm.
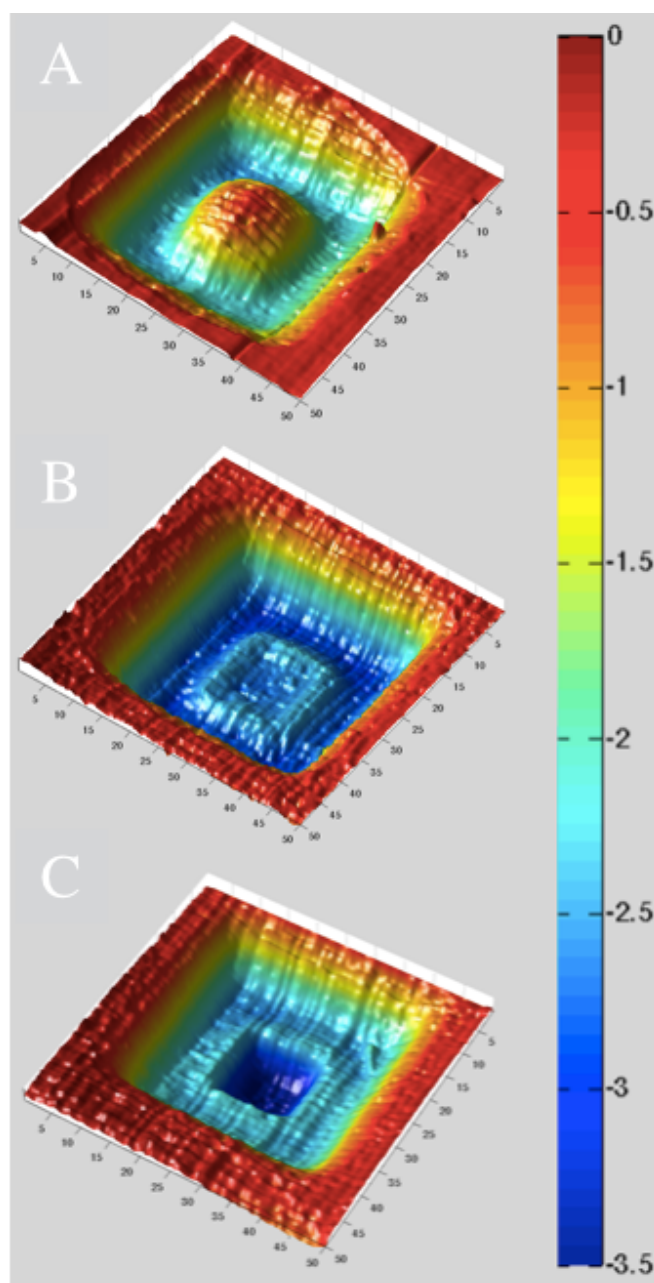
Figure 3.2: Sequential feature creation and subtraction. (A – C) AFM surface representations of protein pads that were originally flat. A) A 2-μm-tall elevation is first created by imprinting a hollowed square. B) The elevation is nearly eliminated after a secondary laser scan where the inverse photomask from (A) was displayed. C) The central elevation was scanned further to create a depression where the elevation first stood. The figure shows three separate structures. The scan dimensions for the figures are 50 x 50 μm, and the colorbar is in units of μm.

3.4.2 Effect of Laser Shrinking on Elastic Modulus

Dynamic topographical modifications must be created without altering the surface chemistry or modulus in order to decouple the effects of these cues. A major advantage of laser shrinking is that the surface is not exposed; therefore, the original chemical presentation of the surface is maintained. To evaluate the effect of shrinking on the modulus of the gelatin/BSA hydrogels, structures were uniformly imprinted beginning at the base of the hydrogel and stepped axially (1-μm-increments) through heights ranging from 20 - 75% of the nominal height. The scanning procedure was repeated a total of four times. The microscale compressive modulus was measured using an AFM, and relative comparisons were made between scanned structures and un-scanned controls.

Topographies can be created without perturbing the apparent modulus of the protein hydrogel, shown in **Figure 3.3**, when scan planes are maintained below 50% of the nominal height. This percentage equates to a distance from the surface of approximately 5 μm. Similar results are obtained for BSA hydrogels and are presented in **section 3.4.4**. In stark contrast to BSA hydrogels, the modulus of BSA/gelatin composite hydrogels decreases as planes approaching the hydrogel surface are scanned. This apparent softening could be due to the crosslinking of residual pre-fabrication solution trapped within the hydrogel. The photosensitizer retained within the matrix is considerably lower for BSA/gelatin composites after rinsing than in BSA hydrogels, a condition that could produce a less stiff matrix than the original fabrication. Another possibility is that bonds are being broken rather than formed during laser shrinking, degrading the gelatin.

How AFM modulus measurements relate to cellular mechanosensing is unclear. It is generally accepted that cells can detect stiffness variations at depths approximately equal to their radius, although depths up to 100 μm have also been reported [93-97].

106

Reported differences for critical thickness most likely depend on the behavior and cell phenotype being evaluated, as well as the mechanical properties of the gel [98]. Engler and colleagues monitored smooth muscle cell spreading on thin films of polyacrylamide with thicknesses and moduli ranging from 5 – 70 μm and 1 – 8 kPa, respectively. No changes in cell morphology were observed at any gel thickness, even on the softest gels [99]. These results suggest that imprinting can be achieved without triggering additional mechanotransduction pathways, as long as sufficient distances from the surface are maintained during scanning.
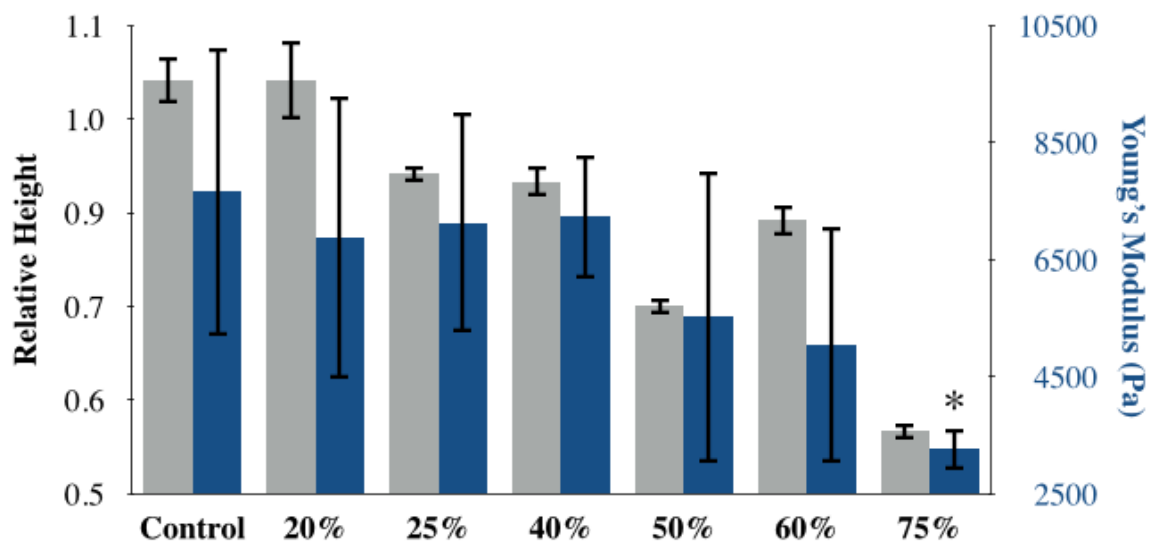
Figure 3.3: Effect of imprinting on Young's modulus of gelatin/BSA protein hydrogels. The relative height (gray bars, left axis) measured as the final/initial height is displayed to show hydrogel contraction is achieved. The corresponding average Young's modulus (blue bars, right axis) of a minimum of 3 hydrogel is also plotted. The x-axis represents the percentage of the nominal height where the laser was scanned during imprinting. The error bars represent standard deviations (+/-) of the measured structure height and modulus (* - p value < 0.05 with respect to all other groups).

3.4.3 *In Situ* Imprinting

One application for this technology is studying cellular responses to dynamic changes in substrate topography. Since laser shrinking is conducted below the surface, substrates can be imprinted directly under adherent cells as shown in **Figure 3.4** and **Figure 3.5**. This technique also allows for feature localization relative to the position of an adherent cell, unlike SMPs that have predefined features. Topographical manipulations are rapid, requiring only minutes to complete. Although there is a possibility for oxidative damage due to singlet oxygen generation from rose bengal, the adherent cells remain vital and motile for many hours after imprinting.

In **Figure 3.4**, a protein hydrogel is imprinted within 30 minutes of plating fibroblasts and before the cell of interest flattened on the substrate. The cell is recessed into a 2-μm-deep, 10-μm-wide divot located in the center of an elevated "island," that was also created via laser shrinking. The depth of the "island" is 4 μm larger because the entire height of the hydrogel was scanned. Caution is taken to avoid scanning the laser beam directly through the cell by remaining a minimum of 3 μm below the nominal pad height. The cell interacts with the features and remains motile for 12 hours after imprinting, the maximum observation time. No specific or adverse effects on the cells from the imprinted features are qualitatively observed.

In **Figure 3.5**, spirals are imprinted beneath the lamellipodium of two SCs that are adhered to a collagen coated, BSA hydrogel. Both cells extend filopodia into the patterns, and eventually migrate in the direction of the imprinted features. Other feature architectures that were generated *in situ* are shown in **Figure 3.6**. Attempts have not been made to quantify the effects of dynamic topographical presentation on cell behaviors. Studies to evaluate cell alignment in response to evolving spatial cues at defined

timepoints are ongoing. In the future, sub-cellular features can be imprinted to study intracellular signaling mechanisms and focal adhesion dynamics of adherent cells.
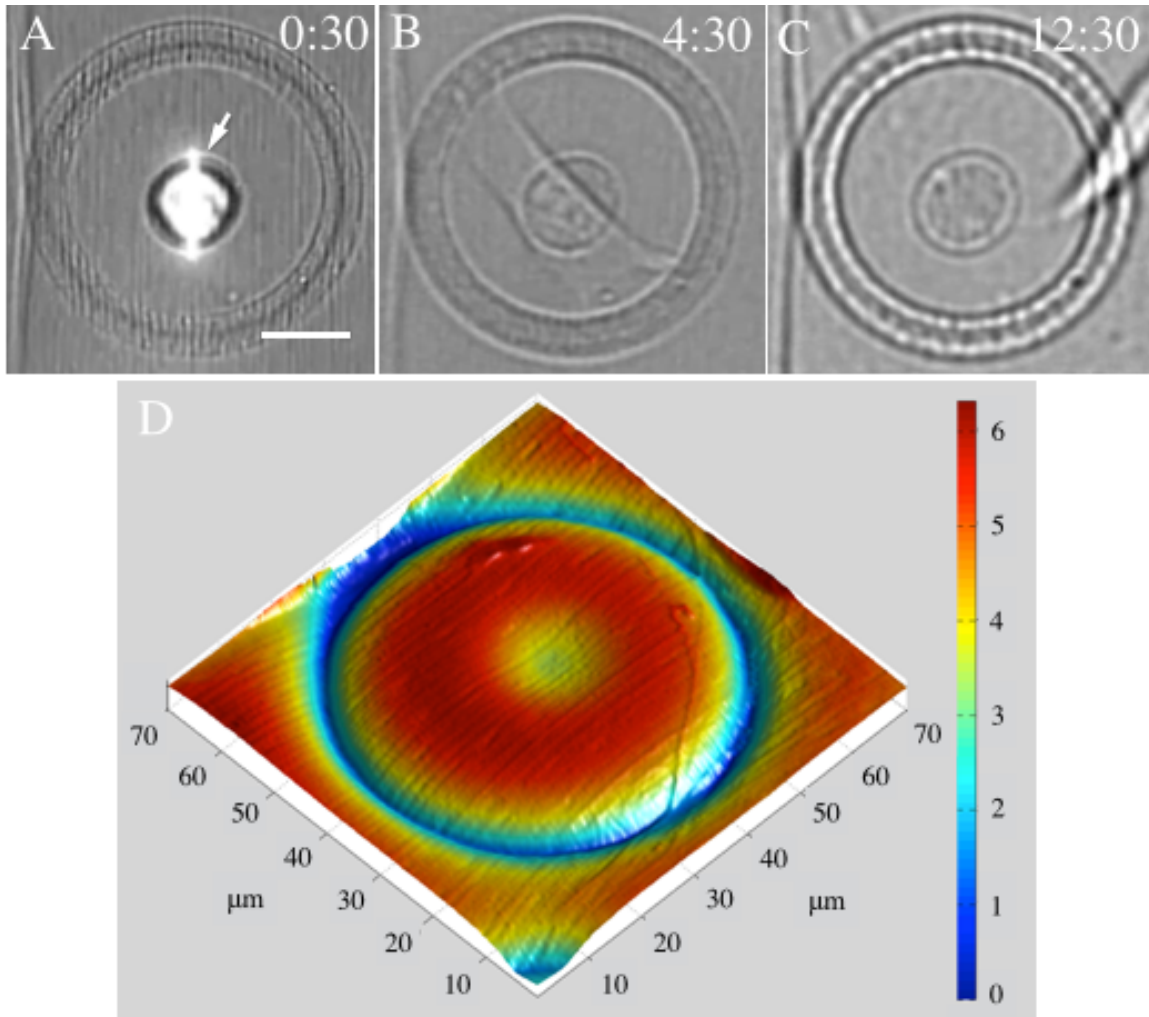
Figure 3.4: Imprinting a BSA/gelatin hydrogel beneath an adherent fibroblast. A) Brightfield image acquired during imprinting procedure. A fibroblast is isolated on an "island" and recessed using laser shrinking 30 min after plating (scale bar = 10 µm). The cell is adherent but is not flattened. The bright line denoted by the white arrow is the reflection of the laser beam. (B - C) Time-lapse acquisition of the cell after hydrogel imprinting. Time stamps, in hours, are located at the top right of each image. The cell flattens and interacts with the imprinted features, as shown in (B). After 12.5 hours, the cell migrates away from the features as shown in (C). D) Topographical map of the imprinted hydrogel acquired using AFM after fixing the sample with formaldehyde. The "island" height is 6 µm, and the centralized divot is approximately 3-µm-deep. Colorbar scale is in units of µm.

111
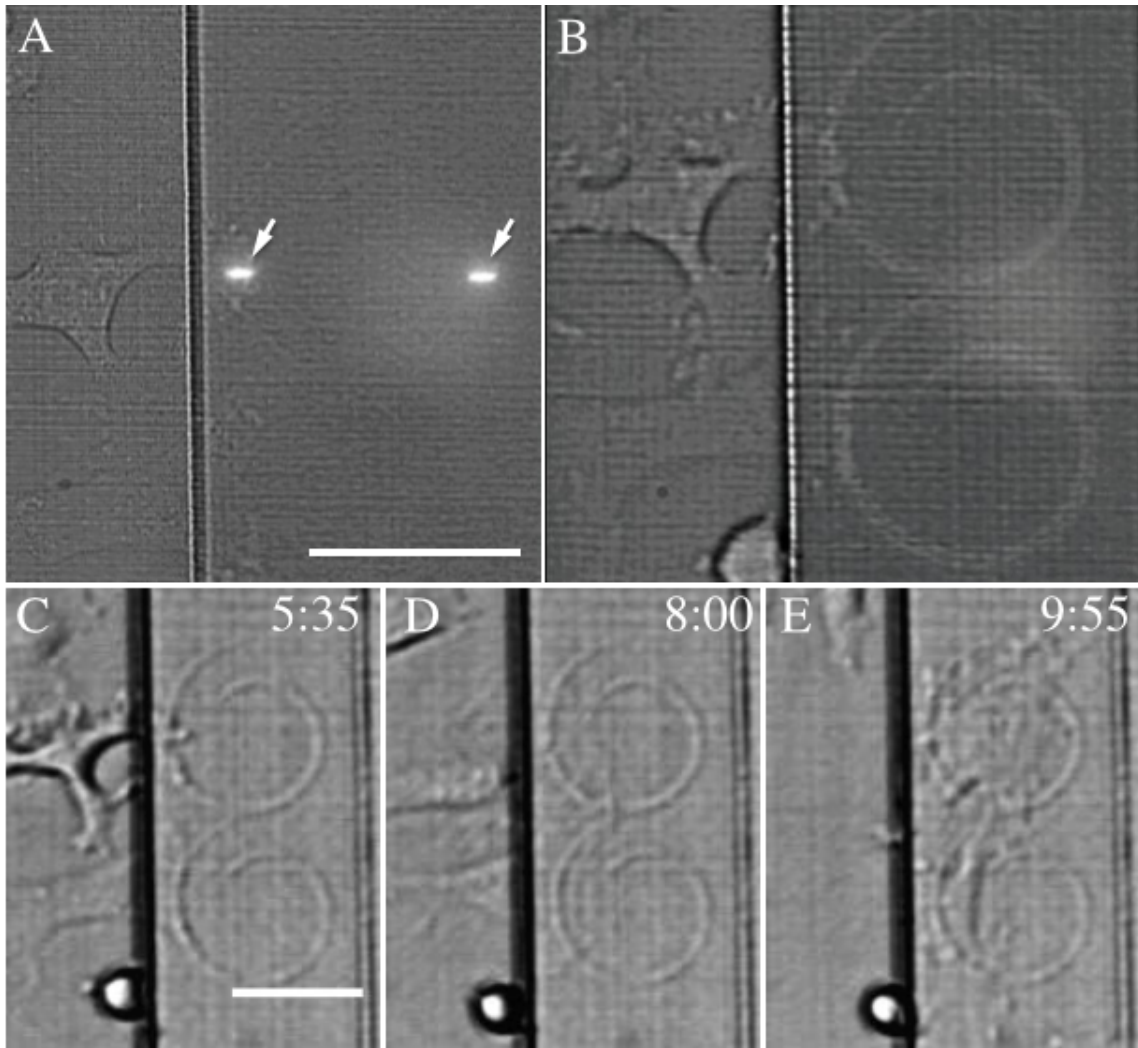
Figure 3.5: Imprinting beneath adherent SCs. A) A brightfield image captured during imprinting, conducted after cells adhered to collagen coated, BSA hydrogels (~4.5 hours after initially plating the cells). The lamellipodia of the SCs are specifically targeted with this scan. The reflection of the laser beam, denoted by white arrows, is displayed to show the beam position directly below the cell. B) A brightfield image of the resultant structure after the conclusion of the imprinting process. Two spirals are imprinted to target adjacent cells. (C – E) Time-lapse of the cells was after imprinting. Time stamps, in hours, are displayed at the top right of each frame. C) Shortly after imprinting, SC filopodia are observed extending into the spiral features. E) The SCs migrate onto the imprinted spirals ~ 5 hours after imprinting. Scale bars = 50 µm.
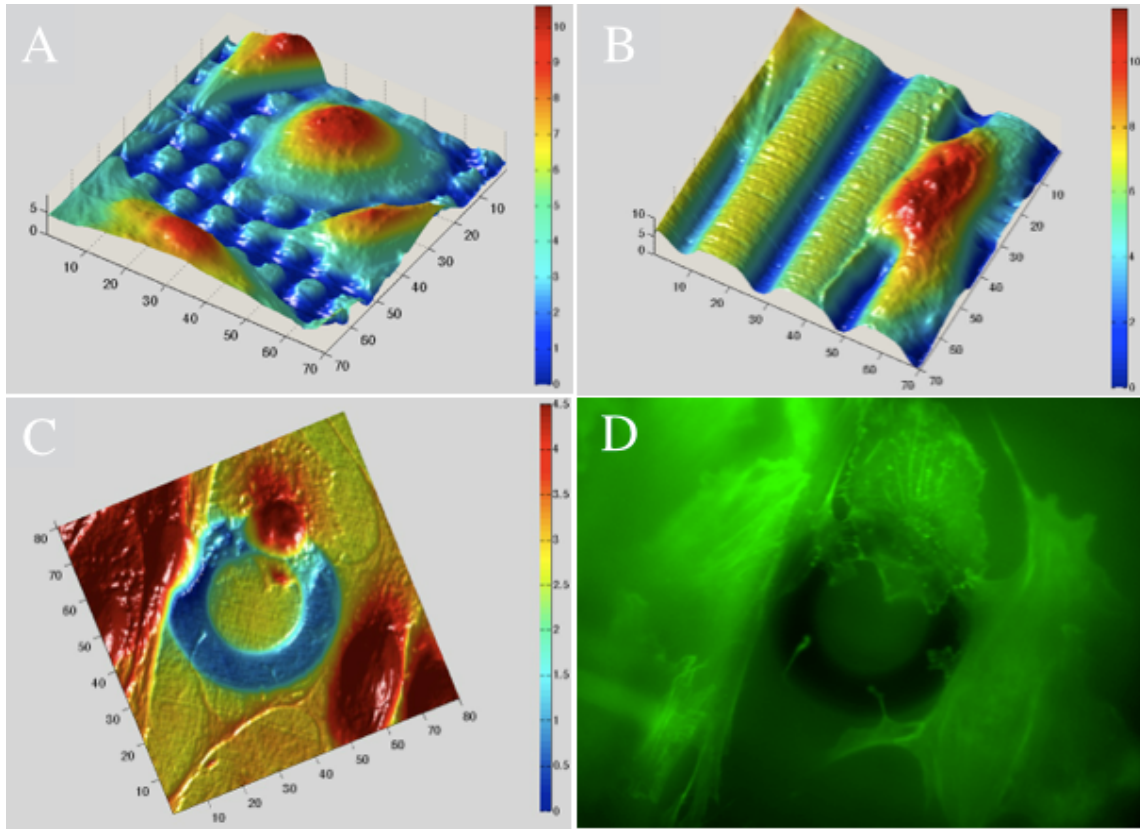
Figure 3.6: Surface representations of cells on gelatin/BSA hydrogels with imprinted features. Numerous features are imprinted below cells; micropost arrays (A), grooves (B), and an annulus (C). All axes are in units of μm, including the colorbars. D) Fluorescence image that corresponds to the image area in (C). Cells were stained with Alexa fluor 488 phalloidin, and imaged using a fluorescein filter set.

3.4.4 Tuning the Elastic Modulus

Matrix stiffening is a common pathological trait associated with tumor development and artherosclerosis [100]. Whether a stiffer matrix is an outcome or cause of disease is still contested, as few technologies exist to study dynamic effects of matrix stiffening on cell behavior. In addition, currently outfitted technologies cannot decouple the effects of changes in modulus from other structural or chemical stimuli. To demonstrate that the hydrogel modulus is tunable via laser shrinking, BSA hydrogels were fabricated to a nominal height of 14 μm. Laser shrinking was conducted through a 3-μm-axial-section of the hydrogel. A single plane was laser scanned 4 times, and then the focal plane was axially stepped 1 μm toward the surface prior to repeating the laser scan. The initial scan plane was set at defined distances from the base of the hydrogel using a motorized stage.

When planes closer to the hydrogel surface are scanned with the laser, the apparent modulus of the hydrogels increases up to five-fold as shown in **Figure 3.7**. The larger standard deviation observed at higher stiffness is a product of the probe limitations and quality of the Hertz model fit (decreased r-squared values). For AFM measurements, it is important to match the probe spring constant with the matrix mechanics. Here, relative values are desired; therefore, the same probe and conditions are used to acquire all force curves. The apparent hydrogel modulus is only affected when scanning within a 4-μm-distance from the surface, similar to the results obtained in **section 3.4.2** with BSA/gelatin composite hydrogels. Alternative laser scanning protocols may expand the range of or provide finer control over the apparent modulus. For these studies specifically, the surface of the structure is not always avoided during the laser scan.

Furthermore, the reduction in height is consistent regardless of the position of the initial scan plane as shown in **Figure 3.7B**. Since indistinguishable topographies can be

114

created with dramatically different moduli, this will provide a means to study the interplay of topography and stiffness in a more serial, systematic fashion. Few studies have assessed the effects of these two properties independently, and the majority of substrates have moduli outside of physiologically relevant ranges [100-104]. Collectively, these examples suggest stiffer matrices promote cell alignment and migration: however, only a limited number of parameters and cell types have been evaluated.

The absolute range of modulus demonstrated in these studies is theoretically tunable using a plethora of available parameters. Hydrogel composition, fabrication solution concentrations (protein and photosensitizer), fabrication laser power, and objective selection are some options for tuning the resultant hydrogel modulus during fabrication [89]. Post-fabrication modifications such as photobleaching or solution pH can also have profound effects on the swelling properties and modulus of the hydrogels [92, 105]. Here, the impact of photobleaching on the elastic modulus of hydrogels is evaluated. When stated, BSA hydrogels were laser reduced prior to photobleaching by scanning through the entire height of the structure. Photobleaching was performed using a 30 minute exposure to the "full" output of a halogen arc lamp. A nearly 30% increase in the height is measured for control structures after photobleaching, which corresponds to a 50% reduction in the modulus as shown in **Figure 3.8**. Hydrogels that are laser scanned prior to photobleaching were more resistant to swelling, and additional scans enhanced this effect. Photobleaching also mitigates the matrix stiffening effect of laser shrinking, reducing the achievable range to 12 – 58 kPa from 15 – 90 kPa. Other options should be explored to target lower modulus regimes for neuronal and tumorigenic cell studies, as the ranges demonstrated here apply to myocytes and fibroblasts. Ultimately, significant stiffening of BSA hydrogels can be accomplished via laser-induced shrinking.
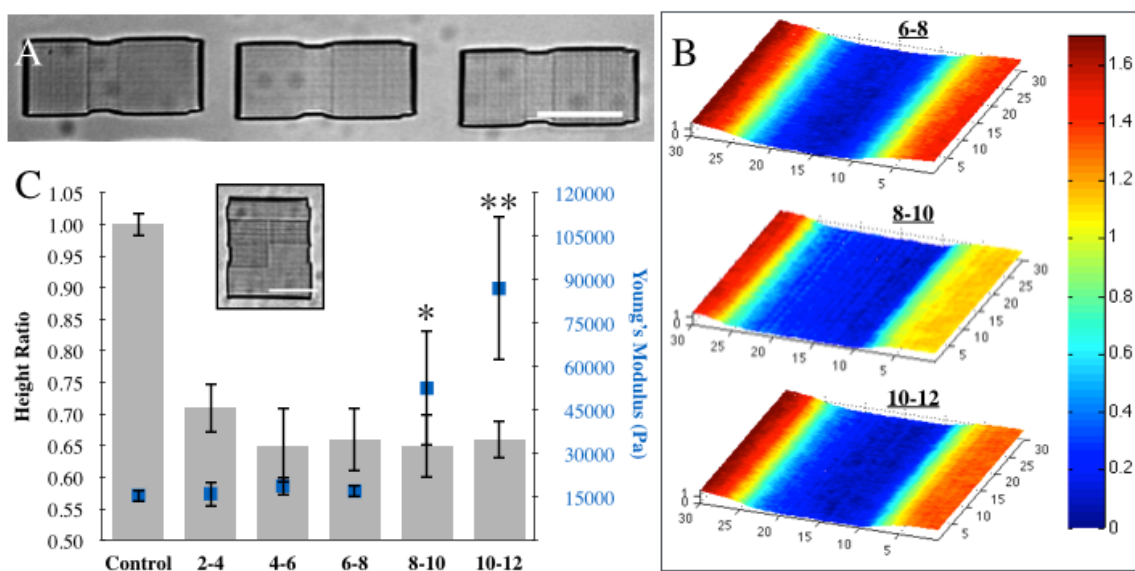
Figure 3.7: Tuning the modulus independent of topography. A) A brightfield image of BSA pads (14 μm-tall nominally) with a 20 μm contracted region near the center (scale bar = 50 μm). The structures are indistinguishable, but are created by scanning different optical planes within the structure (left: 6 - 8 μm, middle: 8 – 10 μm, right: 10 – 12 μm). B) Surface representation acquired using an AFM of each structure in the image to show that the surfaces are indistinguishable. All axes are in units of μm. C) Three regions are imprinted on a single BSA pad by scanning the laser through different optical planes (inset image). The plot displays the height ratio (scanned height/non-scanned height) represented by the gray bars and the apparent Young's modulus (blue dots) of each region. Data for a minimum of three separate regions were acquired and averaged per point. All scans resulted in nearly the same degree of contraction, but the apparent modulus increased significantly as the surface was approached (* - p-value < 0.05 when measured against the control, ** - p-value < 0.05 when measured against the 8 – 10 μm data set). The error bars represent the standard deviation (+/-).

116
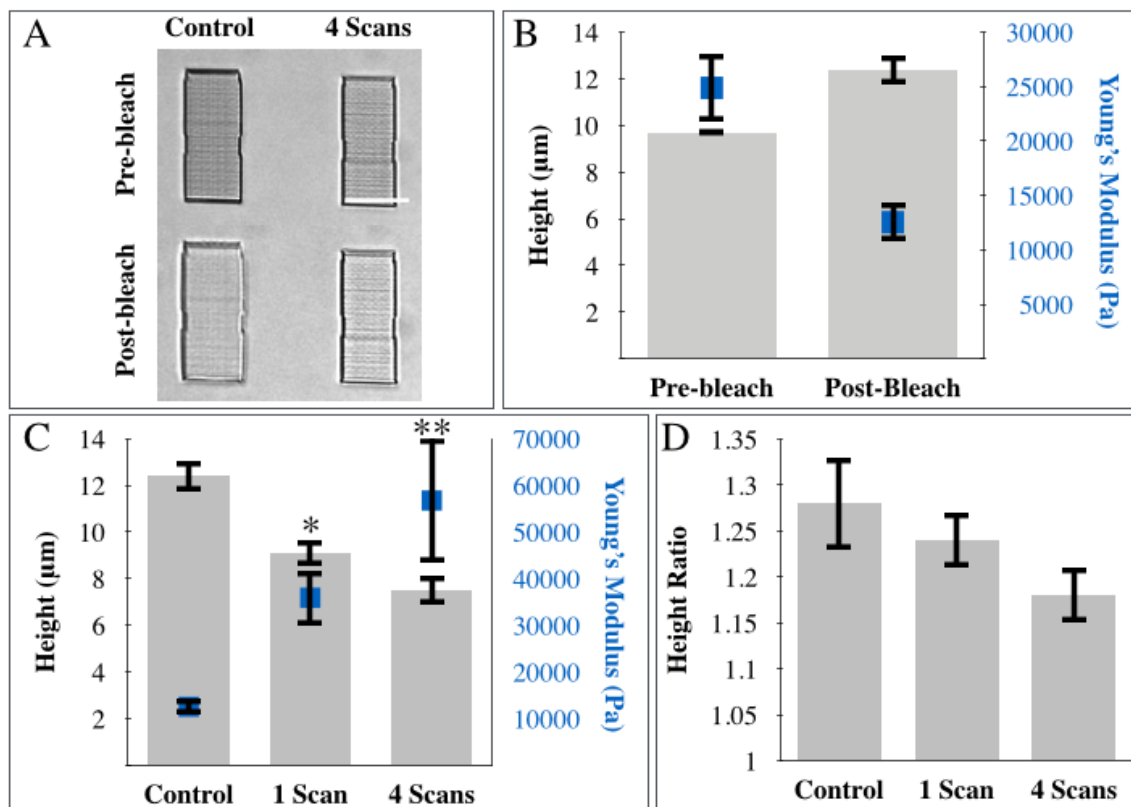
Figure 3.8: Effects of photobleaching on the modulus and swelling properties of BSA hydrogels. A) Brightfield image showing control and laser scanned structures before and after photobleaching (scale bar = 50 μm). B) A plot of the height (gray bars) and modulus (blue dots) of control structures before and after photobleaching. All values are significant (p-value < 0.05). C) Plot of the height (gray bars) and modulus (blue dots) measured after photobleaching of control and laser scanned hydrogels. The hydrogels laser scanned prior to photobleaching using either a single scan or 4 scans are stiffer than unscanned controls. All values are significantly different (n = 3; * - p-value < 0.05 when measured against the control, ** - p-value < 0.05 when measured against the single scan data set). D) The height ratio (height after photobleaching/height prior to photobleaching) as a result of photobleaching is reduced when laser shrinking was used to increase the crosslinking density. Height measurements were acquired before and after photobleaching. No values are statistically significant (n = 3).

117

3.4.5 Stiffness Gradients

Gradients of matrix stiffness promote cell migration and polarization through a process known as durotaxis. The majority of studies generate gradients by varying the crosslinking density of polyacrylamide hydrogels [106-108]. Gradient strengths of 1 and 10 Pa/μm represent physiological and pathological conditions, respectively [106]. Here, variable power laser shrinking is used to generate stiffness gradients. The average laser power is modulated at set frequencies with a Pockels cell to control the extent of contraction. The input frequency is adjusted such that the entire power range (3 – 22 mW) is spanned over a 200-μm distance, the length of the BSA hydrogels. The matrix was stiffened from 10 – 60 kPa as shown in **Figure 3.9**, equivalent to a gradient strength of 333 Pa/μm. Laser powers less than 9 mW did not produce significant changes to the hydrogel modulus. The input to the Pockels cell is adjustable, such that the gradient strength and absolute range can be controlled as shown in **Chapter 2**. If gradients are generated without scanning through the surface of the hydrogel, the effects of the stiffness gradient can be decoupled from other chemical and structural cues; which offers this technique a distinct advantage over polyacrylamide hydrogels.
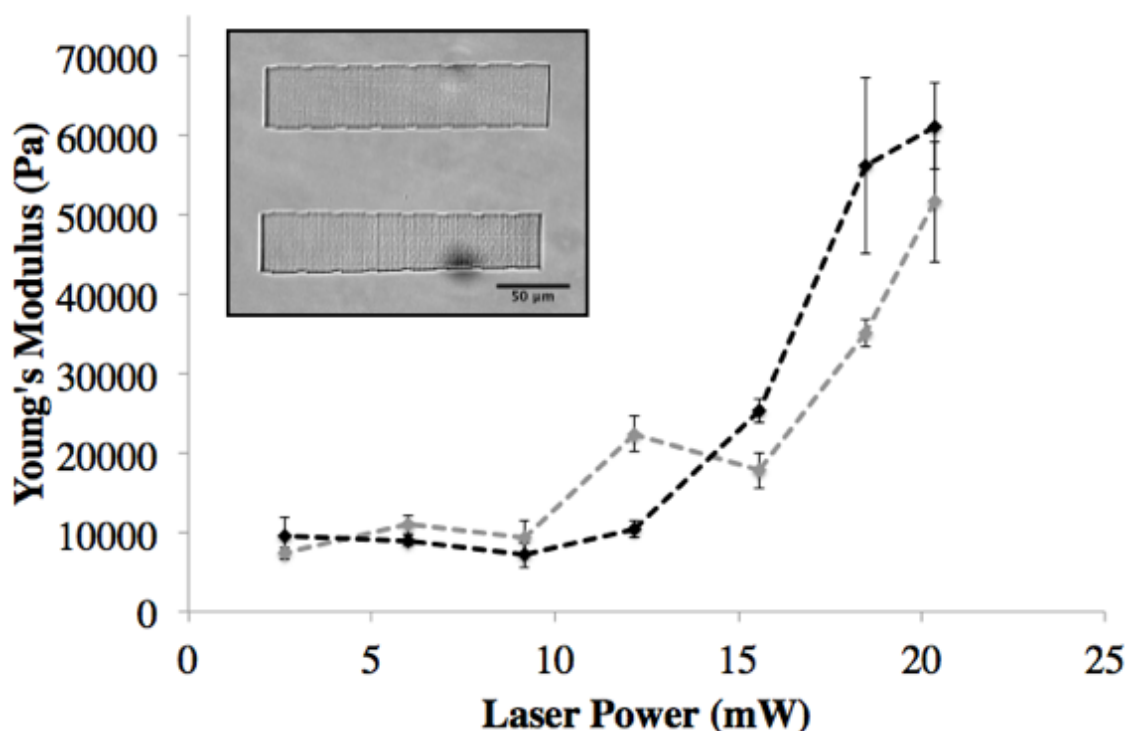
Figure 3.9: Modulus gradients created using variable power laser shrinking. Inset) BSA pads are fabricated using a consistent protocol. A control (top) and gradient (bottom) structure are shown in the inset image. The power used for laser shrinking increased from left to right for the gradient structure, noticeable by the reduction in area. Plot) A Pockels cell is used to modulate the laser power during laser shrinking over a 200-μm-distance. The entirety of the structure is laser scanned using 1-μm-axial-steps. The shrinking protocol is repeated two (gray) or four (black) times to achieve a six-fold increase in the elastic modulus. To generate the plot, force curves were acquired at notch positions spaced 25 μm apart along the long axis. Four curves were acquired at each position and averaged. The error bars represent the standard deviation (+/-) of four force curves taken at a single position on the hydrogel. The phase input to the Pockels cell was adjusted to represent each notch position for back aperture power estimates. Control structures had an average modulus of 12.7 kPa (standard deviation = 1.8 kPa).

3.5 CONCLUSIONS

This chapter introduces a novel, photolithographic method to dynamically tune the topographical and mechanical presentation of protein hydrogels. The effect of laser shrinking on the structural and mechanical properties is characterized to demonstrate that surface topography and stiffness can be manipulated independently, allowing for decoupled analyses. Furthermore, proof-of-concept studies show that dynamic, spatiotemporal modifications made in the presence of adherent cells do not cause cell death.

Future studies are needed to optimize hydrogel shrinking through a series of studies assessing the effects of fabrication and post-fabrication conditions. Additionally, efforts should be made to evaluate the responses of cells to spatiotemporal changes in their microenvironment. Some behaviors of interest are polarization, migration, and mechanotransduction signaling cascades, as these relate to embryonic development and disease progression. In addition to planar surfaces, the Shear Group has recently demonstrated that mammalian cells can be trapped within 3D protein hydrogels [109]. Combining cell trapping with laser shrinking could offer an easy and powerful approach for single cell analysis.

3.6 REFERENCES

1.   Curtis, A. and C. Wilkinson, *Topographical control of cells*. Biomaterials, 1997. **18**(24): p. 1573-83.

2.   Wells, R.G., *The role of matrix stiffness in regulating cell behavior*. Hepatology, 2008. **47**(4): p. 1394-400.

3.   Jaalouk, D.E. and J. Lammerding, *Mechanotransduction gone awry*. Nature Reviews Molecular Cell Biology, 2009. **10**(1): p. 63-73.

4.   Ingber, D.E., *Cellular mechanotransduction: putting all the pieces together again*. FASEB Journal, 2006. **20**(7): p. 811-827.

5.   Chen, C.S., J. Tan, and J. Tien, *Mechanotransduction at cell-matrix and cell-cell contacts*. Annual Review Biomedical Engineering, 2004. **6**: p. 275-302.

6.   Burdick, J.A. and W.L. Murphy, *Moving from static to dynamic complexity in hydrogel design*. Nature Communications, 2012. **3**: p. 1269.

7.   Lu, P., et al., *Extracellular matrix degradation and remodeling in development and disease*. Cold Spring Harbor Perspectives in Biology, 2011. **3**(12).

8.   Larsen, M., et al., *The matrix reorganized: extracellular matrix remodeling and integrin signaling*. Current Opinion in Cell Biology, 2006. **18**(5): p. 463-71.

9.   Nielson, R., B. Kaehr, and J.B. Shear, *Microreplication and design of biological architectures using dynamic-mask multiphoton lithography*. Small, 2009. **5**(1): p. 120-5.

10.   Seidlits, S.K., C.E. Schmidt, and J.B. Shear, *High-resolution patterning of hydrogels in three dimensions using direct-write photofabrication for cell guidance*. Advanced Functional Materials, 2009. **19**(22): p. 3543-3551.

11.   Kaehr, B. and J.B. Shear, *Multiphoton fabrication of chemically responsive protein hydrogels for microactuation*. Proceedings of the National Academy of Sciences, 2008. **105**(26): p. 8850-4.

12.   Goody, M.F. and C.A. Henry, *Dynamic interactions between cells and their extracellular matrix mediate embryonic development*. Molecular Reproduction and Development, 2010. **77**(6): p. 475-88.

13.   Frantz, C., K.M. Stewart, and V.M. Weaver, *The extracellular matrix at a glance*. Journal of Cell Science, 2010. **123**(Pt 24): p. 4195-200.

14.   Bettinger, C.J., R. Langer, and J.T. Borenstein, *Engineering substrate topography at the micro- and nanoscale to control cell function*. Angewandte Chemie International Edition, 2009. **48**(30): p. 5406-15.

15. Webb, A., et al., *Guidance of oligodendrocytes and their progenitors by substratum topography*. Journal of Cell Science, 1995. **108 (Pt 8)**: p. 2747-60.

16. Teixeira, A.I., et al., *Epithelial contact guidance on well-defined micro- and nanostructured substrates*. Journal of Cell Science, 2003. **116**(Pt 10): p. 1881-92.

17. Mitchel, J.A. and D. Hoffman-Kim, *Cellular scale anisotropic topography guides Schwann cell motility*. PLOS One, 2011. **6**(9): p. e24316.

18. Fraser, S.A., et al., *Sub-micron and nanoscale feature depth modulates alignment of stromal fibroblasts and corneal epithelial cells in serum-rich and serum-free media*. Journal of Biomedical Materials Research A, 2008. **86**(3): p. 725-35.

19. Fozdar, D.Y., et al., *Selective axonal growth of embryonic hippocampal neurons according to topographic features of various sizes and shapes*. International Journal of Nanomedicine, 2011. **6**: p. 45-57.

20. Tocce, E.J., et al., *The influence of biomimetic topographical features and the extracellular matrix peptide RGD on human corneal epithelial contact guidance*. Acta Biomaterialia, 2013. **9**(2): p. 5040-51.

21. Teo, B.K.K., et al., *Nanotopography modulates mechanotransduction of stem cells and induces differentiation through focal adhesion kinase*. ACS Nano, 2013. **7**(6): p. 4785-4798.

22. Wood, M.A., P. Bagnaninchi, and M.J. Dalby, *The beta integrins and cytoskeletal nanoimprinting*. Experimental Cell Research, 2008. **314**(4): p. 927-35.

23. Curtis, A.S., M.J. Dalby, and N. Gadegaard, *Nanoprinting onto cells*. Journal of the Royal Society Interface, 2006. **3**(8): p. 393-8.

24. Dalby, M.J., N. Gadegaard, and R.O. Oreffo, *Harnessing nanotopography and integrin-matrix interactions to influence stem cell fate*. Nature Materials, 2014. **13**(6): p. 558-69.

25. Uttayarat, P., et al., *Topographic guidance of endothelial cells on silicone surfaces with micro- to nanogrooves: orientation of actin filaments and focal adhesions*. Journal of Biomedical Materials Research A, 2005. **75**(3): p. 668-80.

26. Dalby, M.J., et al., *Nucleus alignment and cell signaling in fibroblasts: response to a micro-grooved topography*. Experimental Cell Research, 2003. **284**(2): p. 272-280.

27. Thomas, C.H., et al., *Engineering gene expression and protein synthesis by modulation of nuclear shape*. Proceedings of the National Academy of Sciences, 2002. **99**(4): p. 1972-7.

28. O'Rourke, N.A., et al., *Tangential migration of neurons in the developing cerebral cortex*. Development, 1995. **121**(7): p. 2165-76.

29.   Rakic, P., *Mode of cell migration to the superficial layers of fetal monkey neocortex*. Journal of Computational Neurology, 1972. **145**(1): p. 61-83.

30.   Ortino, B., et al., *Substrates and routes of migration of early generated neurons in the developing rat thalamus*. European Journal of Neuroscience, 2003. **18**(2): p. 323-32.

31.   Ono, K. and K. Kawamura, *Migration of immature neurons along tangentially oriented fibers in the subpial part of the fetal mouse medulla oblongata*. Experimental Brain Research, 1989. **78**(2): p. 290-300.

32.   Miller, R.K. and P.D. McCrea, *Wnt to build a tube: contributions of Wnt signaling to epithelial tubulogenesis*. Developmental Dynamics, 2010. **239**(1): p. 77-93.

33.   Petrie, R.J., A.D. Doyle, and K.M. Yamada, *Random versus directionally persistent cell migration*. Nature Reviews Molecular Cell Biology, 2009. **10**(8): p. 538-49.

34.   Bryant, D.M. and K.E. Mostov, *From cells to organs: building polarized tissue*. Nature Reviews Molecular Cell Biology, 2008. **9**(11): p. 887-901.

35.   Provenzano, P.P., et al., *Contact guidance mediated three-dimensional cell migration is regulated by Rho/ROCK-dependent matrix reorganization*. Biophysical Journal, 2008. **95**(11): p. 5374-84.

36.   Olsen, O., et al., *Renal defects associated with improper polarization of the CRB and DLG polarity complexes in MALS-3 knockout mice*. Journal of Cell Biology, 2007. **179**(1): p. 151-64.

37.   Willis, B.C., R.M. duBois, and Z. Borok, *Epithelial origin of myofibroblasts during fibrosis in the lung*. Proceedings of the American Thoracic Society, 2006. **3**(4): p. 377-82.

38.   Geiger, B., J.P. Spatz, and A.D. Bershadsky, *Environmental sensing through focal adhesions*. Nature Reviews Molecular Cell Biology, 2009. **10**(1): p. 21-33.

39.   Kuo, C.H., et al., *Complex stiffness gradient substrates for studying mechanotactic cell migration*. Advanced Materials, 2012. **24**(45): p. 6059-64.

40.   Nemir, S., H.N. Hayenga, and J.L. West, *PEGDA hydrogels with patterned elasticity: novel tools for the study of cell response to substrate rigidity*. Biotechnology and Bioengineering, 2010. **105**(3): p. 636-44.

41.   Tseng, P. and D. Di Carlo, *Substrates with patterned extracellular matrix and subcellular stiffness gradients reveal local biomechanical responses*. Advanced Materials, 2014. **26**(8): p. 1242-1247.

42. Cheung, Y.K., et al., *Microscale control of stiffness in a cell-adhesive substrate using microfluidics-based lithography*. Angewandte Chemie International Edition, 2009. **48**(39): p. 7188-7192.

43. Even-Ram, S. and K.M. Yamada, *Cell migration in 3D matrix*. Current Opinion in Cell Biology, 2005. **17**(5): p. 524-32.

44. Steffensen, B., L. Hakkinen, and H. Larjava, *Proteolytic events of wound-healing--coordinated interactions among matrix metalloproteinases (MMPs), integrins, and extracellular matrix molecules*. Critical Reviews in Oral Biological Medicine, 2001. **12**(5): p. 373-98.

45. van Dijk, M., S.A. Goransson, and S. Stromblad, *Cell to extracellular matrix interactions and their reciprocal nature in cancer*. Experimental Cell Research, 2013.

46. Ng, M.R. and J.S. Brugge, *A stiff blow from the stroma: collagen crosslinking drives tumor progression*. Cancer Cell, 2009. **16**(6): p. 455-7.

47. DeGroot, J., *The AGE of the matrix: chemistry, consequence and cure*. Current Opinion in Pharmacology, 2004. **4**(3): p. 301-5.

48. Huynh, J., et al., *Age-related intimal stiffening enhances endothelial permeability and leukocyte transmigration*. Science Translational Medicine, 2011. **3**(112): p. 112ra122.

49. Paszek, M.J., et al., *Tensional homeostasis and the malignant phenotype*. Cancer Cell, 2005. **8**(3): p. 241-54.

50. Georges, P.C., et al., *Increased stiffness of the rat liver precedes matrix deposition: implications for fibrosis*. American Journal of Physiology Gastrointestinal Liver Physiology, 2007. **293**(6): p. G1147-54.

51. Liu, F., et al., *Feedback amplification of fibrosis through matrix stiffening and COX-2 suppression*. Journal of Cell Biology, 2010. **190**(4): p. 693-706.

52. Krishnan, R., et al., *Substrate stiffening promotes endothelial monolayer disruption through enhanced physical forces*. American Journal of Physiology Cell Physiology, 2011. **300**(1): p. C146-54.

53. Baker, A.M., et al., *Lysyl oxidase enzymatic function increases stiffness to drive colorectal cancer progression through FAK*. Oncogene, 2013. **32**(14): p. 1863-8.

54. King, G.L. and M. Brownlee, *The cellular and molecular mechanisms of diabetic complications*. Endocrinology Metabolism Clinics of North America, 1996. **25**(2): p. 255-70.

55. Kumar, S. and V.M. Weaver, *Mechanics, malignancy, and metastasis: the force journey of a tumor cell*. Cancer Metastasis Review, 2009. **28**(1-2): p. 113-27.

56. Zaman, M.H., et al., *Migration of tumor cells in 3D matrices is governed by matrix stiffness along with cell-matrix adhesion and proteolysis.* Proceedings of the National Academy of Sciences, 2006. **103**(29): p. 10889-94.

57. West, J.L. and J.A. Hubbell, *Polymeric biomaterials with degradation sites for proteases involved in cell migration.* Macromolecules, 1998. **32**(1): p. 241-244.

58. Lutolf, M.P., et al., *Synthetic matrix metalloproteinase-sensitive hydrogels for the conduction of tissue regeneration: Engineering cell-invasion characteristics.* Proceedings of the National Academy of Sciences, 2003. **100**(9): p. 5413-5418.

59. Straley, K.S. and S.C. Heilshorn, *Dynamic, 3D-pattern formation within enzyme-responsive hydrogels.* Advanced Materials, 2009. **21**(41): p. 4148-4152.

60. Lam, M.T., W.C. Clem, and S. Takayama, *Reversible on-demand cell alignment using reconfigurable microtopography.* Biomaterials, 2008. **29**(11): p. 1705-12.

61. Guvendiren, M. and J.A. Burdick, *Stem cell response to spatially and temporally displayed and reversible surface topography.* Advanced Healthcare Materials, 2013. **2**(1): p. 155-164.

62. Riveline, D., et al., *Focal contacts as mechanosensors: externally applied local mechanical force induces growth of focal contacts by an mDia1-dependent and ROCK-independent mechanism.* Journal of Cell Biology, 2001. **153**(6): p. 1175-86.

63. Galbraith, C.G., K.M. Yamada, and M.P. Sheetz, *The relationship between force and focal complex development.* Journal of Cell Biology, 2002. **159**(4): p. 695-705.

64. Gillette, B.M., et al., *Dynamic hydrogels: switching of 3D microenvironments using two-component naturally derived extracellular matrices.* Advanced Materials, 2010. **22**(6): p. 686-91.

65. Clapham, D.E., *Calcium signaling.* Cell, 2007. **131**(6): p. 1047-1058.

66. Jiang, F.X., et al., *The relationship between fibroblast growth and the dynamic stiffnesses of a DNA crosslinked hydrogel.* Biomaterials, 2010. **31**(6): p. 1199-212.

67. Young, J.L. and A.J. Engler, *Hydrogels with time-dependent material properties enhance cardiomyocyte differentiation in vitro.* Biomaterials, 2011. **32**(4): p. 1002-9.

68. Yoshikawa, H.Y., et al., *Quantitative evaluation of mechanosensing of cells on dynamically tunable hydrogels.* Journal of the American Chemical Society, 2011. **133**(5): p. 1367-74.

69.   von Recum, H.A., et al., *Novel thermally reversible hydrogel as detachable cell culture substrate*. Journal of Biomedical Materials Research, 1998. **40**(4): p. 631-9.

70.   Tekin, H., et al., *Responsive microgrooves for the formation of harvestable tissue constructs*. Langmuir, 2011. **27**(9): p. 5671-9.

71.   Yamaki, K., et al., *Regulation of cellular morphology using temperature-responsive hydrogel for integrin-mediated mechanical force stimulation*. Biomaterials, 2009. **30**(7): p. 1421-7.

72.   Frisman, I., et al., *Stimulus-responsive hydrogels made from biosynthetic fibrinogen conjugates for tissue engineering: structural characterization*. Langmuir, 2011. **27**(11): p. 6977-86.

73.   Davis, K.A., et al., *Dynamic cell behavior on shape memory polymer substrates*. Biomaterials, 2011. **32**(9): p. 2285-93.

74.   Nelson, B.A., W.P. King, and K. Gall, *Shape recovery of nanoscale imprints in a thermoset "shape memory" polymer*. Applied Physics Letters, 2005. **86**(10): p. -.

75.   Xie, T., *Tunable polymer multi-shape memory effect*. Nature, 2010. **464**(7286): p. 267-70.

76.   Sonna, L.A., et al., *Invited review: effects of heat and cold stress on mammalian gene expression*. Journal of Applied Physiology, 2002. **92**(4): p. 1725-42.

77.   Kloxin, A.M., et al., *Photodegradable hydrogels for dynamic tuning of physical and chemical properties*. Science, 2009. **324**(5923): p. 59-63.

78.   Kloxin, A.M., J.A. Benton, and K.S. Anseth, *In situ elasticity modulation with dynamic substrates to direct cell phenotype*. Biomaterials, 2010. **31**(1): p. 1-8.

79.   Kirschner, C.M., et al., *Clickable, photodegradable hydrogels to dynamically modulate valvular interstitial cell phenotype*. Advanced Healthcare Materials, 2014. **3**(5): p. 649-57.

80.   Kirschner, C.M. and K.S. Anseth, *In situ control of cell substrate microtopographies using photolabile hydrogels*. Small, 2013. **9**(4): p. 578-84.

81.   Tibbitt, M.W., et al., *Controlled two-photon photodegradation of PEG hydrogels to study and manipulate subcellular interactions on soft materials*. Soft Matter, 2010. **6**(20): p. 5100-5108.

82.   Khetan, S., J.S. Katz, and J.A. Burdick, *Sequential crosslinking to control cellular spreading in 3-dimensional hydrogels*. Soft Matter, 2009. **5**(8): p. 1601-1606.

83.   Marklein, R.A., D.E. Soranno, and J.A. Burdick, *Magnitude and presentation of mechanical signals influence adult stem cell behavior in 3-dimensional macroporous hydrogels*. Soft Matter, 2012. **8**(31): p. 8113-8120.

84. Muraoka, T., et al., *Light-triggered bioactivity in three dimensions*. Angewandte Chemie International Edition, 2009. **48**(32): p. 5946-5949.

85. Spivey, E.C., et al., *Multiphoton lithography of unconstrained three-dimensional protein microstructures*. Advanced Functional Materials, 2013. **23**(3): p. 333-339.

86. Ritschdorff, E.T., R. Nielson, and J.B. Shear, *Multi-focal multiphoton lithography*. Lab on a Chip, 2012. **12**(5): p. 867-71.

87. Ritschdorff, E.T. and J.B. Shear, *Multiphoton lithography using a high-repetition rate microchip laser*. Analytical Chemistry, 2010. **82**(20): p. 8733-8737.

88. Kaehr, B. and J.B. Shear, *Mask-directed multiphoton lithography*. Journal of the American Chemical Society, 2007. **129**(7): p. 1904-5.

89. Spivey, E.C., *Multiphoton lithography of mechanically and functionally tunable hydrogels*. 2012, The University of Texas at Austin.

90. Forciniti, L., et al., *Schwann cell response on polypyrrole substrates upon electrical stimulation*. Acta Biomaterialia, 2014. **10**(6): p. 2423-2433.

91. Pitts, J.D., et al., *Submicron multiphoton free-form fabrication of proteins and polymers: studies of reaction efficiencies and applications in sustained release*. Macromolecules, 2000. **33**(5): p. 1514-1523.

92. Khripin, C.Y., C.J. Brinker, and B. Kaehr, *Mechanically tunable multiphoton fabricated protein hydrogels investigated using atomic force microscopy*. Soft Matter, 2010. **6**(12): p. 2842-2848.

93. Sen, S., A.J. Engler, and D.E. Discher, *Matrix strains induced by cells: computing how far cells can feel*. Cell Molecular Bioengineering, 2009. **2**(1): p. 39-48.

94. Mullender, M.G., et al., *Osteocyte density and histomorphometric parameters in cancellous bone of the proximal femur in five mammalian species*. Journal of Orthopaedic Research, 1996. **14**(6): p. 972-979.

95. Merkel, R., et al., *Cell force microscopy on elastic layers of finite thickness*. Biophysical Journal, 2007. **93**(9): p. 3314-23.

96. Buxboim, A., et al., *How deeply cells feel: methods for thin gels*. Journal of Physics Condensed Matter, 2010. **22**(19): p. 194116.

97. Kraning-Rush, C.M., et al., *Quantifying traction stresses in adherent cells*. Methods in Cell Biology, 2012. **110**: p. 139-78.

98. Maloney, J.M., et al., *Influence of finite thickness and stiffness on cellular adhesion-induced deformation of compliant substrata*. Physical Review E, 2008. **78**(4): p. 041923.

99. Engler, A.J., et al., *Surface probe measurements of the elasticity of sectioned tissue, thin gels and polyelectrolyte multilayer films: Correlations between*

substrate stiffness and cell adhesion. Surface Science, 2004. **570**(1–2): p. 142-154.

100. Kraning-Rush, C.M. and C.A. Reinhart-King, *Controlling matrix stiffness and topography for the study of tumor cell migration*. Cell Adhesion and Migration, 2012. **6**(3): p. 274-9.

101. Park, J., et al., *Quantitative analysis of the combined effect of substrate rigidity and topographic guidance on cell morphology*. IEEE Transactions on Nanobioscience, 2012. **11**(1): p. 28-36.

102. Charest, J.M., et al., *Fabrication of substrates with defined mechanical properties and topographical features for the study of cell migration*. Macromolecular Bioscience, 2012. **12**(1): p. 12-20.

103. Al-Haque, S., et al., *Hydrogel substrate stiffness and topography interact to induce contact guidance in cardiac fibroblasts*. Macromolecular Bioscience, 2012. **12**(10): p. 1342-53.

104. Pathak, A. and S. Kumar, *Independent regulation of tumor cell migration by matrix stiffness and confinement*. Proceedings of the National Academy of Sciences, 2012.

105. Connell, J.L., *Characterization and microfabrication of environmentally sensitive materials for studying bacterial group behaviors*. 2012, The University of Texas at Austin.

106. Vincent, L.G., et al., *Mesenchymal stem cell durotaxis depends on substrate stiffness gradient strength*. Biotechnology Journal, 2013. **8**(4): p. 472-84.

107. Isenberg, B.C., et al., *Vascular smooth muscle cell durotaxis depends on substrate stiffness gradient strength*. Biophysical Journal, 2009. **97**(5): p. 1313-22.

108. Lo, C.-M., et al., *Cell movement Is guided by the rigidity of the substrate*. Biophysical Journal, 2000. **79**(1): p. 144-152.

109. Hoppe, T.J., *Laser-Based Techniques for Manipulating the Single-Cell Environment*. 2013, The University of Texas at Austin.

Chapter 4: Evaluation of Fluorescent Nitric Oxide Probes for Live Cell Imaging Applications

4.1 CHAPTER SUMMARY

Highly reactive small molecules, such as free radicals, have garnered significant attention for their contribution to many physiological and pathological responses [1]. They are known to generate oxidative stress and mediate many regulatory effects, including apoptosis, angiogenesis, and cell migration [2-6]. The most prominent endogenously produced reactive small molecules are superoxide and nitric oxide (NO). Substantial efforts have revealed that NO is an important signaling component in many transduction pathways [7-11], and NO has been shown to exhibit both protective and toxic effects on cells [12-14]. However, underlying mechanisms for the paradoxical behavior of NO are still being elucidated [15]. To better classify roles of NO in physiological and pathological processes, methods that can selectively detect vital NO concentrations with high sensitivity are required.

Collaborative efforts between Eric Anslyn, Jason Shear, and co-workers focused on the development and evaluation of NO_{550}, a fluorescent probe for live cell NO detection [16]. They demonstrated this probe was much more selective than alternative technologies; however, the product formed via a reaction with dinitrogen trioxide (N_2O_3), the oxidized product of solution phase NO, was not highly fluorescent. In addition, the probe is hydrophobic, and its limited water solubility complicates intracellular loading. Despite the limitations of NO_{550}, it has been used in a handful of studies to detect NO in living cells [17-19].

Recently, Anslyn and colleagues have developed new fluorescent probes for NO detection that are derivatives of NO_{550}. In bench studies, these probes provide superior spectral and photophysical properties (refer to **Table 1** for more details on the probes).

Here, further characterization of the probes for live cell imaging applications is presented. Fibroblasts (NIH-3T3s) are used for comparative detection analysis of the new probes with their predecessor, NO_{550}, and a commercial competitor, 4-amino-5-methylamino-2',7'-difluorofluorescein diacetate (DAF-FM). Similar to NO_{550}, the new probes display minimal nuclear fluorescence, punctate cytosolic signal, and low extracellular background fluorescence. Additionally, the novel probes produce significantly more signal (between four- and fifteen-fold higher) than NO_{550} after one and 24 hour incubations at equimolar (10 μM) concentrations, demonstrating their potential for biological applications. As expected, signal intensity is dependent on the loading concentration, as demonstrated via probe #10 optimization experiments. Nuclear fluorescence, an indicator of cell health, is observed at loading concentrations above 50 μM. To provide sufficient evidence that NO was in fact being detected, an exogenous NO donor, S-nitroso-N-acetyl-D,L-penicillamine (SNAP), is added to culture wells during probe incubations. The response of the probes to NO was evaluated via fluorescence after 4 and 24 hours. Significantly higher intra- and extracellular fluorescence was detected in the presence of SNAP compared to controls. Additionally, ratiometric imaging is conducted using probe #10 to assess cytosolic loading and signal localization within the cells over 24 hours. Visualization of the unreacted probe and reacted product is possible due to the large spectral shift (~100 nm) in the absorbance maximum. The probe and product are visualized using common 4',6-diamidino-2-phenylindole (DAPI) and fluorescein isothiocyanate (FITC) filter sets, respectively. These novel probes represent some of the first reported ratiometric capable probes for NO detection, and they provide a substantial improvement over current alternatives for the fluorescence detection of localized, intracellular NO dynamics [20].

4.2 BACKGROUND AND MOTIVATION

The endogenous production of NO was first realized in the 1980s when it was identified as the endothelium-derived relaxation factor [21-23]. Concurrent studies also revealed that NO was synthesized by macrophages in response to inflammatory signals [24, 25]. These inaugural studies inspired an inundation of research over the last 30 years to uncover the biological functions of NO. At present, NO synthesis has been credited to numerous cell types, including endothelial cells, macrophages, neuronal cells, glial cells, and fibroblasts [23, 25-28]. Moreover, the effects of NO are not limited to the cells from which it is produced [7, 29-31]. NO is a highly diffusible molecule with a half-life of 1-30 seconds in physiological fluid, allowing it to remain active at long-range distances approaching 500 micrometers [32-36]. The dynamic inter- and intracellular signaling capacity of NO demands real-time visualization methods, similar to those developed for calcium imaging, to truly understand its physiological and pathological roles [37, 38].

4.2.1 Biological Relevance of NO

NO is a ubiquitous signaling molecule that is associated with a number of physiological and pathological responses. Its versatility is emphasized by its involvement in mediating vasodilation, inflammation, and neuronal transmission [39-41]. Deficiencies in NO signaling pathways are implicated in many diseases including artherosclerosis, cancer, and neuropathy [42-45]. Strong evidence also suggests that specific intracellular transduction pathways are activated by distinct concentrations of NO [46-49]. Intracellular NO concentration estimates span from 10 nM to above one μM, and these concentrations are generally associated with cell survival and nitrosative stress or apoptosis, respectively [50]. However, the intracellular dynamics of NO signaling with respect to localized production and targeting are not well understood because there is a dearth of capable, analytical methods to evaluate such effects.

Cells generate NO via nitric oxide synthase (NOS) enzymes. Three isoforms of NOS have been discovered to date: endothelial NOS (eNOS), neuronal NOS (nNOS), and inducible NOS (iNOS) [51]. Two of these enzymes, nNOS and eNOS, are expressed constitutively, associated with normal physiological behavior, and mediated by intracellular calcium levels [52, 53]. Conversely, the expression of iNOS is activated by calcium-independent exposure to cytokines, produces significantly higher quantities of NO, and can ultimately lead to cell death or disease [25, 54-56]. All NOS isoforms catalyze the production of NO through an L-arginine dependent oxidation pathway [57-59]. The most widely used inhibitors of NOS activity target the binding site of L-arginine, including the competitive molecule L-NMMA, whose reported 50% inhibitory concentration is ~5 μM [59, 60].

In addition to chemical mediation, the sub-cellular distribution of NOS enzymes also plays an important regulatory role [61-63]. The most convincing study published by Barouch and colleagues revealed divergent contractile responses to NO by cardiomyocytes with different intracellular distributions of NOS [64]. This regulatory effect is in part driven by the necessity for proximity between an NO source and target due to the short half-life of NO. As such, NOS isoforms are primarily associated with the plasma membrane, endoplasmic reticulum (ER), and mitochondria within cells, although other organelles have also been suggested [65-69]. Unfortunately the mechanisms and motivations for sub-cellular localization of NOS remain ambiguous, despite its inference of cell function and health.

4.2.2 NO Detection Methods

Due to the short half-life of NO in physiological fluids, most methods of detection target NO reaction products, such as nitrate, nitrite, or N_2O_3. Their half-lives in

physiological media are reported to be orders of magnitude longer than NO, at approximately 5-8 hours, 110 seconds, and 7 minutes, respectively, which makes them suitable targets for indirect detection schemes [34, 70]. Current detection methodologies can be divided into two categories: 1) media-based approaches, via the Griess reagent or electrochemistry, and 2) intracellular detection using fluorescent probes [15].

The most established technique for quantifying NO production uses the Griess reagent, first developed in 1879 by Peter Griess to evaluate nitrite in saliva, which reacts with nitrite to form a chromophoric azo dye that absorbs strongly at 540 nm [71, 72]. Media nitrite concentrations can be determined colorimetrically using external calibration standards. To estimate the total NO content in solution, the reduction of all nitrate to nitrite is required using a secondary step. Despite its comprehensive use, reported nitrite concentrations in plasma and other biological systems can vary by over two orders of magnitude (0.1 – 20 μM) [72]. These differences are largely attributed to inefficient nitrate conversion or molecular interference [15, 72]. Other reported techniques for analyzing nitrate and nitrite content from media include high-performance liquid chromatography, capillary electrophoresis, and mass spectrophotometry [73-76]. These methods offer extremely low limits of detection (~ nM), but similar to the Griess reagent, these methods do not provide pertinent spatial information. Electrochemical detection methods developed to date can measure NO directly with significantly higher selectivity and provide discrete detection. Many of the sensors used for electrochemical NO detection are not biocompatible or are quickly fouled in biological fluid [77-79]. While media-based detection methods currently dominate the field, fluorescence microscopy-based approaches are becoming increasing popular because they can convey valuable spatial and temporal information within complex biological systems.

Fluorescent probes offer significant promise for delineating some of the underlying mechanisms of NO signaling and its involvement in intracellular transduction pathways. The most prominent mechanism used for detection via fluorescent probes eliminates the emission quenching photoinduced electron transfer (PET) upon reaction with NO directly or with its oxidation products, rendering the probe fluorescently active; a notable example being DAF and its derivatives [80, 81]. For DAF specifically, the PET mechanism enhances the fluorescence quantum yield ~160 fold, and detection limits as low as 2 nM have been reported [82]. Potential pitfalls of DAF and other probes are low selectivity for binding NO equivalents, pH sensitivity, interferences, and quenching by other molecules [83, 84]. Additionally, the simple, non-ratiometric "turn on" approach does not allow for the assessment of potential probe compartmentalization within organelles. The irreversibility of the PET mechanism limits its temporal resolution, and could potentially impact downstream signaling cascades [85]. Transition metal probes have been employed as a remedy, because they reversibly react with NO [85-88]. However, metal ions themselves are components of many biological processes and may independently alter cell signaling or enzyme activity [89, 90]. Many of these limitations were addressed with the introduction of NO_{550} [16]. The novel synthetic probes presented in this chapter address two primary shortcomings of NO_{550}, fluorescence intensity and longer wavelength activity. They represent a major step forward for the detection of intracellular NO, and should prove useful for a multitude of biological applications.

4.3 MATERIALS AND METHODS

4.3.1 Reagents

All cell culture reagents including Dulbecco's modified eagle's medium (DMEM, high glucose), Leibovitz media (L-15), bovine calf serum (BCS), DMSO (BP-231),

Trypsin (SH3004201), and penicillin-streptomycin antibiotic (PSA) were purchased from Fisher Scientific. Sterile phosphate buffered saline (PBS, SH3026401) solution was purchased from Thermo Scientific (Waltham, MA). DAF-FM (D-23841) was obtained from Life Technologies. NO probes were provided as 100 nanomole aliquots by Eric Anslyn and colleagues. The chemical structures and absorbance/emission spectra of all probes used are shown in **Table 1**. SNAP (N3398) was purchased from Sigma Aldrich. All products were used and stored in a manner consistent with the supplier recommendations.
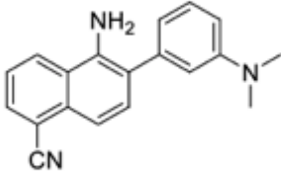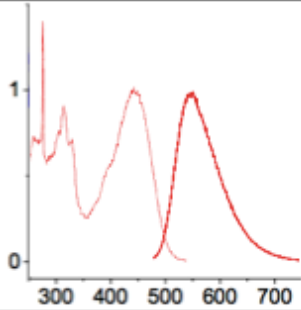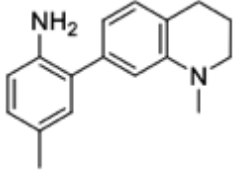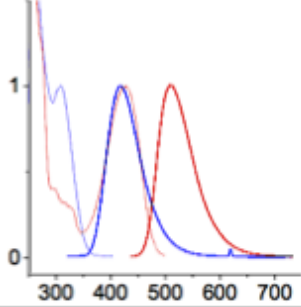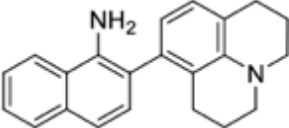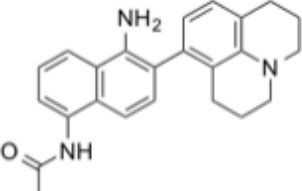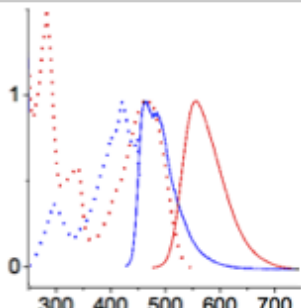
NO$_{550}$		
#6		
#8		
#10		

Table 4.1: Chemical structures and spectral properties of NO probes. The probe name or identification number (column 1) and chemical structure (column 2) are provided. The excitation (lighter or dotted lines) and emission (darker or solid lines) spectrum for each probe (blue) and the corresponding azo product (red) are displayed in column 3. Spectral information was provided by Eric Anlsyn's Group.

136

4.3.2 Cell Culture

Fibroblasts (NIH-3T3s) were purchased from the American Type Culture Collection (ATCC). Cell cultures were maintained in DMEM, high glucose growth media supplemented with 10% (v/v) BCS. Cells were passaged every 4 – 7 days. For experiments, cells were cultured on No. 1.5, 8-welled coverslips (12565388, Fisher Scientific) with L-15 or DMEM media containing 1 - 10% (v/v) BCS and 1% (v/v) PSA.

4.3.3 Fluorescence Imaging

Fluorescence images were acquired using a Zeiss Axiovert microscope system with either an Axiocam HRm camera and Axiovision software or an Orca Flash camera (Hamamatsu, Japan) and HCImage Live software (Hamamatsu). A 10X objective (NeoFluar, 0.3 NA or NeoFluar, 0.5 NA) was used to acquire images unless otherwise stated. DAPI and FITC filter sets purchased from Zeiss (DAPI - #34, FITC - #44) or Chroma (DAPI - 49000, FITC – 41001) were used to acquire images of the probes NO_{550}, #8, and #10. A violet longpass (#05, Zeiss) filter set was used to acquire images of probe #6. Within a single experiment, all exposures and post-acquisition processing in ImageJ software were consistent and optimized for visualization.

4.3.4 Comparative Assays

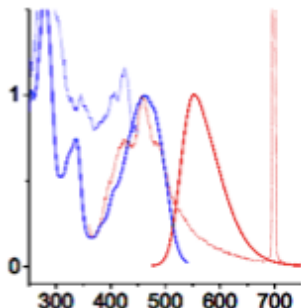Cells were allowed to adhere to the culture wells for 24 hours prior to loading. Cells were loaded and imaged in L-15 media with 1% BCS, 1% PSA, and 1% DMSO to improve probe solubility. Solutions containing equimolar concentrations of each probe (10 μM), based on absorbance measurements, were made and loaded in separate wells. All wells were imaged after 1 and 24 hours of loading without exchanging the media.

4.3.5 NO Donor Experiments

Fibroblasts were cultured on 8 well coverslips 24 hours prior to use. All experiments were conducted in L-15 media supplemented with 1% (v/v) BCS and 1% (v/v) PSA. SNAP (250 μM) or cPTIO (500 μM) was co-loaded with probe #10 (20 μM) and DAF-FM (5 μM) for 24 hours and 30 minutes, respectively. SNAP and cPTIO solutions were made just prior to use. Fluorescence images were acquired after 30 minutes for DAF-FM wells and after 1, 2, 4, and 24 hours for probe #10 wells.

4.3.6 Ratiometric Imaging

Fibroblasts were cultured on 8-well coverslips in L-15 medium with 1% (v/v) BCS, and 1% (v/v) PSA. The culture media was replaced with working medium that included probe #10 at a concentration of 10 μM and 1% (v/v) DMSO. Cells were immediately transported to an environmental chamber situated on the stage of an inverted Zeiss microscope for imaging. The environmental chamber is described in detail in **section 2.3.7**. Images were acquired with a 40X, 0.95 NA objective using both DAPI and FITC filter sets. An overlay of the spectra for the filter sets and probe is displayed in **Figure 4.1**. Metamorph software was set up to acquire images at 10 minute-intervals for one hour. A short exposure time (50 ms) was used to avoid photobleaching. Corresponding images were divided (azo product/probe) after acquisition in ImageJ software to produce the ratiometric image.
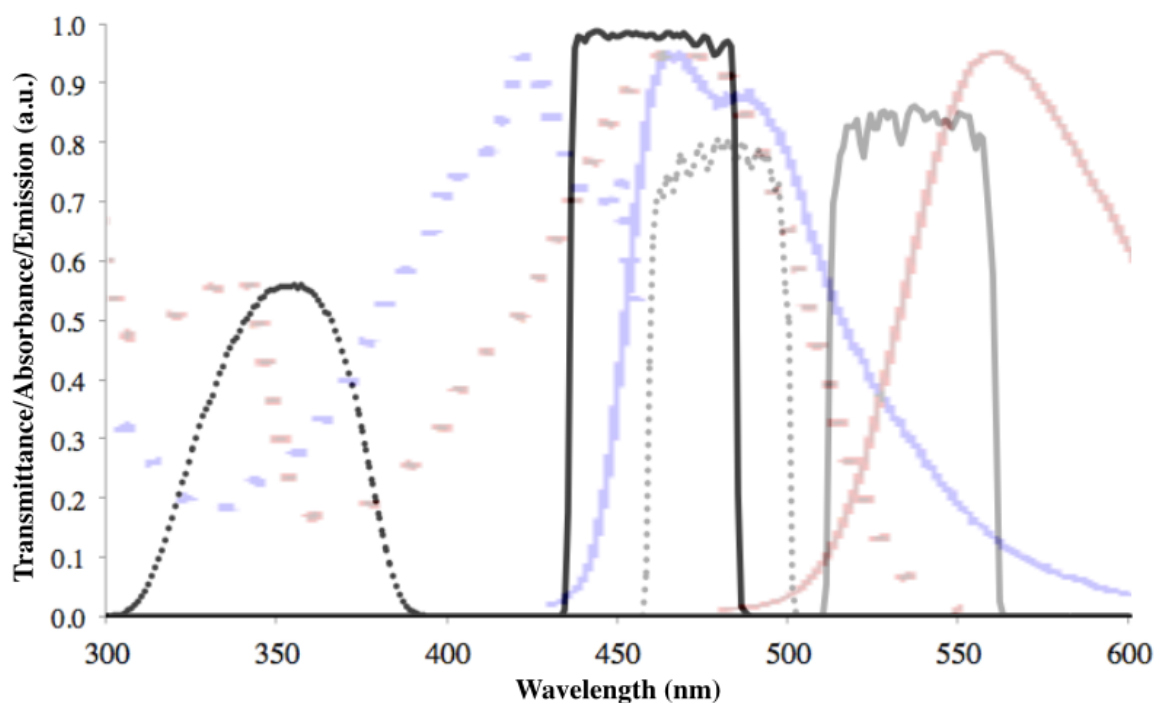
Figure 4.1: Spectra of filters used for ratiometric imaging of probe #10. The excitation (dotted lines) and emission (solid lines) curves for the DAPI filters (black), FITC filters (gray), probe #10 (blue), and the azo product of probe #10 (red). The DAPI emission captures only the fluorescence emission of the unreacted probe, while the FITC filter set overlaps a larger percentage of the excitation and emission spectra of the azo product. Only the azo product is observed using the FITC filters because it is approximately 1000 times brighter than the unreacted probe (data not shown). Data for the filters were obtained from Chroma. Data for probe #10 were provided by Eric Anlsyn's Group.

4.4 RESULTS AND DISCUSSION

4.4.1 Equimolar Studies

Equimolar loading studies were conducted to evaluate the relative intracellular brightness of each probe. Absolute concentrations were derived for probe #10 and NO_{550}, as these probes were pure solids. Relative aliquot concentrations for probes #6 and #8 were determined spectrophotemetrically, by comparing the absorbance of equally diluted aliquots at their respective maximum absorbance wavelength with probe #10. Aliquots were diluted with DMSO to make 1 mM stock solutions. The stock solutions were diluted 1:100 (v/v) in cell culture media for cell loading. DAF-FM loading was conducted at 5 μM concentrations and imaged after 45 minutes. All cells were imaged without exchanging the probe-containing media.

After one hour of probe loading, cytosolic fluorescence of the azo product is visible for all probes tested, as shown in **Figure 4.2**. The intracellular signal in fibroblasts, which express both constitutive and inducible isoforms of NOS, is highly localized and punctate [26]. Brightest fluorescence is detected in close proximity to the nucleus, in what is thought to be ER where NOS is highly expressed [68]. We hypothesize the punctate signal throughout the cytosol is detecting mitochondrial or peroxisomal NO production [66, 67, 91]. The localized signal is likely the result of the higher specificity of the probes for N_2O_3 than DAF-FM, which can react with numerous NO motifs [83]. All probes generate significantly brighter fluorescence than NO_{550} at identical conditions, and appear to maintain specificity for N_2O_3. In contrast to DAF-FM, minimal nuclear fluorescence is observed for the probes. After one hour, the background subtracted fluorescence intensity of probe #8 is nearly equivalent to DAF-FM. The probe concentrations can be increased as shown in the next section, to optimize the fluorescence intensity.

140

The cell density after 24 hours of loading is qualitatively similar to the 1 hour timepoint, implying the probes are not cytotoxic at these low concentrations. The signal intensities for NO_{550}, #6, and #10 increases at longer incubation times, which makes them suitable candidates for long-term NO detection. The intracellular fluorescence intensity remains localized and punctate, and the extracellular background is unchanged. For probe #8 however, the intracellular fluorescence is diminished after 24 hours. This observation is most likely due hydrolysis of the probe, and it should only be used for short-term observations. DAF-FM images are completely saturated after 24 hours because of the extracellular signal, and it is not a suitable probe for long-term imaging applications.

In summary, the efficacy of the probes as intracellular NO indicators is demonstrated. The probes can be loaded for hours without compromising the vitality of the cells. All probes are significantly brighter than NO_{550}; therefore, shorter exposure times can be used during imaging to minimize cell exposure to high intensity light. Probe #6 requires a specialized filter set to image appropriately, and is thus not optimal for most researchers. Probes #8 and #10 are optically comparable, but differ in regards to cell loading and persistence. Probe #8 is best suited for short-term assays, and #10 can be used for either short or long-term NO monitoring. Probe #10 is used for all subsequent studies in this chapter because it produced sufficiently bright intracellular signal, can be imaged using commonly owned FITC filter sets, and has ratiometric potential. Ultimately, all the fluorescent probes tested represent a substantial improvement over currently available alternatives because of their specificity, brightness, and ratiometric capabilities (discussed in **section 4.4.4**).
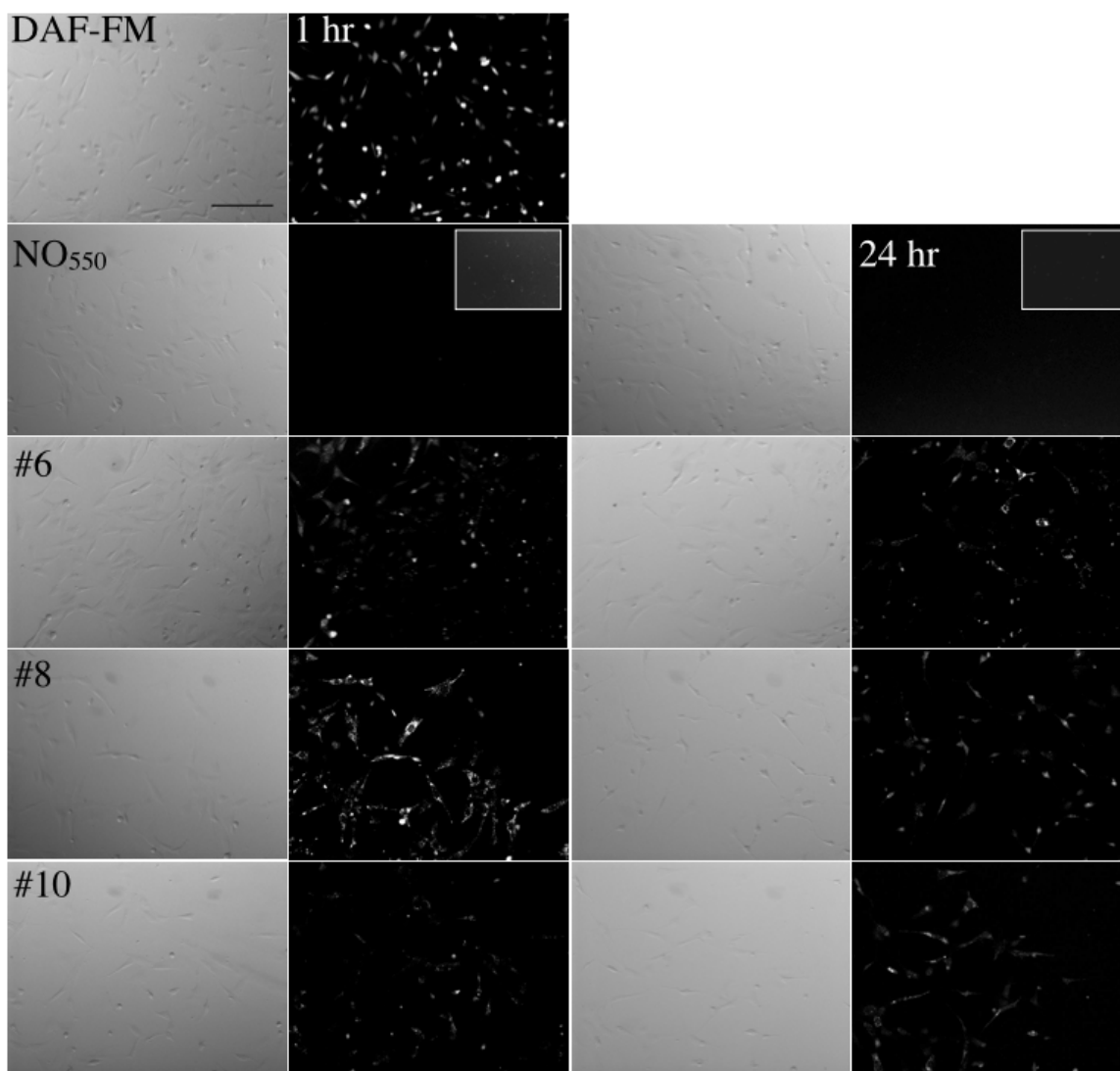
Figure 4.2: Equimolar comparison of all probes for intracellular NO detection. Fibroblasts were incubated in media containing 10 μM of each probe (except for DAF-FM, where a 5 μM loading concentration was used). Brightfield and fluorescence images were acquired after 1 and 24 hours of incubation in loading media. All probe images captured with the FITC filter set (DAF-FM, NO_{550}, #8, and #10) were acquired and adjusted equally for direct comparison. All probes produce significantly higher fluorescence intensities than NO_{550}, which is not visible without additional image processing (insets). The signal intensity from probe #8 is comparable to DAF-FM at 1 hour, but is much lower after 24 hours. Probes #6 and #10 are substantially bright after 1 hour and remain loaded in the cells over the course of 24 hours, when an even brighter signal is observed. All probes display more punctate and localized signal within the cells than DAF-FM. In addition, the DAF-FM extracellular background at 24 hours produced a saturated image (not shown), as it is not a suitable probe for long-term cell monitoring. Scale bar = 50 μm.

4.4.2 Probe #10 Concentration Optimization

To optimize the visualization of probe #10, cells were incubated for 1.5 hours with media containing 10, 20, 50, or 100 μM of the probe. Concentrations were achieved via a variable dilution of 100 nanomole aliquots in DMSO to maintain a 1% (v/v) DMSO working solution. Precipitation of the probe was not evident by visual inspection at any concentration tested. As expected, the intracellular fluorescence increases at higher loading concentrations, as demonstrated in **Figure 4.3**. At loading concentrations of 50 μM and above, the intracellular fluorescence is no longer punctate and localized, and instead resembles a cytosolic stain, showing disperse fluorescence throughout the cell body. Nuclear fluorescence, indicative of cellular damage, is apparent at loading concentrations of 50 and 100 μM. Furthermore, cell death also occurs at 50 and 100 μM loading concentrations over a period of 24 hours (not quantified). To avoid these shortcomings, a 20 μM loading concentration of probe #10 is selected as the optimum concentration for our culture system. It is reasonable to assume that this concentration is not ideal for all cells, and the probe concentration should be adjusted based on the spatiotemporal dynamics of the experiment.
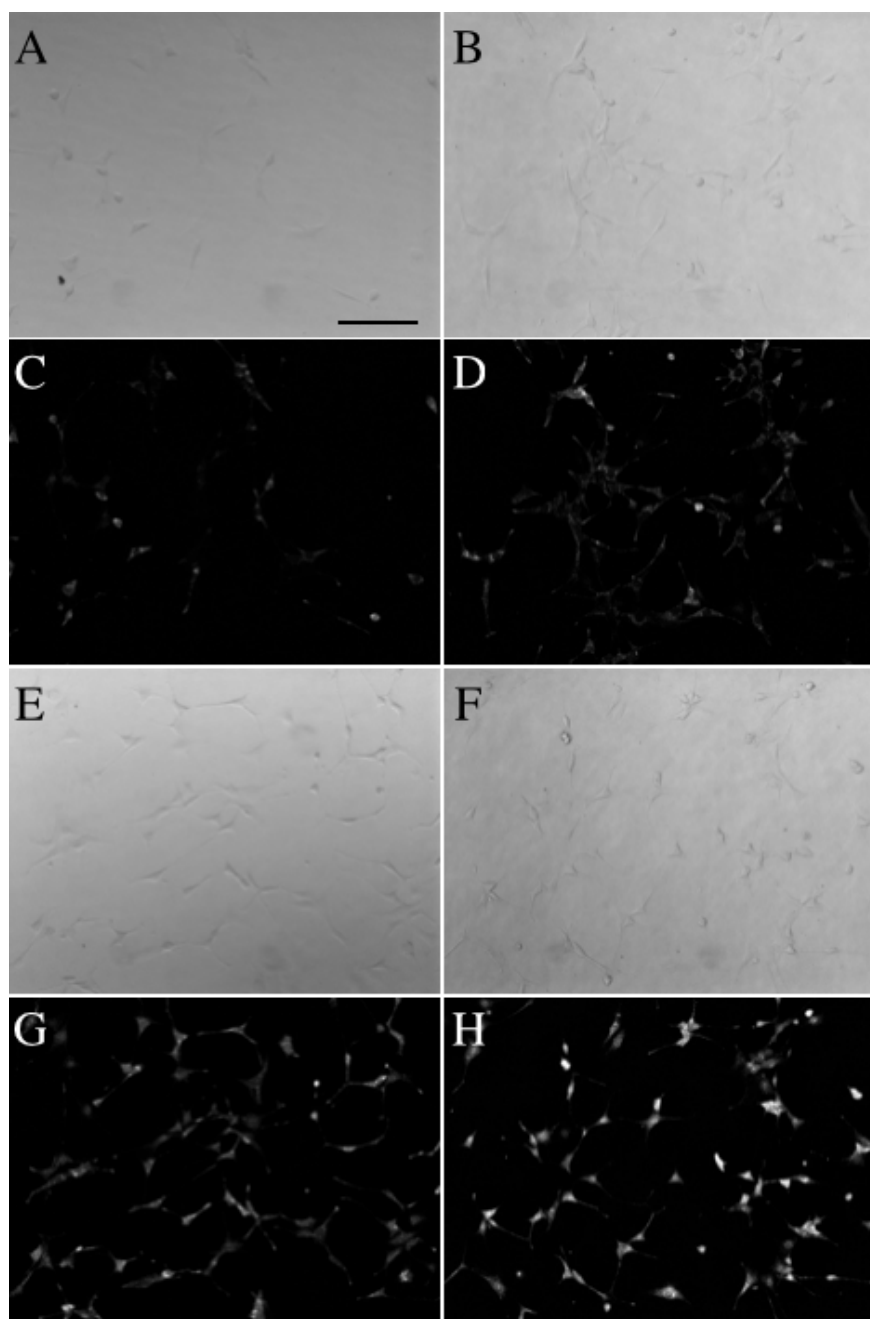
Figure 4.3: Concentration optimization for probe #10. Brightfield and corresponding fluorescence images for 10 μM (A, C), 20 μM (B, D), 50 μM (E, G), and 100 μM (F, H) loading concentrations of probe #10, acquired 1.5 hours after loading was initiated. Nuclear fluorescence, representative of cellular damage, is observed in fibroblasts at concentrations above 50 μM. Scale bar = 50 μm.

4.4.3 Response of Probe #10 to an Exogenous NO donor

SNAP is an S-nitrosothiol that decomposes in aqueous solution to form NO, and its half-life is approximately 6 hours [92, 93]. For every 1 mole of SNAP in solution, approximately 0.0232 moles of NO gas are produced after 15 minutes [93]. Therefore, the 250 μM concentration of SNAP used in these studies should generate an estimated 5.8 μM concentration of NO in the media. The co-loading protocol and effectiveness of SNAP were verified using DAF-FM as a control. After fibroblasts were incubated for 30 minutes in media containing DAF-FM and SNAP, fluorescence images were acquired. The media was not exchanged prior to imaging in order to visualize and compare the intra- and extracellular fluorescence intensities. The well with SNAP exhibited approximately a ten-fold increase in both intra- and extracellular signal over a control well absent of SNAP, as shown in **Figure 4.4**, confirming the efficacy of the protocol.

Cells are co-loaded simultaneously with probe #10 at a concentration of 20 μM and SNAP. A well containing only probe #10 is used as a control. Fluorescence images are acquired 0.5, 1, 2, 4, and 24 hours after loading. For all images that are acquired prior to 4 hours, there is an indiscernible difference in fluorescence intensity. However, images that are acquired at 4 and 24 hours display a noticeable increase in extracellular fluorescence intensity (**Figure 4.4**). In fact, the extracellular signal produced by the SNAP addition saturated the 24 hour image at exposure times typically used for detection (200 ms). In order to see the cells, the exposure time was reduced to 50 ms and some saturation still occurred. The intracellular signal attributable to probe #10 is difficult to quantify because of its punctate presentation, but the fluorescence distribution appears more homogenously distributed when SNAP is present.

This study confirms that probe #10 is responding to NO in the presence of cells. The slower "turn-on" kinetics of probe #10 relative to DAF-FM in response to the SNAP

addition may be due to its higher specificity for N_2O_3, as NO radicals can form numerous reaction products in solution. Future studies should evaluate the response of additional probes to SNAP. Endogenous stimulation of iNOS activity via the introduction of cytokines could provide further evidence to support the value of the probes for sub-cellular imaging applications.
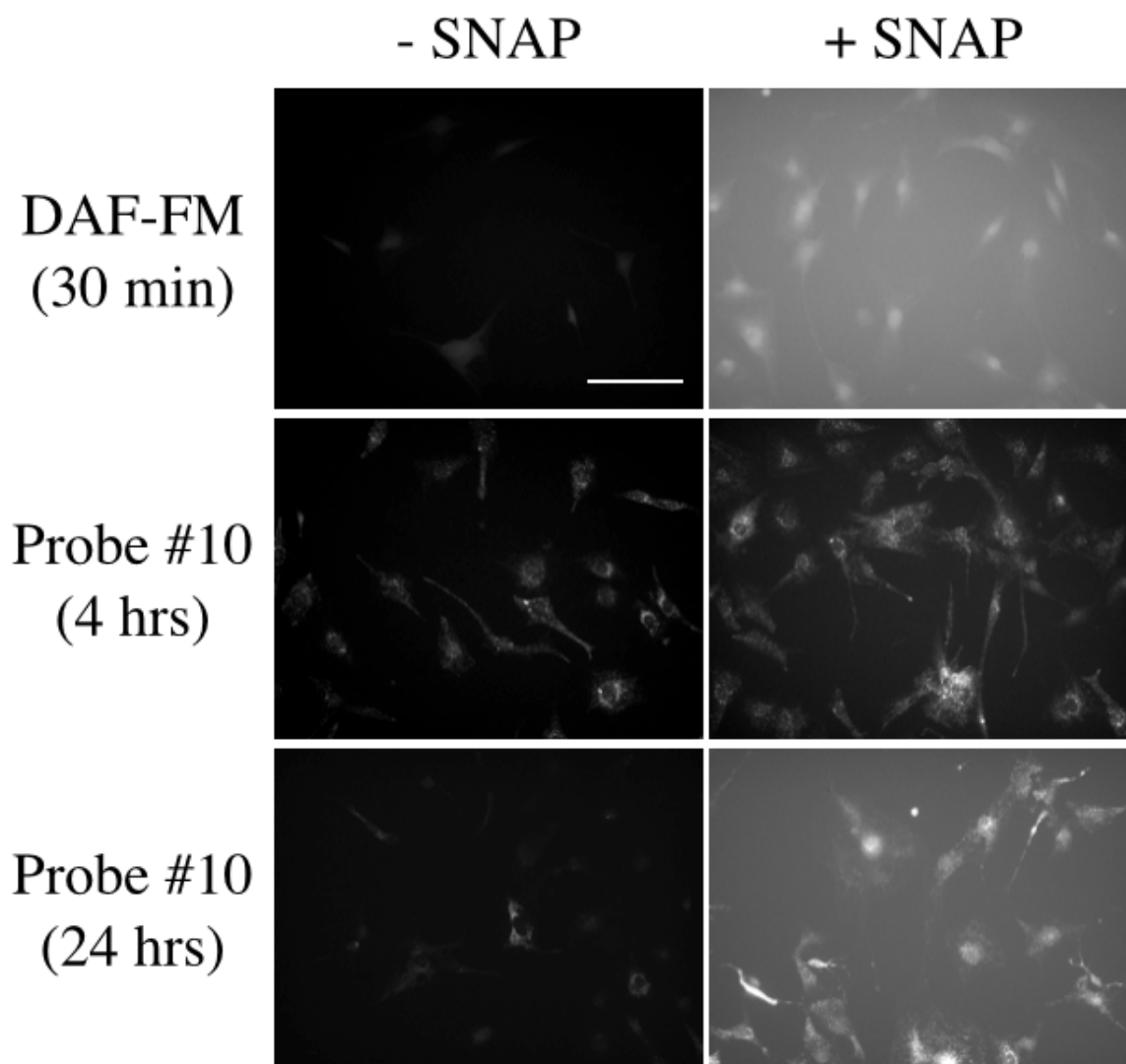
Figure 4.4: Response of probe #10 and DAF-FM to SNAP. Fibroblasts are loaded with DAF-FM (5 μM) and probe #10 (20 μM) in the absence (left column) and presence of SNAP (250 μM). The increase in intra- and extracellular fluorescence is substantial for wells containing SNAP compared to control wells acquired at the same time. For an image pair (+/- SNAP), the acquisition and post-processing parameters are consistent. Scale bar = 50 μM.

4.4.4 Ratiometry

Ratiometry is a powerful, well-established microscopic technique used to quantify intracellular ion concentrations for common cations, such as Ca^{2+} [94]. The technique considerably reduces the effects of variable loading and differential cell thickness. Similarly to Ca^{2+} indicators, all probes discussed in this chapter undergo an excitation and emission wavelength shift of nearly 100 nm after reaction with N_2O_3. Here, the ratiometric capability of probe #10 for monitoring intracellular NO production using time-lapse fluorescence microscopy is demonstrated (**Figure 4.5**). Fibroblasts cells were incubated with media containing 10 μM of probe #10. Immediately after loading was initiated, image pairs were acquired at 10 minute-intervals using a DAPI and FITC filter set for a total of one hour. More rapid acquisition times (2-minute-intervals) were attempted, but cell death occurred.

Fluorescence images collected with the DAPI filter reveal vital information regarding the intracellular loading and compartmentalization of the probe. A nearly homogenous intracellular distribution of the probe is observed initially. The probe loads into the cell over the course of one hour. Probe compartmentalization is observed within a few regions of the cells, and these regions always correspond to higher fluorescence signal of the azo product. It is not clear what causes the probe compartmentalization, but the cell-to-cell heterogeneity suggests that a single organelle is not responsible. After 20 minutes, intracellular fluorescence from the azo product is observed, resulting in an increase in the product/probe ratio. The highest concentration of N_2O_3 is detected around the cell nuclei, where the maximum intracellular ratio approaches 1.7. Filter optimization for detection of the azo product should amplify this ratio even further. Nonetheless, this ratiometric approach provides valuable spatial information regarding the intracellular localization of NO production. Shorter exposure times are necessary to yield more

resolved temporal information without deleterious effects on cells. Future work should employ calibration standards to determine the absolute intracellular concentrations of the probe and N_2O_3.
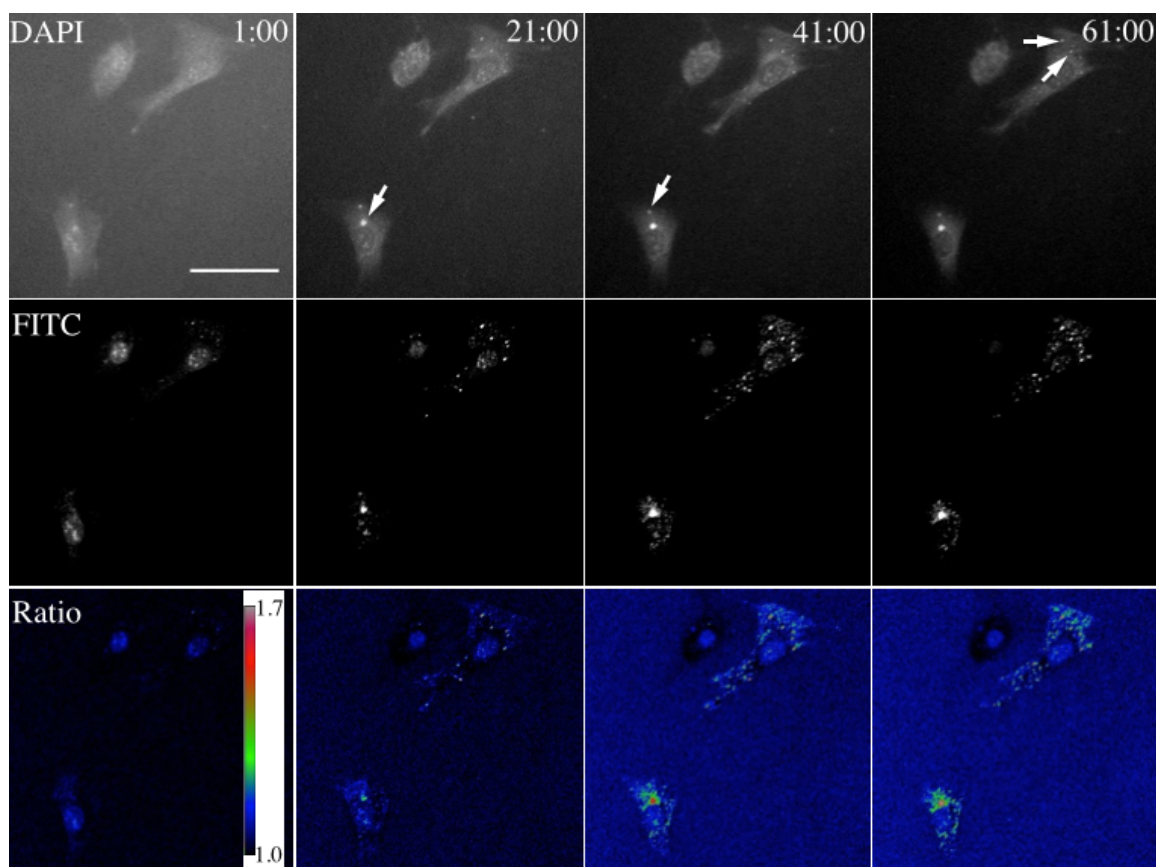
Figure 4.5: Intracellular ratiometric time-lapse of probe #10. Image acquisition began immediately after the culture media was replaced by media + probe (10 μM). Image pairs were captured using both a DAPI (top row) and FITC (middle row) filter set every 10 minutes for a total of 1 hour. The time stamp, in minutes, for each set of images is located at the top right of each column. The DAPI images reveal some degree of compartmentalization within the fibroblasts in areas indicated by the white arrows. The FITC filter set captures the emission of the reacted azo product. The ratiometric images (bottom row) are generated by dividing the FITC image by the DAPI image. The initial extracellular baseline was adjusted to a value of 1. A "rainbow-RGB" look-up table is applied to the ratiometric images, and the scale is compressed as shown (colorbar inset). All images are optimized for visualization. Images within a single row have the same brightness and contrast settings. Scale bar = 20 μm.

4.5 CONCLUSIONS

This chapter demonstrated the efficacy of a series of N_2O_3 reactive fluorescent probes for live-cell imaging. The probes exhibited significantly enhanced fluorescence over NO_{550}, and were competitively bright when compared to the commercially available DAF-FM probe. Other advantages of the probes are selectivity, ability to monitor long-term intracellular dynamics, and ratiometric potential to detect localized N_2O_3 concentrations. Because of these advantages, the novel synthetic probes are considered to be broadly applicable to detect NO production within many biological systems.

Considering the versatility of NO signaling and its involvement in several signal transduction cascades, a multitude of possible studies can be envisioned. Future work should focus on improving probe solubility and establishing a reversible mechanism for detection. These enhancements will provide the spatiotemporal resolution necessary to answer many of the questions surrounding NO signaling within biological systems. In addition, these probes could be used to evaluate cellular responses to dynamic, topographical or mechanical changes to the extracellular environment, as demonstrated in **Chapter 3**. Furthermore, the incorporation of the probes into protein hydrogels could offer a novel platform for the evaluation of NO production and extracellular signaling of in vitro tissue culture systems.

4.6 REFERENCES

1. Droge, W., *Free radicals in the physiological control of cell function*. Physiological Reviews, 2002. **82**(1): p. 47-95.

2. Ray, P.D., B.W. Huang, and Y. Tsuji, *Reactive oxygen species (ROS) homeostasis and redox regulation in cellular signaling*. Cell Signaling, 2012. **24**(5): p. 981-90.

3. Ushio-Fukai, M. and R.W. Alexander, *Reactive oxygen species as mediators of angiogenesis signaling: role of NAD(P)H oxidase*. Molecular Cell Biochemistry, 2004. **264**(1-2): p. 85-97.

4. Colavitti, R., et al., *Reactive oxygen species as downstream mediators of angiogenic signaling by vascular endothelial growth factor receptor-2/KDR*. Journal of Biological Chemistry, 2002. **277**(5): p. 3101-8.

5. Simon, H.U., A. Haj-Yehia, and F. Levi-Schaffer, *Role of reactive oxygen species (ROS) in apoptosis induction*. Apoptosis, 2000. **5**(5): p. 415-8.

6. Wang, Y., et al., *Regulation of VEGF-induced endothelial cell migration by mitochondrial reactive oxygen species*. American Journal of Physiology Cell Physiology, 2011. **301**(3): p. C695-704.

7. Blaise, G.A., et al., *Nitric oxide, cell signaling and cell death*. Toxicology, 2005. **208**(2): p. 177-92.

8. Gupta, S.K. and N.E. Vlahakis, *Integrin alpha9beta1 mediates enhanced cell migration through nitric oxide synthase activity regulated by Src tyrosine kinase*. Journal of Cell Science, 2009. **122**(Pt 12): p. 2043-54.

9. Rudic, R.D., et al., *Direct evidence for the importance of endothelium-derived nitric oxide in vascular remodeling*. Journal of Clinical Investigation, 1998. **101**(4): p. 731-6.

10. Murohara, T., et al., *Nitric oxide synthase modulates angiogenesis in response to tissue ischemia*. Journal of Clinical Investigation, 1998. **101**(11): p. 2567-78.

11. Brune, B., *Nitric oxide: NO apoptosis or turning it ON?* Cell Death and Differentiation, 2003. **10**(8): p. 864-9.

12. Wiley, J.W., *The many faces of nitric oxide: cytotoxic, cytoprotective or both*. Neurogastroenterology and Motility, 2007. **19**(7): p. 541-4.

13. Wink, D.A. and J.B. Mitchell, *Chemical biology of nitric oxide: insights into regulatory, cytotoxic, and cytoprotective mechanisms of nitric oxide*. Free Radical Biology and Medicine, 1998. **25**(4–5): p. 434-456.

14.   Kroncke, K.D., K. Fehsel, and V. Kolb-Bachofen, *Nitric oxide: cytotoxicity versus cytoprotection--how, why, when, and where?* Nitric Oxide, 1997. **1**(2): p. 107-20.

15.   Bryan, N.S. and M.B. Grisham, *Methods to detect nitric oxide and its metabolites in biological samples*. Free Radical Biology and Medicine, 2007. **43**(5): p. 645-57.

16.   Yang, Y., et al., *A highly selective low-background fluorescent imaging agent for nitric oxide*. Journal of the American Chemical Society, 2010. **132**(38): p. 13114-6.

17.   Ghebremariam, Y.T., et al., *Characterization of a fluorescent probe for imaging nitric oxide*. Journal of Vascular Research, 2014. **51**(1): p. 68-79.

18.   Lv, X., et al., *A specific fluorescent probe for NO based on a new NO-binding group*. Chemical Communications, 2014. **50**(56): p. 7499-7502.

19.   Yang, L., et al., *A targetable nanogenerator of nitric oxide for light-triggered cytotoxicity*. Journal of Materials Chemistry B, 2013. **1**(44): p. 6115-6122.

20.   Yu, H., et al., *From a BODIPY-rhodamine scaffold to a ratiometric fluorescent probe for nitric oxide*. New Journal of Chemistry, 2013. **37**(6): p. 1688-1691.

21.   Furchgott, R.F. and P.M. Vanhoutte, *Endothelium-derived relaxing and contracting factors*. FASEB Journal, 1989. **3**(9): p. 2007-18.

22.   Palmer, R.M., D.S. Ashton, and S. Moncada, *Vascular endothelial cells synthesize nitric oxide from L-arginine*. Nature, 1988. **333**(6174): p. 664-6.

23.   Ignarro, L.J., et al., *Endothelium-derived relaxing factor produced and released from artery and vein is nitric oxide*. Proceedings of the National Academy of Sciences, 1987. **84**(24): p. 9265-9.

24.   Stuehr, D.J. and C.F. Nathan, *Nitric oxide. A macrophage product responsible for cytostasis and respiratory inhibition in tumor target cells*. Journal of Experimental Medicine, 1989. **169**(5): p. 1543-55.

25.   Nathan, C.F. and J.B. Hibbs, Jr., *Role of nitric oxide synthesis in macrophage antimicrobial activity*. Current Opinion in Immunology, 1991. **3**(1): p. 65-70.

26.   Wang, R., et al., *Human dermal fibroblasts produce nitric oxide and express both constitutive and inducible nitric oxide synthase isoforms*. Journal of Investigative Dermatology, 1996. **106**(3): p. 419-27.

27.   Boje, K.M. and P.K. Arora, *Microglial-produced nitric oxide and reactive nitrogen oxides mediate neuronal cell death*. Brain Research, 1992. **587**(2): p. 250-6.

28.   Hope, B.T., et al., *Neuronal NADPH diaphorase is a nitric oxide synthase*. Proceedings of the National Academy of Sciences, 1991. **88**(7): p. 2811-4.

29. Nathan, C., *Nitric oxide as a secretory product of mammalian cells*. FASEB Journal, 1992. **6**(12): p. 3051-64.

30. Schuman, E.M. and D.V. Madison, *A requirement for the intercellular messenger nitric oxide in long-term potentiation*. Science, 1991. **254**(5037): p. 1503-6.

31. Stamler, J.S., *Redox signaling: nitrosylation and related target interactions of nitric oxide*. Cell, 1994. **78**(6): p. 931-6.

32. Porterfield, D.M., et al., *Proteins and lipids define the diffusional field of nitric oxide*. American Journal of Physiology Lung Cell Molecular Physiology, 2001. **281**(4): p. L904-12.

33. Kelm, M. and J. Schrader, *Nitric oxide release from the isolated guinea pig heart*. European Journal of Pharmacology, 1988. **155**(3): p. 317-21.

34. Kelm, M., *Nitric oxide metabolism and breakdown*. Biochimica et Biophysica Acta, 1999. **1411**(2-3): p. 273-89.

35. Liu, X., et al., *Nitric oxide diffusion rate is reduced in the aortic wall*. Biophysical Journal, 2008. **94**(5): p. 1880-9.

36. Lancaster, J.R., Jr., *A tutorial on the diffusibility and reactivity of free nitric oxide*. Nitric Oxide, 1997. **1**(1): p. 18-30.

37. Grienberger, C. and A. Konnerth, *Imaging calcium in neurons*. Neuron, 2012. **73**(5): p. 862-85.

38. Grewe, B.F., et al., *High-speed in vivo calcium imaging reveals neuronal network activity with near-millisecond precision*. Nature Methods, 2010. **7**(5): p. 399-405.

39. Ignarro, L.J., *Nitric oxide as a unique signaling molecule in the vascular system: a historical overview*. Journal of Physiology and Pharmacology, 2002. **53**(4 Pt 1): p. 503-14.

40. Bogdan, C., *Nitric oxide and the immune response*. Nature Immunology, 2001. **2**(10): p. 907-16.

41. Prast, H. and A. Philippu, *Nitric oxide as modulator of neuronal function*. Progress in Neurobiology, 2001. **64**(1): p. 51-68.

42. Kawashima, S. and M. Yokoyama, *Dysfunction of endothelial nitric oxide synthase and atherosclerosis*. Arteriosclerosis Thrombosis and Vascular Biology, 2004. **24**(6): p. 998-1005.

43. Xu, W., et al., *The role of nitric oxide in cancer*. Cell Research, 2002. **12**(5-6): p. 311-20.

44. Vareniuk, I., et al., *Peripheral neuropathy in mice with neuronal nitric oxide synthase gene deficiency*. International Journal of Molecular Medicine, 2009. **23**(5): p. 571-80.

45.   Pacher, P., J.S. Beckman, and L. Liaudet, *Nitric oxide and peroxynitrite in health and disease*. Physiological Reviews, 2007. **87**(1): p. 315-424.

46.   Thomas, D.D., et al., *Hypoxic inducible factor 1alpha, extracellular signal-regulated kinase, and p53 are regulated by distinct threshold concentrations of nitric oxide*. Proceedings of the National Academy of Sciences, 2004. **101**(24): p. 8894-9.

47.   Prueitt, R.L., et al., *Inflammation and IGF-I activate the Akt pathway in breast cancer*. International Journal of Cancer, 2007. **120**(4): p. 796-805.

48.   Pervin, S., et al., *Nitric oxide in physiologic concentrations targets the translational machinery to increase the proliferation of human breast cancer cells: involvement of mammalian target of rapamycin/eIF4E pathway*. Cancer Research, 2007. **67**(1): p. 289-99.

49.   Ridnour, L.A., et al., *The chemistry of nitrosative stress induced by nitric oxide and reactive nitrogen oxide species. Putting perspective on stressful biological situations*. Journal of Biological Chemistry, 2004. **385**(1): p. 1-10.

50.   Thomas, D.D., et al., *The chemical biology of nitric oxide: implications in cellular signaling*. Free Radical Biology and Medicine, 2008. **45**(1): p. 18-31.

51.   Nathan, C. and Q.W. Xie, *Nitric oxide synthases: roles, tolls, and controls*. Cell, 1994. **78**(6): p. 915-8.

52.   Zhou, L. and D.Y. Zhu, *Neuronal nitric oxide synthase: structure, subcellular localization, regulation, and clinical implications*. Nitric Oxide, 2009. **20**(4): p. 223-30.

53.   Sessa, W.C., *Regulation of endothelial derived nitric oxide in health and disease*. Memorias de Instituto Oswaldo Cruz, 2005. **100 Suppl 1**: p. 15-8.

54.   Weisz, A., et al., *Dual mechanism for the control of inducible-type NO synthase gene expression in macrophages during activation by interferon-gamma and bacterial lipopolysaccharide. Transcriptional and post-transcriptional regulation*. Journal of Biological Chemistry, 1994. **269**(11): p. 8324-33.

55.   MacMicking, J.D., et al., *Altered responses to bacterial infection and endotoxic shock in mice lacking inducible nitric oxide synthase*. Cell, 1995. **81**(4): p. 641-50.

56.   Nussler, A.K., et al., *Stimulation of the nitric oxide synthase pathway in human hepatocytes by cytokines and endotoxin*. Journal of Experimental Medicine, 1992. **176**(1): p. 261-4.

57.   Moncada, S., R.M. Palmer, and E.A. Higgs, *Biosynthesis of nitric oxide from L-arginine. A pathway for the regulation of cell function and communication*. Biochemical Pharmacology, 1989. **38**(11): p. 1709-15.

58.   Moncada, S. and A. Higgs, *The L-arginine-nitric oxide pathway*. New England Journal of Medicine, 1993. **329**(27): p. 2002-12.

59.   Alderton, W.K., C.E. Cooper, and R.G. Knowles, *Nitric oxide synthases: structure, function and inhibition*. Biochemical Journal, 2001. **357**(Pt 3): p. 593-615.

60.   Young, R.J., et al., *Inhibition of inducible nitric oxide synthase by acetamidine derivatives of hetero-substituted lysine and homolysine*. Bioorganic and Medicine Chemistry Letters, 2000. **10**(6): p. 597-600.

61.   Shaul, P.W., *Regulation of endothelial nitric oxide synthase: location, location, location*. Annual RevIew Physiology, 2002. **64**: p. 749-74.

62.   Villanueva, C. and C. Giulivi, *Subcellular and cellular locations of nitric oxide synthase isoforms as determinants of health and disease*. Free Radical Biology and Medicine, 2010. **49**(3): p. 307-16.

63.   Jagnandan, D., W.C. Sessa, and D. Fulton, *Intracellular location regulates calcium-calmodulin-dependent activation of organelle-restricted eNOS*. American Journal of Physiology Cell Physiology, 2005. **289**(4): p. C1024-33.

64.   Barouch, L.A., et al., *Nitric oxide regulates the heart by spatial confinement of nitric oxide synthase isoforms*. Nature, 2002. **416**(6878): p. 337-9.

65.   Feron, O., et al., *Endothelial nitric oxide synthase targeting to caveolae. Specific interactions with caveolin isoforms in cardiac myocytes and endothelial cells*. Journal of Biological Chemistry, 1996. **271**(37): p. 22810-4.

66.   Gao, S., et al., *Docking of endothelial nitric oxide synthase (eNOS) to the mitochondrial outer membrane: a pentabasic amino acid sequence in the autoinhibitory domain of eNOS targets a proteinase K-cleavable peptide on the cytoplasmic face of mitochondria*. Journal of Biological Chemistry, 2004. **279**(16): p. 15968-74.

67.   Brookes, P.S., *Mitochondrial nitric oxide synthase*. Mitochondrion, 2004. **3**(4): p. 187-204.

68.   Martinez-Moreno, M., et al., *Direct interaction between the reductase domain of endothelial nitric oxide synthase and the ryanodine receptor*. FEBS Letters, 2005. **579**(14): p. 3159-63.

69.   O'Brien, A.J., et al., *Nitric oxide synthase is localized predominantly in the Golgi apparatus and cytoplasmic vesicles of vascular endothelial cells*. Histochemistry and Cell Biology, 1995. **103**(3): p. 221-5.

70.   Rafikova, O., R. Rafikov, and E. Nudler, *Catalysis of S-nitrosothiols formation by serum albumin: the mechanism and implication in vascular control*. Proceedings of the National Academy of Sciences, 2002. **99**(9): p. 5913-8.

71. Griess, P., *Bemerkungen zu der Abhandlung der HH. Weselsky und Benedikt „Ueber einige Azoverbindungen"* . Berichte der deutschen chemischen Gesellschaft, 1879. **12**(1): p. 426-428.

72. Tsikas, D., *Analysis of nitrite and nitrate in biological fluids by assays based on the Griess reaction: appraisal of the Griess reaction in the L-arginine/nitric oxide area of research*. Journal of Chromatogr B Analytical Technologies in the Biomedical Life Sciences, 2007. **851**(1-2): p. 51-70.

73. Jobgen, W.S., et al., *Analysis of nitrite and nitrate in biological samples using high-performance liquid chromatography*. Journal of Chromatogr B Analytical Technologies in the Biomedical Life Sciences, 2007. **851**(1-2): p. 71-82.

74. Leone, A.M., et al., *A rapid and simple method for the measurement of nitrite and nitrate in plasma by high performance capillary electrophoresis*. Biochemical and Biophysical Research Communications, 1994. **200**(2): p. 951-7.

75. Boudko, D.Y., *High-resolution capillary electrophoresis of nitrite and nitrate in biological samples*. Methods in Molecular Biology, 2004. **279**: p. 9-19.

76. Tsikas, D., *Simultaneous derivatization and quantification of the nitric oxide metabolites nitrite and nitrate in biological fluids by gas chromatography/mass spectrometry*. Analytical Chemistry, 2000. **72**(17): p. 4064-72.

77. Allen, B.W., J. Liu, and C.A. Piantadosi, *Electrochemical detection of nitric oxide in biological fluids*. Methods in Enzymology, 2005. **396**: p. 68-77.

78. Boo, Y.C., et al., *Detection of low levels of nitric oxide using an electrochemical sensor*. Methods in Molecular Biology, 2011. **704**: p. 81-9.

79. Privett, B.J., J.H. Shin, and M.H. Schoenfisch, *Electrochemical nitric oxide sensors for physiological measurements*. Chemical Society Reviews, 2010. **39**(6): p. 1925-1935.

80. de Silva, P.A., N.H.Q. Gunaratne, and C.P. McCoy, *A molecular photoionic AND gate based on fluorescent signalling*. Nature, 1993. **364**(6432): p. 42-44.

81. Valeur, B. and I. Leray, *Design principles of fluorescent molecular sensors for cation recognition*. Coordination Chemistry Reviews, 2000. **205**(1): p. 3-40.

82. Kojima, H., et al., *Fluorescent indicators for imaging nitric oxide production*. Angew Chemie International Edition, 1999. **38**(21): p. 3209-3212.

83. Rodriguez, J., et al., *Performance of diamino fluorophores for the localization of sources and targets of nitric oxide*. Free Radical Biology and Medicine, 2005. **38**(3): p. 356-68.

84. Wardman, P., *Fluorescent and luminescent probes for measurement of oxidative and nitrosative species in cells and tissues: progress, pitfalls, and prospects*. Free Radical Biology and Medicine, 2007. **43**(7): p. 995-1022.

85.   McQuade, L.E. and S.J. Lippard, *Fluorescent probes to investigate nitric oxide and other reactive nitrogen species in biology (truncated form: fluorescent probes of reactive nitrogen species)*. Current Opinion in Chemical Biology, 2010. **14**(1): p. 43-9.

86.   Lim, M.H. and S.J. Lippard, *Metal-based turn-on fluorescent probes for sensing nitric oxide*. Accounts of Chemical Research, 2007. **40**(1): p. 41-51.

87.   Smith, R.C., et al., *Conjugated polymer-based fluorescence turn-on sensor for nitric oxide*. Organic Letters, 2005. **7**(16): p. 3573-5.

88.   Ford, P.C. and I.M. Lorkovic, *Mechanistic aspects of the reactions of nitric oxide with transition-metal complexes*. Chemical Reviews, 2002. **102**(4): p. 993-1018.

89.   Williams, R.J.P., *Role of transition metal ions in biological processes*. Royal Institute of Chemistry, Reviews, 1968. **1**(1): p. 13-38.

90.   Anastassopoulou, J. and T. Theophanides, *The role of metal ions in biological systems and medicine*, in *Bioinorganic Chemistry*, D. Kessissoglou, Editor. 1995, Springer Netherlands. p. 209-218.

91.   Stolz, D.B., et al., *Peroxisomal localization of inducible nitric oxide synthase in hepatocytes*. Hepatology, 2002. **36**(1): p. 81-93.

92.   Singh, R.J., et al., *Mechanism of nitric oxide release from S-nitrosothiols*. Journal of Biological Chemistry, 1996. **271**(31): p. 18596-603.

93.   Ferrero, R., et al., *Comparative effects of several nitric oxide donors on intracellular cyclic GMP levels in bovine chromaffin cells: correlation with nitric oxide production*. British Journal of Pharmacology, 1999. **127**(3): p. 779-87.

94.   Demchenko, A.P., *The concept of lambda-ratiometry in fluorescence sensing and imaging*. Journal of Fluorescence, 2010. **20**(5): p. 1099-128.

Chapter 5: Overall Perspectives

This dissertation has outlined multiphoton excitation-based techniques to dynamically control the chemical, mechanical, and topographical presentation of cellular microenvironments. The work is demonstrated using micro-three dimensional protein hydrogels, which have been used as *in vitro* cell culture platforms to promote cell behaviors, including adhesion, alignment, and migration [1-5]. This work augments technologies developed previously in the Shear Group by providing means to introduce localized, sub-cellular contact guidance cues within protein hydrogels after fabrication. Efforts to extend these methods to other polymeric systems are planned, and they should be used to gain a better understanding of the spatiotemporal complexity of the cell-matrix interaction.

Numerous researchers have demonstrated that chemotaxis and durotaxis are viable solutions for dictating cell migration, yet a dearth of 3D capable platforms exists [6-9]. Currently, studies are underway to investigate the effects of chemical and mechanical gradients generated using the laser-based methods introduced in this dissertation on cell migration, with the hope of translating these results to 3D hydrogel scaffolds. Furthermore, future efforts should exploit the decoupling potential of these methods to evaluate the interplay between cues, and then optimize cue combinations within hydrogel scaffolds to promote successful tissue regeneration.

Research involving dynamic culture systems is still in its infancy, and many questions regarding the roles of extracellular matrix changes in embryonic and pathological development remain unanswered [10]. One potential method to monitor cellular responses to dynamic extracellular changes in real-time is via the fluorescent nitric oxide probes characterized in this work. Nitric oxide is a ubiquitous signaling

molecule that mediates many cell behaviors, including vasodilation, mechanotransduction, cell migration, and cell death [11-15]. By combining the probes with dynamic protein hydrogels via cell loading or direct hydrogel conjugation, specific roles for nitric oxide in cellular responses to dynamic extracellular changes can be defined. Additional research is recommended to quantify the impacts of on-the-fly changes to the mechanical or topographical properties of protein hydrogels on cell behavior.

The field of tissue engineering has progressed at an incredibly rapid pace within the last 20 years; however, translational technologies continue to elude researchers [16]. Some challenges associated with the transition from *in vitro* studies to clinical trials have been overcome through the development of more representative, 3D culture systems, such as hydrogels. The added ability to control the presentation of extracellular matrix properties differentially and independently with a high degree of spatiotemporal resolution within hydrogels is a significant advance in the field. Additionally, the innovative approaches discussed in this dissertation can complement existing technologies, and should have wide-ranging impacts on the design of next-generation scaffolds for tissue engineering.

REFERENCES

1.   Seidlits, S.K., C.E. Schmidt, and J.B. Shear, *High-resolution patterning of hydrogels in three dimensions using direct-write photofabrication for cell guidance*. Advanced Functional Materials, 2009. **19**(22): p. 3543-3551.

2.   Kaehr, B., et al., *Direct-write fabrication of functional protein matrixes using a low-cost Q-switched laser*. Analytical Chemistry, 2006. **78**(9): p. 3198-202.

3.   Pins, G.D., et al., *Multiphoton excited fabricated nano and micro patterned extracellular matrix proteins direct cellular morphology*. Journal of Biomedical Materials Research A, 2006. **78**(1): p. 194-204.

4.   Kaehr, B., et al., *Guiding neuronal development with in situ microfabrication*. Proceedings of the National Academy of Sciences, 2004. **101**(46): p. 16104-16108.

5.   Chen, X., et al., *Cell adhesion on micro-structured fibronectin gradients fabricated by multiphoton excited photochemistry*. Cellular and Molecular Bioengineering, 2012. **5**(3): p. 307-319.

6.   Kapur, T.A. and M.S. Shoichet, *Immobilized concentration gradients of nerve growth factor guide neurite outgrowth*. Journal of Biomedical Materials Research A, 2004. **68**(2): p. 235-43.

7.   DeLong, S.A., J.J. Moon, and J.L. West, *Covalently immobilized gradients of bFGF on hydrogel scaffolds for directed cell migration*. Biomaterials, 2005. **26**(16): p. 3227-34.

8.   Vincent, L.G., et al., *Mesenchymal stem cell durotaxis depends on substrate stiffness gradient strength*. Biotechnology Journal, 2013. **8**(4): p. 472-84.

9.   Isenberg, B.C., et al., *Vascular smooth muscle cell durotaxis depends on substrate stiffness gradient strength*. Biophysical Journal, 2009. **97**(5): p. 1313-1322.

10.   Burdick, J.A. and W.L. Murphy, *Moving from static to dynamic complexity in hydrogel design*. Nature Communications, 2012. **3**: p. 1269.

11.   Bogdan, C., *Nitric oxide and the regulation of gene expression*. Trends in Cell Biology, 2001. **11**(2): p. 66-75.

12.   Ignarro, L.J., *Nitric oxide as a unique signaling molecule in the vascular system: a historical overview*. Journal of Physiology and Pharmacology, 2002. **53**(4 Pt 1): p. 503-14.

13.   Shyy, J.Y. and S. Chien, *Role of integrins in endothelial mechanosensing of shear stress*. Circulation Research, 2002. **91**(9): p. 769-75.

14. Harrison, D.G., et al., *Endothelial mechanotransduction, nitric oxide and vascular inflammation*. Journal of Internal Medicine, 2006. **259**(4): p. 351-63.

15. Blaise, G.A., et al., *Nitric oxide, cell signaling and cell death*. Toxicology, 2005. **208**(2): p. 177-92.

16. Fisher, M.B. and R.L. Mauck, *Tissue engineering and regenerative medicine: recent innovations and the transition to translation*. Tissue Engingeering Part B Reviews, 2013. **19**(1): p. 1-13.

Bibliography

Adams, DN, et al., Growth cones turn and migrate up an immobilized gradient of the laminin ikvav peptide. Journal of Neurobiology, 2005. 62(1): p. 134-147.

Ahmed, Z and Brown, RA, Adhesion, alignment, and migration of cultured schwann cells on ultrathin fibronectin fibres. Cell Motility and the Cytoskeleton, 1999. 42(4): p. 331-343.

Akira, S, Uematsu, S, and Takeuchi, O, Pathogen recognition and innate immunity. Cell, 2006. 124(4): p. 783-801.

Al-Haque, S, et al., Hydrogel substrate stiffness and topography interact to induce contact guidance in cardiac fibroblasts. Macromolecular Bioscience, 2012. 12(10): p. 1342-1353.

Alderton, WK, Cooper, CE, and Knowles, RG, Nitric oxide synthases: Structure, function and inhibition. Biochemical Journal, 2001. 357(Pt 3): p. 593-615.

Alfa, RW, Tuszynski, MH, and Blesch, A, A novel inducible tyrosine kinase receptor to regulate signal transduction and neurite outgrowth. Journal of Neuroscience Research, 2009. 87(12): p. 2624-2631.

Allen, BW, Liu, J, and Piantadosi, CA, Electrochemical detection of nitric oxide in biological fluids. Methods in Enzymology, 2005. 396: p. 68-77.

Anastassopoulou, J and Theophanides, T, The role of metal ions in biological systems and medicine, in Bioinorganic chemistry, 1995, p. 209-218.

Artavanis-Tsakonas, S, Rand, MD, and Lake, RJ, Notch signaling: Cell fate control and signal integration in development. Science, 1999. 284(5415): p. 770-776.

Baker, AM, et al., Lysyl oxidase enzymatic function increases stiffness to drive colorectal cancer progression through fak. Oncogene, 2013. 32(14): p. 1863-1868.

Baker, BM and Chen, CS, Deconstructing the third dimension: How 3d culture microenvironments alter cellular cues. Journal of Cell Science, 2012. 125(Pt 13): p. 3015-3024.

Balgude, AP, et al., Agarose gel stiffness determines rate of drg neurite extension in 3d cultures. Biomaterials, 2001. 22(10): p. 1077-1084.

Banerjee, A, et al., The influence of hydrogel modulus on the proliferation and differentiation of encapsulated neural stem cells. Biomaterials, 2009. 30(27): p. 4695-4699.

Barouch, LA, et al., Nitric oxide regulates the heart by spatial confinement of nitric oxide synthase isoforms. Nature, 2002. 416(6878): p. 337-339.

Basu, S and Campagnola, PJ, Properties of crosslinked protein matrices for tissue engineering applications synthesized by multiphoton excitation. Journal of Biomedical Materials Research A, 2004. 71(2): p. 359-368.

Basu, S, et al., Multiphoton excited fabrication of collagen matrixes cross-linked by a modified benzophenone dimer: Bioactivity and enzymatic degradation. Biomacromolecules, 2005. 6(3): p. 1465-1474.

Becker, MM and Wang, Z, Origin of ultraviolet damage in DNA. Journal of Molecular Biology, 1989. 210(3): p. 429-438.

Bellido, E, et al., Controlling the number of proteins with dip-pen nanolithography. Advanced Materials, 2010. 22(3): p. 352-355.

Bettinger, CJ, Langer, R, and Borenstein, JT, Engineering substrate topography at the micro- and nanoscale to control cell function. Angewandte Chemie International Edition, 2009. 48(30): p. 5406-5415.

Binder, WH and Sachsenhofer, R, 'Click' chemistry in polymer and materials science. Macromolecular Rapid Communications, 2007. 28(1): p. 15-54.

Blaise, GA, et al., Nitric oxide, cell signaling and cell death. Toxicology, 2005. 208(2): p. 177-192.

Bogdan, C, Nitric oxide and the immune response. Nature Immunology, 2001. 2(10): p. 907-916.

Bogdan, C, Nitric oxide and the regulation of gene expression. Trends in Cell Biology, 2001. 11(2): p. 66-75.

Boje, KM and Arora, PK, Microglial-produced nitric oxide and reactive nitrogen oxides mediate neuronal cell death. Brain Research, 1992. 587(2): p. 250-256.

Bonneh-Barkay, D and Wiley, CA, Brain extracellular matrix in neurodegeneration. Brain Pathology, 2009. 19(4): p. 573-585.

Boo, YC, et al., Detection of low levels of nitric oxide using an electrochemical sensor. Methods in Molecular Biology, 2011. 704: p. 81-89.

Boote Jones, EN and Mallapragada, SK, Directed growth and differentiation of stem cells towards neural cell fates using soluble and surface-mediated cues. Journal of Biomaterials Science Polymer Edition, 2007. 18(8): p. 999-1015.

Boudko, DY, High-resolution capillary electrophoresis of nitrite and nitrate in biological samples. Methods in Molecular Biology, 2004. 279: p. 9-19.

Bozkurt, A, et al., In vitro cell alignment obtained with a schwann cell enriched microstructured nerve guide with longitudinal guidance channels. Biomaterials, 2009. 30(2): p. 169-179.

Brookes, PS, Mitochondrial nitric oxide synthase. Mitochondrion, 2004. 3(4): p. 187-204.

Brune, B, Nitric oxide: No apoptosis or turning it on? Cell Death and Differentiation, 2003. 10(8): p. 864-869.

Bryan, NS and Grisham, MB, Methods to detect nitric oxide and its metabolites in biological samples. Free Radical Biology and Medicine, 2007. 43(5): p. 645-657.

Bryant, DM and Mostov, KE, From cells to organs: Building polarized tissue. Nature Reviews Molecular Cell Biology, 2008. 9(11): p. 887-901.

Bryant, SJ, Nuttelman, CR, and Anseth, KS, Cytocompatibility of uv and visible light photoinitiating systems on cultured nih/3t3 fibroblasts in vitro. Journal of Biomaterials Science Polymer Edition, 2000. 11(5): p. 439-457.

Burdick, JA, et al., Controlled degradation and mechanical behavior of photopolymerized hyaluronic acid networks. Biomacromolecules, 2005. 6(1): p. 386-391.

Burdick, JA and Murphy, WL, Moving from static to dynamic complexity in hydrogel design. Nature Communications, 2012. 3: p. 1269.

Buxboim, A, et al., How deeply cells feel: Methods for thin gels. Journal of Physics Condensed Matter, 2010. 22(19): p. 194116.

Cai, L, et al., Photocured biodegradable polymer substrates of varying stiffness and microgroove dimensions for promoting nerve cell guidance and differentiation. Langmuir, 2012. 28(34): p. 12557-12568.

Camci-Unal, G, et al., Hydrogel surfaces to promote attachment and spreading of endothelial progenitor cells. Journal of Tissue Engineering Regenerative Medicine, 2013. 7(5): p. 337-347.

Cao, X and Shoichet, MS, Defining the concentration gradient of nerve growth factor for guided neurite outgrowth. Neuroscience, 2001. 103(3): p. 831-840.

Cao, X and Shoichet, MS, Investigating the synergistic effect of combined neurotrophic factor concentration gradients to guide axonal growth. Neuroscience, 2003. 122(2): p. 381-389.

Carrel, AaB, Montrose T., Cultivation of tissues in vitro and its technique. Journal of Experimental Medicine, 1911. 13: p. 387-396.

Chao, MV, Neurotrophins and their receptors: A convergence point for many signalling pathways. Nature Reviews Neuroscience, 2003. 4(4): p. 299-309.

Charest, JL, Garcia, AJ, and King, WP, Myoblast alignment and differentiation on cell culture substrates with microscale topography and model chemistries. Biomaterials, 2007. 28(13): p. 2202-2210.

Charest, JM, et al., Fabrication of substrates with defined mechanical properties and topographical features for the study of cell migration. Macromolecular Bioscience, 2012. 12(1): p. 12-20.

Chen, B, et al., Geometric control of cell migration. Scientific Reports, 2013. 3: p. 2827.

Chen, CS, et al., Geometric control of cell life and death. Science, 1997. 276(5317): p. 1425-1428.

Chen, CS, Tan, J, and Tien, J, Mechanotransduction at cell-matrix and cell-cell contacts. Annual Review Biomedical Engineering, 2004. 6: p. 275-302.

Chen, X, et al., Cell adhesion on micro-structured fibronectin gradients fabricated by multiphoton excited photochemistry. Cellular and Molecular Bioengineering, 2012. 5(3): p. 307-319.

Cheung, YK, et al., Microscale control of stiffness in a cell-adhesive substrate using microfluidics-based lithography. Angewandte Chemie International Edition, 2009. 48(39): p. 7188-7192.

Choi, D-G, et al., Particle arrays with patterned pores by nanomachining with colloidal masks. Journal of the American Chemical Society, 2005. 127(6): p. 1636-1637.

Chou, SY, Krauss, PR, and Renstrom, PJ, Imprint of sub-25 nm vias and trenches in polymers. Applied Physics Letters, 1995. 67(21): p. 3114-3116.

Clapham, DE, Calcium signaling. Cell, 2007. 131(6): p. 1047-1058.

Clark, P, et al., Cell guidance by ultrafine topography in vitro. Journal of Cell Science, 1991. 99 (Pt 1): p. 73-77.

Colavitti, R, et al., Reactive oxygen species as downstream mediators of angiogenic signaling by vascular endothelial growth factor receptor-2/kdr. Journal of Biological Chemistry, 2002. 277(5): p. 3101-3108.

Collinsworth, AM, et al., Apparent elastic modulus and hysteresis of skeletal muscle cells throughout differentiation. American Journal of Physiology Cell Physiology, 2002. 283(4): p. C1219-1227.

Connell, JL, Characterization and microfabrication of environmentally sensitive materials for studying bacterial group behaviors. 2012, The University of Texas at Austin.

Coppola, V, et al., Ablation of trka function in the immune system causes b cell abnormalities. Development, 2004. 131(20): p. 5185-5195.

Curtis, A and Wilkinson, C, Topographical control of cells. Biomaterials, 1997. 18(24): p. 1573-1583.

Curtis, AS, Dalby, MJ, and Gadegaard, N, Nanoprinting onto cells. Journal of the Royal Society Interface, 2006. 3(8): p. 393-398.

Curtis, AS and Varde, M, Control of cell behavior: Topological factors. Journal of the National Cancer Instititute, 1964. 33: p. 15-26.

Dalby, MJ, Gadegaard, N, and Oreffo, RO, Harnessing nanotopography and integrin-matrix interactions to influence stem cell fate. Nature Materials, 2014. 13(6): p. 558-569.

Dalby, MJ, et al., Nucleus alignment and cell signaling in fibroblasts: Response to a micro-grooved topography. Experimental Cell Research, 2003. 284(2): p. 272-280.

Davis, KA, Burdick, JA, and Anseth, KS, Photoinitiated crosslinked degradable copolymer networks for tissue engineering applications. Biomaterials, 2003. 24(14): p. 2485-2495.

Davis, KA, et al., Dynamic cell behavior on shape memory polymer substrates. Biomaterials, 2011. 32(9): p. 2285-2293.

De Silva, PA, Gunaratne, NHQ, and Mccoy, CP, A molecular photoionic and gate based on fluorescent signalling. Nature, 1993. 364(6432): p. 42-44.

Deforest, CA, Polizzotti, BD, and Anseth, KS, Sequential click reactions for synthesizing and patterning three-dimensional cell microenvironments. Nature Materials, 2009. 8(8): p. 659-664.

Degroot, J, The age of the matrix: Chemistry, consequence and cure. Current Opinion in Pharmacology, 2004. 4(3): p. 301-305.

Deister, C, Aljabari, S, and Schmidt, CE, Effects of collagen 1, fibronectin, laminin and hyaluronic acid concentration in multi-component gels on neurite extension. Journal of Biomaterials Science Polymer Edition, 2007. 18(8): p. 983-997.

Delong, SA, Moon, JJ, and West, JL, Covalently immobilized gradients of bfgf on hydrogel scaffolds for directed cell migration. Biomaterials, 2005. 26(16): p. 3227-3234.

Demchenko, AP, The concept of lambda-ratiometry in fluorescence sensing and imaging. Journal of Fluorescence, 2010. 20(5): p. 1099-1128.

Dertinger, SKW, et al., Generation of gradients having complex shapes using microfluidic networks. Analytical Chemistry, 2001. 73(6): p. 1240-1246.

Dhoot, NO, et al., Peptide-modified alginate surfaces as a growth permissive substrate for neurite outgrowth. Journal of Biomedical Materials Research A, 2004. 71(2): p. 191-200.

Dickinson, LE, et al., Endothelial cell responses to micropillar substrates of varying dimensions and stiffness. Journal of Biomedical Materials Research A, 2012. 100(6): p. 1457-1466.

Dimilla, PA, et al., Maximal migration of human smooth muscle cells on fibronectin and type iv collagen occurs at an intermediate attachment strength. Journal of Cell Biology, 1993. 122(3): p. 729-737.

167

Dimitriadis, EK, et al., Determination of elastic moduli of thin layers of soft material using the atomic force microscope. Biophysical Journal. 82(5): p. 2798-2810.

Discher, DE, Janmey, P, and Wang, Y-L, Tissue cells feel and respond to the stiffness of their substrate. Science, 2005. 310(5751): p. 1139-1143.

Donovan, MJ, et al., Brain derived neurotrophic factor is an endothelial cell survival factor required for intramyocardial vessel stabilization. Development, 2000. 127(21): p. 4531-4540.

Dorman, G and Prestwich, GD, Benzophenone photophores in biochemistry. Biochemistry, 1994. 33(19): p. 5661-5673.

Droge, W, Free radicals in the physiological control of cell function. Physiological Reviews, 2002. 82(1): p. 47-95.

Dubey, N, Letourneau, PC, and Tranquillo, RT, Guided neurite elongation and schwann cell invasion into magnetically aligned collagen in simulated peripheral nerve regeneration. Experimental Neurology, 1999. 158(2): p. 338-350.

Edahiro, J-I, et al., In situ control of cell adhesion using photoresponsive culture surface. Biomacromolecules, 2005. 6(2): p. 970-974.

Eguchi, Y, Ogiue-Ikeda, M, and Ueno, S, Control of orientation of rat schwann cells using an 8-t static magnetic field. Neuroscience Letters, 2003. 351(2): p. 130-132.

Engler, AJ, et al., Surface probe measurements of the elasticity of sectioned tissue, thin gels and polyelectrolyte multilayer films: Correlations between substrate stiffness and cell adhesion. Surface Science, 2004. 570(1–2): p. 142-154.

Engler, AJ, et al., Matrix elasticity directs stem cell lineage specification. Cell, 2006. 126(4): p. 677-689.

Esch, T, Lemmon, V, and Banker, G, Local presentation of substrate molecules directs axon specification by cultured hippocampal neurons. Journal of Neuroscience, 1999. 19(15): p. 6417-6426.

Even-Ram, S and Yamada, KM, Cell migration in 3d matrix. Current Opinion in Cell Biology, 2005. 17(5): p. 524-532.

Falconnet, D, et al., Surface engineering approaches to micropattern surfaces for cell-based assays. Biomaterials, 2006. 27(16): p. 3044-3063.

Feneley, MR, Fawcett, JW, and Keynes, RJ, The role of schwann cells in the regeneration of peripheral nerve axons through muscle basal lamina grafts. Experimental Neurololgy, 1991. 114(3): p. 275-285.

Feron, O, et al., Endothelial nitric oxide synthase targeting to caveolae. Specific interactions with caveolin isoforms in cardiac myocytes and endothelial cells. Journal of Biological Chemistry, 1996. 271(37): p. 22810-22814.

Ferrero, R, et al., Comparative effects of several nitric oxide donors on intracellular cyclic gmp levels in bovine chromaffin cells: Correlation with nitric oxide production. British Journal of Pharmacology, 1999. 127(3): p. 779-787.

Fischer, ME, Amine coupling through edc/nhs: A practical approach, in Surface plasmon resonance, N.J. Mol and M.J.E. Fischer, Editors. 2010, Humana Press. p. 55-73.

Fisher, MB and Mauck, RL, Tissue engineering and regenerative medicine: Recent innovations and the transition to translation. Tissue Engingeering Part B Reviews, 2013. 19(1): p. 1-13.

Forciniti, L, et al., Schwann cell response on polypyrrole substrates upon electrical stimulation. Acta Biomaterialia, 2014. 10(6): p. 2423-2433.

Ford, PC and Lorkovic, IM, Mechanistic aspects of the reactions of nitric oxide with transition-metal complexes. Chemical Reviews, 2002. 102(4): p. 993-1018.

Fozdar, DY, et al., Selective axonal growth of embryonic hippocampal neurons according to topographic features of various sizes and shapes. International Journal of Nanomedicine, 2011. 6: p. 45-57.

Frantz, C, Stewart, KM, and Weaver, VM, The extracellular matrix at a glance. Journal of Cell Science, 2010. 123(Pt 24): p. 4195-4200.

Fraser, SA, et al., Sub-micron and nanoscale feature depth modulates alignment of stromal fibroblasts and corneal epithelial cells in serum-rich and serum-free media. Journal of Biomedical Materials Research A, 2008. 86(3): p. 725-735.

Freedman, NJ and Lefkowitz, RJ, Desensitization of g protein-coupled receptors. Recent Progress in Hormonal Research, 1996. 51: p. 319-351; discussion 352-313.

Frisman, I, et al., Stimulus-responsive hydrogels made from biosynthetic fibrinogen conjugates for tissue engineering: Structural characterization. Langmuir, 2011. 27(11): p. 6977-6986.

Fugleholm, K, Schmalbruch, H, and Krarup, C, Early peripheral nerve regeneration after crushing, sectioning, and freeze studied by implanted electrodes in the cat. Journal of Neuroscience, 1994. 14(5 Pt 1): p. 2659-2673.

Furchgott, RF and Vanhoutte, PM, Endothelium-derived relaxing and contracting factors. FASEB Journal, 1989. 3(9): p. 2007-2018.

Gacesa, P, Alginates. Carbohydrate Polymers, 1988. 8(3): p. 161-182.

Galardy, RE, et al., Photoaffinity labeling of peptide hormone binding sites. Journal of Biological Chemistry, 1974. 249(11): p. 3510-3518.

Galbraith, CG and Sheetz, MP, Forces on adhesive contacts affect cell function. Current Opinion Cell Biology, 1998. 10(5): p. 566-571.

Galbraith, CG, Yamada, KM, and Sheetz, MP, The relationship between force and focal complex development. Journal of Cell Biology, 2002. 159(4): p. 695-705.

Gao, S, et al., Docking of endothelial nitric oxide synthase (enos) to the mitochondrial outer membrane: A pentabasic amino acid sequence in the autoinhibitory domain of enos targets a proteinase k-cleavable peptide on the cytoplasmic face of mitochondria. Journal of Biological Chemistry, 2004. 279(16): p. 15968-15974.

Geiger, B, Spatz, JP, and Bershadsky, AD, Environmental sensing through focal adhesions. Nature Reviews Molecular Cell Biology, 2009. 10(1): p. 21-33.

Georges, PC, et al., Increased stiffness of the rat liver precedes matrix deposition: Implications for fibrosis. American Journal of Physiology Gastrointestinal Liver Physiology, 2007. 293(6): p. G1147-1154.

Georges, PC, et al., Matrices with compliance comparable to that of brain tissue select neuronal over glial growth in mixed cortical cultures. Biophysical Journal, 2006. 90(8): p. 3012-3018.

Ghebremariam, YT, et al., Characterization of a fluorescent probe for imaging nitric oxide. Journal of Vascular Research, 2014. 51(1): p. 68-79.

Gillette, BM, et al., Dynamic hydrogels: Switching of 3d microenvironments using two-component naturally derived extracellular matrices. Advanced Materials, 2010. 22(6): p. 686-691.

Goldner, JS, et al., Neurite bridging across micropatterned grooves. Biomaterials, 2006. 27(3): p. 460-472.

Gomez, N, Chen, SC, and Schmidt, CE, Polarization of hippocampal neurons with competitive surface stimuli: Contact guidance cues are preferred over chemical ligands. Journal of the Royal Society Interface, 2007. 4(13): p. 223-233.

Gomez, N, et al., Immobilized nerve growth factor and microtopography have distinct effects on polarization versus axon elongation in hippocampal cells in culture. Biomaterials, 2007. 28(2): p. 271-284.

Goody, MF and Henry, CA, Dynamic interactions between cells and their extracellular matrix mediate embryonic development. Molecular Reproduction and Development, 2010. 77(6): p. 475-488.

Göppert-Mayer, M, Elementary processes with two quantum transitions. Annalen der Physik, 1931. 18(7-8): p. 466-479.

Gray, DS, Tien, J, and Chen, CS, Repositioning of cells by mechanotaxis on surfaces with micropatterned young's modulus. Journal of Biomedical Materials Research A, 2003. 66(3): p. 605-614.

Grewe, BF, et al., High-speed in vivo calcium imaging reveals neuronal network activity with near-millisecond precision. Nature Methods, 2010. 7(5): p. 399-405.

Grienberger, C and Konnerth, A, Imaging calcium in neurons. Neuron, 2012. 73(5): p. 862-885.

Griess, P, Bemerkungen zu der abhandlung der hh. Weselsky und benedikt „ueber einige azoverbindungen" . Berichte der deutschen chemischen Gesellschaft, 1879. 12(1): p. 426-428.

Gulati, AK, Evaluation of acellular and cellular nerve grafts in repair of rat peripheral nerve. Journal of Neurosurgery, 1988. 68(1): p. 117-123.

Gundersen, RW and Barrett, JN, Neuronal chemotaxis: Chick dorsal-root axons turn toward high concentrations of nerve growth factor. Science, 1979. 206(4422): p. 1079-1080.

Gundersen, RW and Barrett, JN, Characterization of the turning response of dorsal root neurites toward nerve growth factor. Journal of Cell Biology, 1980. 87(3 Pt 1): p. 546-554.

Gupta, SK and Vlahakis, NE, Integrin alpha9beta1 mediates enhanced cell migration through nitric oxide synthase activity regulated by src tyrosine kinase. Journal of Cell Science, 2009. 122(Pt 12): p. 2043-2054.

Guvendiren, M and Burdick, JA, The control of stem cell morphology and differentiation by hydrogel surface wrinkles. Biomaterials, 2010. 31(25): p. 6511-6518.

Guvendiren, M and Burdick, JA, Stem cell response to spatially and temporally displayed and reversible surface topography. Advanced Healthcare Materials, 2013. 2(1): p. 155-164.

Hahn, MS, et al., Photolithographic patterning of polyethylene glycol hydrogels. Biomaterials, 2006. 27(12): p. 2519-2524.

Hale, NA, Yang, Y, and Rajagopalan, P, Cell migration at the interface of a dual chemical-mechanical gradient. Applied Materials & Interfaces, 2010. 2(8): p. 2317-2324.

Harburger, DS and Calderwood, DA, Integrin signalling at a glance. Journal of Cell Science, 2009. 122(Pt 2): p. 159-163.

Harrison, DG, et al., Endothelial mechanotransduction, nitric oxide and vascular inflammation. Journal of Internal Medicine, 2006. 259(4): p. 351-363.

Harrison, RG, The outgrowth of the nerve fiber as a mode of protoplasmic movement. Journal of Experimental Zoology, 1910. 9(4): p. 787-846.

Hatten, ME, Central nervous system neuronal migration. Annual Review Neuroscience, 1999. 22: p. 511-539.

Hell, SW, et al., Two-photon near- and far-field fluorescence microscopy with continuous-wave excitation. Optical Letters, 1998. 23(15): p. 1238-1240.

Hennink, WE and Van Nostrum, CF, Novel crosslinking methods to design hydrogels. Advanced Drug Delivery Reviews, 2012. 64, Supplement(0): p. 223-236.

Hermanson, GT, Bioconjugate techniques. 2013: Elsevier Science & Technology Books.

Hertz, H, Über die berührung fester elastischer körper (on the contact of elastic solids). Journal fur die Reine Angewandte Mathematik, 1881. 92: p. 156-171.

Hill, RT, et al., Microfabrication of three-dimensional bioelectronic architectures. Journal of the American Chemical Society, 2005. 127(30): p. 10707-10711.

Hoffman, BD, Grashoff, C, and Schwartz, MA, Dynamic molecular processes mediate cellular mechanotransduction. Nature, 2011. 475(7356): p. 316-323.

Hoffman-Kim, D, Mitchel, JA, and Bellamkonda, RV, Topography, cell response, and nerve regeneration. Annual Review Biomedical Engineering, 2010. 12: p. 203-231.

Hoffmann, JC and West, JL, Three-dimensional photolithographic patterning of multiple bioactive ligands in poly(ethylene glycol) hydrogels. Soft Matter, 2010. 6(20): p. 5056-5063.

Hope, BT, et al., Neuronal nadph diaphorase is a nitric oxide synthase. Proceedings of the National Academy of Sciences, 1991. 88(7): p. 2811-2814.

Hoppe, TJ, Laser-based techniques for manipulating the single-cell environment. 2013, The University of Texas at Austin.

Hu, F, et al., Effects of epidermal growth factor and basic fibroblast growth factor on the proliferation and osteogenic and neural differentiation of adipose-derived stem cells. Cell Reprogramming, 2013. 15(3): p. 224-232.

Hu, ML and Tappel, AL, Potentiation of oxidative damage to proteins by ultraviolet-a and protection by antioxidants. Photochemistry and Photobiology, 1992. 56(3): p. 357-363.

Huang, EJ and Reichardt, LF, Trk receptors: Roles in neuronal signal transduction. Annual Review Biochemistry, 2003. 72: p. 609-642.

Huynh, J, et al., Age-related intimal stiffening enhances endothelial permeability and leukocyte transmigration. Science Translational Medicine, 2011. 3(112): p. 112ra122.

Hynes, RO, Integrins: Versatility, modulation, and signaling in cell adhesion. Cell, 1992. 69(1): p. 11-25.

Hypolite, CL, et al., Formation of microscale gradients of protein using heterobifunctional photolinkers. Bioconjugate Chemistry, 1997. 8(5): p. 658-663.

Ide, C, et al., Schwann cell basal lamina and nerve regeneration. Brain Research, 1983. 288(1-2): p. 61-75.

Ifkovits, JL and Burdick, JA, Review: Photopolymerizable and degradable biomaterials for tissue engineering applications. Tissue Engineering, 2007. 13(10): p. 2369-2385.

Ignarro, LJ, Nitric oxide as a unique signaling molecule in the vascular system: A historical overview. Journal of Physiology and Pharmacology, 2002. 53(4 Pt 1): p. 503-514.

Ignarro, LJ, et al., Endothelium-derived relaxing factor produced and released from artery and vein is nitric oxide. Proceedings of the National Academy of Sciences, 1987. 84(24): p. 9265-9269.

Ingber, DE, Cellular mechanotransduction: Putting all the pieces together again. FASEB Journal, 2006. 20(7): p. 811-827.

Isenberg, BC, et al., Vascular smooth muscle cell durotaxis depends on substrate stiffness gradient strength. Biophysical Journal, 2009. 97(5): p. 1313-1322.

Jaalouk, DE and Lammerding, J, Mechanotransduction gone awry. Nature Reviews Molecular Cell Biology, 2009. 10(1): p. 63-73.

Jacobson, MD, Weil, M, and Raff, MC, Programmed cell death in animal development. Cell, 1997. 88(3): p. 347-354.

Jagnandan, D, Sessa, WC, and Fulton, D, Intracellular location regulates calcium-calmodulin-dependent activation of organelle-restricted enos. American Journal of Physiology Cell Physiology, 2005. 289(4): p. C1024-1033.

Jang, JW, Smetana, A, and Stiles, P, Multi-ink pattern generation by dip-pen nanolithography. Scanning, 2010. 32(1): p. 24-29.

Jeon, O, et al., Photocrosslinked alginate hydrogels with tunable biodegradation rates and mechanical properties. Biomaterials, 2009. 30(14): p. 2724-2734.

Jiang, FX, et al., The relationship between fibroblast growth and the dynamic stiffnesses of a DNA crosslinked hydrogel. Biomaterials, 2010. 31(6): p. 1199-1212.

Jiang, X, et al., Directing cell migration with asymmetric micropatterns. Proceedings of the National Academy of Sciences, 2005. 102(4): p. 975-978.

Jobgen, WS, et al., Analysis of nitrite and nitrate in biological samples using high-performance liquid chromatography. Journal of Chromatogr B Analytical Technologies in the Biomedical Life Sciences, 2007. 851(1-2): p. 71-82.

Johansson, F, et al., Axonal outgrowth on nano-imprinted patterns. Biomaterials, 2006. 27(8): p. 1251-1258.

Kaehr, B, et al., Guiding neuronal development with in situ microfabrication. Proceedings of the National Academy of Sciences, 2004. 101(46): p. 16104-16108.

Kaehr, B, et al., Direct-write fabrication of functional protein matrixes using a low-cost q-switched laser. Analytical Chemistry, 2006. 78(9): p. 3198-3202.

Kaehr, B and Shear, JB, Mask-directed multiphoton lithography. Journal of the American Chemical Society, 2007. 129(7): p. 1904-1905.

Kaehr, B and Shear, JB, Multiphoton fabrication of chemically responsive protein hydrogels for microactuation. Proceedings of the National Academy of Sciences, 2008. 105(26): p. 8850-8854.

Kaiser, W and Garrett, CGB, Two-photon excitation in ca. Physical Review Letters, 1961. 7(6): p. 229-231.

Kalia, J and Raines, RT, Advances in bioconjugation. Current Organic Chemistry, 2010. 14(2): p. 138-147.

Kapur, TA and Shoichet, MS, Immobilized concentration gradients of nerve growth factor guide neurite outgrowth. Journal of Biomedical Materials Research A, 2004. 68(2): p. 235-243.

Katsamanis, F and Raftopoulos, DD, Determination of mechanical properties of human femoral cortical bone by the hopkinson bar stress technique. Journal of Biomechanics, 1990. 23(11): p. 1173-1184.

Kawashima, S and Yokoyama, M, Dysfunction of endothelial nitric oxide synthase and atherosclerosis. Arteriosclerosis Thrombosis and Vascular Biology, 2004. 24(6): p. 998-1005.

Keenan, TM and Folch, A, Biomolecular gradients in cell culture systems. Lab on a Chip, 2008. 8(1): p. 34-57.

Kelm, M, Nitric oxide metabolism and breakdown. Biochimica et Biophysica Acta, 1999. 1411(2-3): p. 273-289.

Kelm, M and Schrader, J, Nitric oxide release from the isolated guinea pig heart. European Journal of Pharmacology, 1988. 155(3): p. 317-321.

Khetan, S, Katz, JS, and Burdick, JA, Sequential crosslinking to control cellular spreading in 3-dimensional hydrogels. Soft Matter, 2009. 5(8): p. 1601-1606.

Khripin, CY, Brinker, CJ, and Kaehr, B, Mechanically tunable multiphoton fabricated protein hydrogels investigated using atomic force microscopy. Soft Matter, 2010. 6(12): p. 2842-2848.

King, GL and Brownlee, M, The cellular and molecular mechanisms of diabetic complications. Endocrinology Metabolism Clinics of North America, 1996. 25(2): p. 255-270.

Kirschner, CM, et al., Clickable, photodegradable hydrogels to dynamically modulate valvular interstitial cell phenotype. Advanced Healthcare Materials, 2014. 3(5): p. 649-657.

Kirschner, CM and Anseth, KS, In situ control of cell substrate microtopographies using photolabile hydrogels. Small, 2013. 9(4): p. 578-584.

Kloxin, AM, Benton, JA, and Anseth, KS, In situ elasticity modulation with dynamic substrates to direct cell phenotype. Biomaterials, 2010. 31(1): p. 1-8.

Kloxin, AM, et al., Photodegradable hydrogels for dynamic tuning of physical and chemical properties. Science, 2009. 324(5923): p. 59-63.

Koepsel, JT and Murphy, WL, Patterning discrete stem cell culture environments via localized self-assembled monolayer replacement. Langmuir, 2009. 25(21): p. 12825-12834.

Kojima, H, et al., Fluorescent indicators for imaging nitric oxide production. Angew Chemie International Edition, 1999. 38(21): p. 3209-3212.

Kolb, HC, Finn, MG, and Sharpless, KB, Click chemistry: Diverse chemical function from a few good reactions. Angew Chemie International Edition, 2001. 40(11): p. 2004-2021.

Kosaka, N, et al., Fgf-4 regulates neural progenitor cell proliferation and neuronal differentiation. FASEB Journal, 2006. 20(9): p. 1484-1485.

Kraning-Rush, CM, et al., Quantifying traction stresses in adherent cells. Methods in Cell Biology, 2012. 110: p. 139-178.

Kraning-Rush, CM and Reinhart-King, CA, Controlling matrix stiffness and topography for the study of tumor cell migration. Cell Adhesion and Migration, 2012. 6(3): p. 274-279.

Krishnan, R, et al., Substrate stiffening promotes endothelial monolayer disruption through enhanced physical forces. American Journal of Physiology Cell Physiology, 2011. 300(1): p. C146-154.

Kroncke, KD, Fehsel, K, and Kolb-Bachofen, V, Nitric oxide: Cytotoxicity versus cytoprotection--how, why, when, and where? Nitric Oxide, 1997. 1(2): p. 107-120.

Kuberka, M, et al., Magnification of the pore size in biodegradable collagen sponges. The International Journal of Artificial Organs, 2002. 25(1): p. 67-73.

Kumar, A, Biebuyck, HA, and Whitesides, GM, Patterning self-assembled monolayers: Applications in materials science. Langmuir, 1994. 10(5): p. 1498-1511.

Kumar, A and Whitesides, G, Features of gold having micrometer to centimeter dimensions can be formed through a combination of stamping with an elastomeric stamp and an alkanethiol "ink" followed by chemical etching. Applied Physics Letters, 1993. 63(14): p. 2002-2004.

Kumar, S and Weaver, VM, Mechanics, malignancy, and metastasis: The force journey of a tumor cell. Cancer Metastasis Review, 2009. 28(1-2): p. 113-127.

Kuo, CH, et al., Complex stiffness gradient substrates for studying mechanotactic cell migration. Advanced Materials, 2012. 24(45): p. 6059-6064.

Kuo, CK and Ma, PX, Ionically crosslinked alginate hydrogels as scaffolds for tissue engineering: Part 1. Structure, gelation rate and mechanical properties. Biomaterials, 2001. 22(6): p. 511-521.

Lafratta, CN, et al., Multiphoton fabrication. Angewandte Chemie International Edition, 2007. 46(33): p. 6238-6258.

Lafratta, CN, Li, L, and Fourkas, JT, Soft-lithographic replication of 3d microstructures with closed loops. Proceedings of the National Academy of Sciences, 2006. 103(23): p. 8589-8594.

Lam, MT, Clem, WC, and Takayama, S, Reversible on-demand cell alignment using reconfigurable microtopography. Biomaterials, 2008. 29(11): p. 1705-1712.

Lancaster, JR, Jr., A tutorial on the diffusibility and reactivity of free nitric oxide. Nitric Oxide, 1997. 1(1): p. 18-30.

Larsen, M, et al., The matrix reorganized: Extracellular matrix remodeling and integrin signaling. Current Opinion in Cell Biology, 2006. 18(5): p. 463-471.

Leach, JB, et al., Development of photocrosslinkable hyaluronic acid-polyethylene glycol-peptide composite hydrogels for soft tissue engineering. Journal of Biomedical Materials Research A, 2004. 70(1): p. 74-82.

Lee, KY and Mooney, DJ, Alginate: Properties and biomedical applications. Progress in Polymer Science, 2012. 37(1): p. 106-126.

Lee, MR, et al., Direct differentiation of human embryonic stem cells into selective neurons on nanoscale ridge/groove pattern arrays. Biomaterials, 2010. 31(15): p. 4360-4366.

Lee, S-H, Moon, JJ, and West, JL, Three-dimensional micropatterning of bioactive hydrogels via two-photon laser scanning photolithography for guided 3d cell migration. Biomaterials, 2008. 29(20): p. 2962-2968.

Lee, SH, et al., Proteolytically degradable hydrogels with a fluorogenic substrate for studies of cellular proteolytic activity and migration. Biotechnology Progress, 2005. 21(6): p. 1736-1741.

Leone, AM, et al., A rapid and simple method for the measurement of nitrite and nitrate in plasma by high performance capillary electrophoresis. Biochemical and Biophysical Research Communications, 1994. 200(2): p. 951-957.

Letourneau, PC, Chemotactic response of nerve fiber elongation to nerve growth factor. Developmental Biology, 1978. 66(1): p. 183-196.

Leung, WY, et al., Fabrication of photonic band gap crystal using microtransfer molded templates. Journal of Applied Physics, 2003. 93(10): p. 5866-5870.

Li, GN and Hoffman-Kim, D, Tissue-engineered platforms of axon guidance. Tissue Engineering Part B Review, 2008. 14(1): p. 33-51.

Li, GN, Liu, J, and Hoffman-Kim, D, Multi-molecular gradients of permissive and inhibitory cues direct neurite outgrowth. Annals of Biomedical Engineering, 2008. 36(6): p. 889-904.

Li, H, et al., Two-photon optical properties of novel branched conjugated derivatives carrying benzophenone moiety with various electron donor-acceptor substituent groups. Journal of Fluorescence, 2011. 21(1): p. 393-407.

Li, N and Folch, A, Integration of topographical and biochemical cues by axons during growth on microfabricated 3-d substrates. Experimental Cell Research, 2005. 311(2): p. 307-316.

Li, Z, et al., Differential regulation of stiffness, topography, and dimension of substrates in rat mesenchymal stem cells. Biomaterials, 2013. 34(31): p. 7616-7625.

Lim, MH and Lippard, SJ, Metal-based turn-on fluorescent probes for sensing nitric oxide. Accounts of Chemical Research, 2007. 40(1): p. 41-51.

Lim, SH, et al., The effect of nanofiber-guided cell alignment on the preferential differentiation of neural stem cells. Biomaterials, 2010. 31(34): p. 9031-9039.

Lindsay, RM, Role of neurotrophins and trk receptors in the development and maintenance of sensory neurons: An overview. Philosophical Transactions of the Royal Society of London B: Biological Sciences, 1996. 351(1338): p. 365-373.

Liu, F, et al., Feedback amplification of fibrosis through matrix stiffening and cox-2 suppression. Journal of Cell Biology, 2010. 190(4): p. 693-706.

Liu, X, et al., Nitric oxide diffusion rate is reduced in the aortic wall. Biophysical Journal, 2008. 94(5): p. 1880-1889.

Lo, C-M, et al., Cell movement is guided by the rigidity of the substrate. Biophysical Journal, 2000. 79(1): p. 144-152.

Lo, CM, et al., Cell movement is guided by the rigidity of the substrate. Biophysical Journal, 2000. 79(1): p. 144-152.

Lu, D, et al., Differential regulation of morphology and stemness of mouse embryonic stem cells by substrate stiffness and topography. Biomaterials, 2014. 35(13): p. 3945-3955.

Lu, P, et al., Extracellular matrix degradation and remodeling in development and disease. Cold Spring Harbor Perspectives in Biology, 2011. 3(12).

Lundblad, RL, Chemical reagents for protein modification. Third ed. 2005: Taylor & Francis.

Luo, Y and Shoichet, MS, A photolabile hydrogel for guided three-dimensional cell growth and migration. Nature Materials, 2004. 3(4): p. 249-253.

Lutolf, MP, et al., Synthetic matrix metalloproteinase-sensitive hydrogels for the conduction of tissue regeneration: Engineering cell-invasion characteristics. Proceedings of the National Academy of Sciences, 2003. 100(9): p. 5413-5418.

Lutz, J-F and Zarafshani, Z, Efficient construction of therapeutics, bioconjugates, biomaterials and bioactive surfaces using azide–alkyne "click" chemistry. Advanced Drug Delivery Reviews, 2008. 60(9): p. 958-970.

Lv, X, et al., A specific fluorescent probe for no based on a new no-binding group. Chemical Communications, 2014. 50(56): p. 7499-7502.

Macmicking, JD, et al., Altered responses to bacterial infection and endotoxic shock in mice lacking inducible nitric oxide synthase. Cell, 1995. 81(4): p. 641-650.

Mahmud, G, et al., Directing cell motions on micropatterned ratchets. Nature Physics, 2009. 5(8): p. 606-612.

Mahoney, MJ, et al., The influence of microchannels on neurite growth and architecture. Biomaterials, 2005. 26(7): p. 771-778.

Maloney, JM, et al., Influence of finite thickness and stiffness on cellular adhesion-induced deformation of compliant substrata. Physical Review E, 2008. 78(4): p. 041923.

Marklein, RA, Soranno, DE, and Burdick, JA, Magnitude and presentation of mechanical signals influence adult stem cell behavior in 3-dimensional macroporous hydrogels. Soft Matter, 2012. 8(31): p. 8113-8120.

Martin, GR and Timpl, R, Laminin and other basement membrane components. Annual Review of Cell Biology, 1987. 3(1): p. 57-85.

Martinez-Moreno, M, et al., Direct interaction between the reductase domain of endothelial nitric oxide synthase and the ryanodine receptor. FEBS Letters, 2005. 579(14): p. 3159-3163.

Maruo, S, Nakamura, O, and Kawata, S, Three-dimensional microfabrication with two-photon-absorbed photopolymerization. Optical Letters, 1997. 22(2): p. 132-134.

Masaki, T, Polarization and myelination in myelinating glia. ISRN Neurology, 2012. 2012: p. 28.

Mcbeath, R, et al., Cell shape, cytoskeletal tension, and rhoa regulate stem cell lineage commitment. Developmental Cell, 2004. 6(4): p. 483-495.

Mccarthy, JB, Palm, SL, and Furcht, LT, Migration by haptotaxis of a schwann cell tumor line to the basement membrane glycoprotein laminin. Journal of Cell Biology, 1983. 97(3): p. 772-777.

Mcdonald, JA, Extracellular matrix assembly. Annual Review of Cell Biology, 1988. 4: p. 183-207.

Mckerracher, L, Chamoux, M, and Arregui, CO, Role of laminin and integrin interactions in growth cone guidance. Molecular Neurobiology, 1996. 12(2): p. 95-116.

Mcquade, LE and Lippard, SJ, Fluorescent probes to investigate nitric oxide and other reactive nitrogen species in biology (truncated form: Fluorescent probes of reactive nitrogen species). Current Opinion in Chemical Biology, 2010. 14(1): p. 43-49.

Merkel, R, et al., Cell force microscopy on elastic layers of finite thickness. Biophysical Journal, 2007. 93(9): p. 3314-3323.

Miller, C, et al., Oriented schwann cell growth on micropatterned biodegradable polymer substrates. Biomaterials, 2001. 22(11): p. 1263-1269.

Miller, K, et al., Mechanical properties of brain tissue in-vivo: Experiment and computer simulation. Journal of Biomechanics, 2000. 33(11): p. 1369-1376.

Miller, RK and Mccrea, PD, Wnt to build a tube: Contributions of wnt signaling to epithelial tubulogenesis. Developmental Dynamics, 2010. 239(1): p. 77-93.

Mitchel, JA and Hoffman-Kim, D, Cellular scale anisotropic topography guides schwann cell motility. PLOS ONE, 2011. 6(9): p. e24316.

Moncada, S and Higgs, A, The l-arginine-nitric oxide pathway. New England Journal of Medicine, 1993. 329(27): p. 2002-2012.

Moncada, S, Palmer, RM, and Higgs, EA, Biosynthesis of nitric oxide from l-arginine. A pathway for the regulation of cell function and communication. Biochemical Pharmacology, 1989. 38(11): p. 1709-1715.

Moore, K, Macsween, M, and Shoichet, M, Immobilized concentration gradients of neurotrophic factors guide neurite outgrowth of primary neurons in macroporous scaffolds. Tissue Engineering, 2006. 12(2): p. 267-278.

Moore, NM, et al., The use of immobilized osteogenic growth peptide on gradient substrates synthesized via click chemistry to enhance mc3t3-e1 osteoblast proliferation. Biomaterials, 2010. 31(7): p. 1604-1611.

Moses, JE and Moorhouse, AD, The growing applications of click chemistry. Chemical Society Review, 2007. 36(8): p. 1249-1262.

Mosna, F, Sensebe, L, and Krampera, M, Human bone marrow and adipose tissue mesenchymal stem cells: A user's guide. Stem Cells and Development, 2010. 19(10): p. 1449-1470.

Mullender, MG, et al., Osteocyte density and histomorphometric parameters in cancellous bone of the proximal femur in five mammalian species. Journal of Orthopaedic Research, 1996. 14(6): p. 972-979.

Muraoka, T, et al., Light-triggered bioactivity in three dimensions. Angewandte Chemie International Edition, 2009. 48(32): p. 5946-5949.

Murohara, T, et al., Nitric oxide synthase modulates angiogenesis in response to tissue ischemia. Journal of Clinical Investigation, 1998. 101(11): p. 2567-2578.

Murphy, CM, Haugh, MG, and O'brien, FJ, The effect of mean pore size on cell attachment, proliferation and migration in collagen-glycosaminoglycan scaffolds for bone tissue engineering. Biomaterials, 2010. 31(3): p. 461-466.

Musoke-Zawedde, P and Shoichet, MS, Anisotropic three-dimensional peptide channels guide neurite outgrowth within a biodegradable hydrogel matrix. Biomedical Materials, 2006. 1(3): p. 162-169.

Nathan, C, Nitric oxide as a secretory product of mammalian cells. FASEB Journal, 1992. 6(12): p. 3051-3064.

Nathan, C and Xie, QW, Nitric oxide synthases: Roles, tolls, and controls. Cell, 1994. 78(6): p. 915-918.

Nathan, CF and Hibbs, JB, Jr., Role of nitric oxide synthesis in macrophage antimicrobial activity. Current Opinion in Immunology, 1991. 3(1): p. 65-70.

Nelson, BA, King, WP, and Gall, K, Shape recovery of nanoscale imprints in a thermoset "shape memory" polymer. Applied Physics Letters, 2005. 86(10): p. -.

Nelson, RD, Quie, PG, and Simmons, RL, Chemotaxis under agarose: A new and simple method for measuring chemotaxis and spontaneous migration of human polymorphonuclear leukocytes and monocytes. Journal of Immunology, 1975. 115(6): p. 1650-1656.

Nemir, S, Hayenga, HN, and West, JL, Pegda hydrogels with patterned elasticity: Novel tools for the study of cell response to substrate rigidity. Biotechnology and Bioengineering, 2010. 105(3): p. 636-644.

Ng, MR and Brugge, JS, A stiff blow from the stroma: Collagen crosslinking drives tumor progression. Cancer Cell, 2009. 16(6): p. 455-457.

Nielson, R, Kaehr, B, and Shear, JB, Microreplication and design of biological architectures using dynamic-mask multiphoton lithography. Small, 2009. 5(1): p. 120-125.

Nussler, AK, et al., Stimulation of the nitric oxide synthase pathway in human hepatocytes by cytokines and endotoxin. Journal of Experimental Medicine, 1992. 176(1): p. 261-264.

Nuzzo, RG and Allara, DL, Adsorption of bifunctional organic disulfides on gold surfaces. Journal of the American Chemical Society, 1983. 105(13): p. 4481-4483.

O'brien, AJ, et al., Nitric oxide synthase is localized predominantly in the golgi apparatus and cytoplasmic vesicles of vascular endothelial cells. Histochemistry and Cell Biology, 1995. 103(3): p. 221-225.

O'rourke, NA, et al., Tangential migration of neurons in the developing cerebral cortex. Development, 1995. 121(7): p. 2165-2176.

Ogaki, R, Alexander, M, and Kingshott, P, Chemical patterning in biointerface science. Materials Today, 2010. 13(4): p. 22-35.

Olsen, O, et al., Renal defects associated with improper polarization of the crb and dlg polarity complexes in mals-3 knockout mice. Journal of Cell Biology, 2007. 179(1): p. 151-164.

Ono, K and Kawamura, K, Migration of immature neurons along tangentially oriented fibers in the subpial part of the fetal mouse medulla oblongata. Experimental Brain Research, 1989. 78(2): p. 290-300.

Ortino, B, et al., Substrates and routes of migration of early generated neurons in the developing rat thalamus. European Journal of Neuroscience, 2003. 18(2): p. 323-332.

Pacher, P, Beckman, JS, and Liaudet, L, Nitric oxide and peroxynitrite in health and disease. Physiological Reviews, 2007. 87(1): p. 315-424.

Paguirigan, AL and Beebe, DJ, Protocol for the fabrication of enzymatically crosslinked gelatin microchannels for microfluidic cell culture. Nature Protocols, 2007. 2(7): p. 1782-1788.

Palm, SL and Furcht, LT, Production of laminin and fibronectin by schwannoma cells: Cell-protein interactions in vitro and protein localization in peripheral nerve in vivo. Journal of Cell Biology, 1983. 96(5): p. 1218-1226.

Palmer, RM, Ashton, DS, and Moncada, S, Vascular endothelial cells synthesize nitric oxide from l-arginine. Nature, 1988. 333(6174): p. 664-666.

Pampaloni, F, Reynaud, EG, and Stelzer, EHK, The third dimension bridges the gap between cell culture and live tissue. Nature Reviews Molecular Cell Biology, 2007. 8(10): p. 839-845.

Panchuk-Voloshina, N, et al., Alexa dyes, a series of new fluorescent dyes that yield exceptionally bright, photostable conjugates. Journal of Histochemistry and Cytochemistry, 1999. 47(9): p. 1179-1188.

Park, J, et al., Quantitative analysis of the combined effect of substrate rigidity and topographic guidance on cell morphology. IEEE Transactions on Nanobioscience, 2012. 11(1): p. 28-36.

Paszek, MJ, et al., Tensional homeostasis and the malignant phenotype. Cancer Cell, 2005. 8(3): p. 241-254.

Pathak, A and Kumar, S, Independent regulation of tumor cell migration by matrix stiffness and confinement. Proceedings of the National Academy of Sciences, 2012.

Pelham, RJ, Jr. and Wang, Y, Cell locomotion and focal adhesions are regulated by substrate flexibility. Proceedings of the National Academy of Sciences, 1997. 94(25): p. 13661-13665.

Pervin, S, et al., Nitric oxide in physiologic concentrations targets the translational machinery to increase the proliferation of human breast cancer cells: Involvement of mammalian target of rapamycin/eif4e pathway. Cancer Research, 2007. 67(1): p. 289-299.

Petrie, RJ, Doyle, AD, and Yamada, KM, Random versus directionally persistent cell migration. Nature Reviews Molecular Cell Biology, 2009. 10(8): p. 538-549.

Pindzola, RR, Doller, C, and Silver, J, Putative inhibitory extracellular matrix molecules at the dorsal root entry zone of the spinal cord during development and after root and sciatic nerve lesions. Developmental Biology, 1993. 156(1): p. 34-48.

Piner, RD, et al., "Dip-pen" nanolithography. Science, 1999. 283(5402): p. 661-663.

Pins, GD, et al., Multiphoton excited fabricated nano and micro patterned extracellular matrix proteins direct cellular morphology. Journal of Biomedical Materials Research A, 2006. 78(1): p. 194-204.

Pitts, JD, et al., Submicron multiphoton free-form fabrication of proteins and polymers: Studies of reaction efficiencies and applications in sustained release. Macromolecules, 2000. 33(5): p. 1514-1523.

Pitts, JD, et al., New photoactivators for multiphoton excited three-dimensional submicron cross-linking of proteins: Bovine serum albumin and type 1 collagen. Photochemistry and Photobiology, 2002. 76(2): p. 135-144.

Porterfield, DM, et al., Proteins and lipids define the diffusional field of nitric oxide. American Journal of Physiology Lung Cell Molecular Physiology, 2001. 281(4): p. L904-912.

Prast, H and Philippu, A, Nitric oxide as modulator of neuronal function. Progress in Neurobiology, 2001. 64(1): p. 51-68.

Privett, BJ, Shin, JH, and Schoenfisch, MH, Electrochemical nitric oxide sensors for physiological measurements. Chemical Society Reviews, 2010. 39(6): p. 1925-1935.

Provenzano, PP, et al., Contact guidance mediated three-dimensional cell migration is regulated by rho/rock-dependent matrix reorganization. Biophysical Journal, 2008. 95(11): p. 5374-5384.

Prueitt, RL, et al., Inflammation and igf-i activate the akt pathway in breast cancer. International Journal of Cancer, 2007. 120(4): p. 796-805.

Qi, L, et al., The effects of topographical patterns and sizes on neural stem cell behavior. PLOS One, 2013. 8(3): p. e59022.

Qin, D, Xia, Y, and Whitesides, GM, Soft lithography for micro- and nanoscale patterning. Nature Protocols, 2010. 5(3): p. 491-502.

Raeber, GP, Lutolf, MP, and Hubbell, JA, Molecularly engineered peg hydrogels: A novel model system for proteolytically mediated cell migration. Biophysical Journal, 2005. 89(2): p. 1374-1388.

Rafikova, O, Rafikov, R, and Nudler, E, Catalysis of s-nitrosothiols formation by serum albumin: The mechanism and implication in vascular control. Proceedings of the National Academy of Sciences, 2002. 99(9): p. 5913-5918.

Rakic, P, Mode of cell migration to the superficial layers of fetal monkey neocortex. Journal of Computational Neurology, 1972. 145(1): p. 61-83.

Rakickas, T, et al., Functional hydrogel density patterns fabricated by dip-pen nanolithography and photografting. Small, 2011. 7(15): p. 2153-2157.

Ray, PD, Huang, BW, and Tsuji, Y, Reactive oxygen species (ros) homeostasis and redox regulation in cellular signaling. Cell Signaling, 2012. 24(5): p. 981-990.

Reichardt, LF, Neurotrophin-regulated signalling pathways. Philosophical Transactions of the Royal Society of London B: Biological Sciences, 2006. 361(1473): p. 1545-1564.

Ridnour, LA, et al., The chemistry of nitrosative stress induced by nitric oxide and reactive nitrogen oxide species. Putting perspective on stressful biological situations. Journal of Biological Chemistry, 2004. 385(1): p. 1-10.

Ritschdorff, ET, Nielson, R, and Shear, JB, Multi-focal multiphoton lithography. Lab on a Chip, 2012. 12(5): p. 867-871.

Ritschdorff, ET and Shear, JB, Multiphoton lithography using a high-repetition rate microchip laser. Analytical Chemistry, 2010. 82(20): p. 8733-8737.

Riveline, D, et al., Focal contacts as mechanosensors: Externally applied local mechanical force induces growth of focal contacts by an mdia1-dependent and rock-independent mechanism. Journal of Cell Biology, 2001. 153(6): p. 1175-1186.

Rodriguez, J, et al., Performance of diamino fluorophores for the localization of sources and targets of nitric oxide. Free Radical Biology and Medicine, 2005. 38(3): p. 356-368.

Rolls, A, et al., Two faces of chondroitin sulfate proteoglycan in spinal cord repair: A role in microglia/macrophage activation. PLOS Medicine, 2008. 5(8): p. e171.

Rosenblatt, J, Devereux, B, and Wallace, DG, Injectable collagen as a ph-sensitive hydrogel. Biomaterials, 1994. 15(12): p. 985-995.

Ross, AM and Lahann, J, Surface engineering the cellular microenvironment via patterning and gradients. Journal of Polymer Science Part B: Polymer Physics, 2013. 51(10): p. 775-794.

Roth, EA, et al., Inkjet printing for high-throughput cell patterning. Biomaterials, 2004. 25(17): p. 3707-3715.

Rudic, RD, et al., Direct evidence for the importance of endothelium-derived nitric oxide in vascular remodeling. Journal of Clinical Investigation, 1998. 101(4): p. 731-736.

Ruoslahti, E, Rgd and other recognition sequences for integrins. Annual Review of Cell and Developmental Biology, 1996. 12(1): p. 697-715.

Saha, K, et al., Substrate modulus directs neural stem cell behavior. Biophysical Journal, 2008. 95(9): p. 4426-4438.

Sasaki, N, et al., Photochemical immobilization of cells onto a glass substrate for in situ DNA analysis. Analytical Sciences, 2012. 28(6): p. 537-539.

Schmidt, CE and Leach, JB, Neural tissue engineering: Strategies for repair and regeneration. Annual Review of Biomedical Engineering, 2003. 5: p. 293-347.

Schmidt, CE, et al., Stimulation of neurite outgrowth using an electrically conducting polymer. Proceedings of the National Academy of Sciences, 1997. 94(17): p. 8948-8953.

Schoof, H, et al., Control of pore structure and size in freeze-dried collagen sponges. Journal of Biomedical Materials Research, 2001. 58(4): p. 352-357.

Schuman, EM and Madison, DV, A requirement for the intercellular messenger nitric oxide in long-term potentiation. Science, 1991. 254(5037): p. 1503-1506.

Schwarz, US and Gardel, ML, United we stand: Integrating the actin cytoskeleton and cell-matrix adhesions in cellular mechanotransduction. Journal of Cell Science, 2012. 125(Pt 13): p. 3051-3060.

Scott, MA, Wissner-Gross, ZD, and Yanik, MF, Ultra-rapid laser protein micropatterning: Screening for directed polarization of single neurons. Lab on a Chip, 2012. 12(12): p. 2265-2276.

Seidlits, SK, et al., The effects of hyaluronic acid hydrogels with tunable mechanical properties on neural progenitor cell differentiation. Biomaterials, 2010. 31(14): p. 3930-3940.

Seidlits, SK, Schmidt, CE, and Shear, JB, High-resolution patterning of hydrogels in three dimensions using direct-write photofabrication for cell guidance. Advanced Functional Materials, 2009. 19(22): p. 3543-3551.

Sekula, S, et al., Multiplexed lipid dip-pen nanolithography on subcellular scales for the templating of functional proteins and cell culture. Small, 2008. 4(10): p. 1785-1793.

Sen, S, Engler, AJ, and Discher, DE, Matrix strains induced by cells: Computing how far cells can feel. Cell Molecular Bioengineering, 2009. 2(1): p. 39-48.

Sessa, WC, Regulation of endothelial derived nitric oxide in health and disease. Memorias de Instituto Oswaldo Cruz, 2005. 100 Suppl 1: p. 15-18.

Shaul, PW, Regulation of endothelial nitric oxide synthase: Location, location, location. Annual RevIew Physiology, 2002. 64: p. 749-774.

Shepherd, DE and Seedhom, BB, The 'instantaneous' compressive modulus of human articular cartilage in joints of the lower limb. Rheumatology, 1999. 38(2): p. 124-132.

Shyy, JY and Chien, S, Role of integrins in endothelial mechanosensing of shear stress. Circulation Research, 2002. 91(9): p. 769-775.

Simon, HU, Haj-Yehia, A, and Levi-Schaffer, F, Role of reactive oxygen species (ros) in apoptosis induction. Apoptosis, 2000. 5(5): p. 415-418.

Singh, RJ, et al., Mechanism of nitric oxide release from s-nitrosothiols. Journal of Biological Chemistry, 1996. 271(31): p. 18596-18603.

Smith, RC, et al., Conjugated polymer-based fluorescence turn-on sensor for nitric oxide. Organic Letters, 2005. 7(16): p. 3573-3575.

Sochol, RD, et al., Unidirectional mechanical cellular stimuli via micropost array gradients. Soft Matter, 2011. 7(10): p. 4606-4609.

Son, YJ and Thompson, WJ, Nerve sprouting in muscle is induced and guided by processes extended by schwann cells. Neuron, 1995. 14(1): p. 133-141.

Son, YJ, Trachtenberg, JT, and Thompson, WJ, Schwann cells induce and guide sprouting and reinnervation of neuromuscular junctions. Trends in Neuroscience, 1996. 19(7): p. 280-285.

Sonna, LA, et al., Invited review: Effects of heat and cold stress on mammalian gene expression. Journal of Applied Physiology, 2002. 92(4): p. 1725-1742.

Spivey, EC, Multiphoton lithography of mechanically and functionally tunable hydrogels. 2012, The University of Texas at Austin.

Spivey, EC, et al., Multiphoton lithography of unconstrained three-dimensional protein microstructures. Advanced Functional Materials, 2013. 23(3): p. 333-339.

Stamler, JS, Redox signaling: Nitrosylation and related target interactions of nitric oxide. Cell, 1994. 78(6): p. 931-936.

Steffensen, B, Hakkinen, L, and Larjava, H, Proteolytic events of wound-healing--coordinated interactions among matrix metalloproteinases (mmps), integrins, and extracellular matrix molecules. Critical Reviews in Oral Biological Medicine, 2001. 12(5): p. 373-398.

Stolz, DB, et al., Peroxisomal localization of inducible nitric oxide synthase in hepatocytes. Hepatology, 2002. 36(1): p. 81-93.

Straley, KS and Heilshorn, SC, Dynamic, 3d-pattern formation within enzyme-responsive hydrogels. Advanced Materials, 2009. 21(41): p. 4148-4152.

Strickler, JH and Webb, WW, Three-dimensional optical data storage in refractive media by two-photon point excitation. Optical Letters, 1991. 16(22): p. 1780-1782.

Stuehr, DJ and Nathan, CF, Nitric oxide. A macrophage product responsible for cytostasis and respiratory inhibition in tumor target cells. Journal of Experimental Medicine, 1989. 169(5): p. 1543-1555.

Sugiura, S, et al., Dynamic three-dimensional micropatterned cell co-cultures within photocurable and chemically degradable hydrogels. Journal of Tissue Engineering and Regenerative Medicine, 2013: p. n/a-n/a.

Sugiura, S, et al., Surface modification of polydimethylsiloxane with photo-grafted poly(ethylene glycol) for micropatterned protein adsorption and cell adhesion. Colloids and Surfaces B: Biointerfaces, 2008. 63(2): p. 301-305.

Suh, KY, et al., A simple soft lithographic route to fabrication of poly(ethylene glycol) microstructures for protein and cell patterning. Biomaterials, 2004. 25(3): p. 557-563.

Sundararaghavan, HG, et al., Fiber alignment directs cell motility over chemotactic gradients. Biotechnology and Bioengineering, 2013. 110(4): p. 1249-1254.

Suri, S and Schmidt, CE, Cell-laden hydrogel constructs of hyaluronic acid, collagen, and laminin for neural tissue engineering. Tissue Engineering Part A, 2010. 16(5): p. 1703-1716.

Ta, HT, Dass, CR, and Dunstan, DE, Injectable chitosan hydrogels for localised cancer therapy. Journal of Controlled Release, 2008. 126(3): p. 205-216.

Tai, G, et al., Electrotaxis and wound healing: Experimental methods to study electric fields as a directional signal for cell migration. Methods in Molecular Biology, 2009. 571: p. 77-97.

Tam, SL and Gordon, T, Mechanisms controlling axonal sprouting at the neuromuscular junction. Journal of Neurocytology, 2003. 32(5-8): p. 961-974.

Tan, H and Marra, KG, Injectable, biodegradable hydrogels for tissue engineering applications. Materials, 2010. 3(3): p. 1746-1767.

186

Tang, MD, Golden, AP, and Tien, J, Molding of three-dimensional microstructures of gels. Journal of the American Chemical Society, 2003. 125(43): p. 12988-12989.

Tashiro, K, et al., A synthetic peptide containing the ikvav sequence from the a chain of laminin mediates cell attachment, migration, and neurite outgrowth. Journal of Biological Chemistry, 1989. 264(27): p. 16174-16182.

Teixeira, AI, et al., Epithelial contact guidance on well-defined micro- and nanostructured substrates. Journal of Cell Science, 2003. 116(Pt 10): p. 1881-1892.

Tekin, H, et al., Responsive microgrooves for the formation of harvestable tissue constructs. Langmuir, 2011. 27(9): p. 5671-5679.

Teo, BKK, et al., Nanotopography modulates mechanotransduction of stem cells and induces differentiation through focal adhesion kinase. ACS Nano, 2013. 7(6): p. 4785-4798.

Thery, M, et al., Anisotropy of cell adhesive microenvironment governs cell internal organization and orientation of polarity. Proceedings of the National Academy of Sciences, 2006. 103(52): p. 19771-19776.

Thomas, CH, et al., Engineering gene expression and protein synthesis by modulation of nuclear shape. Proceedings of the National Academy of Sciences, 2002. 99(4): p. 1972-1977.

Thomas, DD, et al., Hypoxic inducible factor 1alpha, extracellular signal-regulated kinase, and p53 are regulated by distinct threshold concentrations of nitric oxide. Proceedings of the National Academy of Sciences, 2004. 101(24): p. 8894-8899.

Thomas, DD, et al., The chemical biology of nitric oxide: Implications in cellular signaling. Free Radical Biology and Medicine, 2008. 45(1): p. 18-31.

Tibbitt, MW, et al., Controlled two-photon photodegradation of peg hydrogels to study and manipulate subcellular interactions on soft materials. Soft Matter, 2010. 6(20): p. 5100-5108.

Tocce, EJ, et al., The influence of biomimetic topographical features and the extracellular matrix peptide rgd on human corneal epithelial contact guidance. Acta Biomaterialia, 2013. 9(2): p. 5040-5051.

Tropel, P, et al., Functional neuronal differentiation of bone marrow-derived mesenchymal stem cells. Stem Cells, 2006. 24(12): p. 2868-2876.

Tseng, P and Di Carlo, D, Substrates with patterned extracellular matrix and subcellular stiffness gradients reveal local biomechanical responses. Advanced Materials, 2014. 26(8): p. 1242-1247.

Tsikas, D, Simultaneous derivatization and quantification of the nitric oxide metabolites nitrite and nitrate in biological fluids by gas chromatography/mass spectrometry. Analytical Chemistry, 2000. 72(17): p. 4064-4072.

Tsikas, D, Analysis of nitrite and nitrate in biological fluids by assays based on the griess reaction: Appraisal of the griess reaction in the l-arginine/nitric oxide area of research. Journal of Chromatogr B Analytical Technologies in the Biomedical Life Sciences, 2007. 851(1-2): p. 51-70.

Unger, MA, et al., Monolithic microfabricated valves and pumps by multilayer soft lithography. Science, 2000. 288(5463): p. 113-116.

Ushio-Fukai, M and Alexander, RW, Reactive oxygen species as mediators of angiogenesis signaling: Role of nad(p)h oxidase. Molecular Cell Biochemistry, 2004. 264(1-2): p. 85-97.

Uttayarat, P, et al., Topographic guidance of endothelial cells on silicone surfaces with micro- to nanogrooves: Orientation of actin filaments and focal adhesions. Journal of Biomedical Materials Research A, 2005. 75(3): p. 668-680.

Valeur, B and Leray, I, Design principles of fluorescent molecular sensors for cation recognition. Coordination Chemistry Reviews, 2000. 205(1): p. 3-40.

Van Dijk, M, Goransson, SA, and Stromblad, S, Cell to extracellular matrix interactions and their reciprocal nature in cancer. Experimental Cell Research, 2013.

Vareniuk, I, et al., Peripheral neuropathy in mice with neuronal nitric oxide synthase gene deficiency. International Journal of Molecular Medicine, 2009. 23(5): p. 571-580.

Villanueva, C and Giulivi, C, Subcellular and cellular locations of nitric oxide synthase isoforms as determinants of health and disease. Free Radical Biology and Medicine, 2010. 49(3): p. 307-316.

Vincent, LG, et al., Mesenchymal stem cell durotaxis depends on substrate stiffness gradient strength. Biotechnology Journal, 2013. 8(4): p. 472-484.

Von Recum, HA, et al., Novel thermally reversible hydrogel as detachable cell culture substrate. Journal of Biomedical Materials Research, 1998. 40(4): p. 631-639.

Waldbaur, A, et al., Maskless projection lithography for the fast and flexible generation of grayscale protein patterns. Small, 2012. 8(10): p. 1570-1578.

Wan, LQ, et al., Geometric control of human stem cell morphology and differentiation. Integrated Biology, 2010. 2(7-8): p. 346-353.

Wang, CJ, et al., A microfluidics-based turning assay reveals complex growth cone responses to integrated gradients of substrate-bound ecm molecules and diffusible guidance cues. Lab on a Chip, 2008. 8(2): p. 227-237.

Wang, PY, Yu, HT, and Tsai, WB, Modulation of alignment and differentiation of skeletal myoblasts by submicron ridges/grooves surface structure. Biotechnology and Bioengineering, 2010. 106(2): p. 285-294.

Wang, R, et al., Human dermal fibroblasts produce nitric oxide and express both constitutive and inducible nitric oxide synthase isoforms. Journal of Investigative Dermatology, 1996. 106(3): p. 419-427.

Wang, X, et al., Decoupling polymer properties to elucidate mechanisms governing cell behavior. Tissue Engineering Part B Review, 2012. 18(5): p. 396-404.

Wang, Y, et al., Regulation of vegf-induced endothelial cell migration by mitochondrial reactive oxygen species. American Journal of Physiology Cell Physiology, 2011. 301(3): p. C695-704.

Wardman, P, Fluorescent and luminescent probes for measurement of oxidative and nitrosative species in cells and tissues: Progress, pitfalls, and prospects. Free Radical Biology and Medicine, 2007. 43(7): p. 995-1022.

Webb, A, et al., Guidance of oligodendrocytes and their progenitors by substratum topography. Journal of Cell Science, 1995. 108 (Pt 8): p. 2747-2760.

Weiss, P, The problem of specificity in growth and development. Yale Journal of Biological Medicine, 1947. 19(3): p. 235-278.

Weisz, A, et al., Dual mechanism for the control of inducible-type no synthase gene expression in macrophages during activation by interferon-gamma and bacterial lipopolysaccharide. Transcriptional and post-transcriptional regulation. Journal of Biological Chemistry, 1994. 269(11): p. 8324-8333.

Wells, RG, The role of matrix stiffness in regulating cell behavior. Hepatology, 2008. 47(4): p. 1394-1400.

West, JL and Hubbell, JA, Polymeric biomaterials with degradation sites for proteases involved in cell migration. Macromolecules, 1998. 32(1): p. 241-244.

Whitesides, GM, et al., Soft lithography in biology and biochemistry. Annual Review Biomedical Engineering, 2001. 3: p. 335-373.

Wiley, JW, The many faces of nitric oxide: Cytotoxic, cytoprotective or both. Neurogastroenterology and Motility, 2007. 19(7): p. 541-544.

Williams, LN, et al., The anisotropic compressive mechanical properties of the rabbit patellar tendon. Biorheology, 2008. 45(5): p. 577-586.

Williams, RJP, Role of transition metal ions in biological processes. Royal Institute of Chemistry, Reviews, 1968. 1(1): p. 13-38.

Willis, BC, Dubois, RM, and Borok, Z, Epithelial origin of myofibroblasts during fibrosis in the lung. Proceedings of the American Thoracic Society, 2006. 3(4): p. 377-382.

Wink, DA and Mitchell, JB, Chemical biology of nitric oxide: Insights into regulatory, cytotoxic, and cytoprotective mechanisms of nitric oxide. Free Radical Biology and Medicine, 1998. 25(4–5): p. 434-456.

Wong, JY, Leach, JB, and Brown, XQ, Balance of chemistry, topography, and mechanics at the cell–biomaterial interface: Issues and challenges for assessing the role of substrate mechanics on cell response. Surface Science, 2004. 570(1–2): p. 119-133.

Wood, MA, Bagnaninchi, P, and Dalby, MJ, The beta integrins and cytoskeletal nanoimprinting. Experimental Cell Research, 2008. 314(4): p. 927-935.

Wu, C-C, et al., Porous multilayer-coated afm tips for dip-pen nanolithography of proteins. Journal of the American Chemical Society, 2009. 131(22): p. 7526-7527.

Wylie, RG, et al., Spatially controlled simultaneous patterning of multiple growth factors in three-dimensional hydrogels. Nature Materials, 2011. 10(10): p. 799-806.

Wylie, RG and Shoichet, MS, Two-photon micropatterning of amines within an agarose hydrogel. Journal of Materials Chemistry, 2008. 18(23): p. 2716-2721.

Xia, Y, et al., Unconventional methods for fabricating and patterning nanostructures. Chemical Reviews, 1999. 99(7): p. 1823-1848.

Xie, T, Tunable polymer multi-shape memory effect. Nature, 2010. 464(7286): p. 267-270.

Xu, W, et al., The role of nitric oxide in cancer. Cell Research, 2002. 12(5-6): p. 311-320.

Yamaki, K, et al., Regulation of cellular morphology using temperature-responsive hydrogel for integrin-mediated mechanical force stimulation. Biomaterials, 2009. 30(7): p. 1421-1427.

Yamato, M, et al., Thermally responsive polymer-grafted surfaces facilitate patterned cell seeding and co-culture. Biomaterials, 2002. 23(2): p. 561-567.

Yang, L, et al., A targetable nanogenerator of nitric oxide for light-triggered cytotoxicity. Journal of Materials Chemistry B, 2013. 1(44): p. 6115-6122.

Yang, Y, et al., A highly selective low-background fluorescent imaging agent for nitric oxide. Journal of the American Chemical Society, 2010. 132(38): p. 13114-13116.

Yim, EK, Pang, SW, and Leong, KW, Synthetic nanostructures inducing differentiation of human mesenchymal stem cells into neuronal lineage. Experimental Cell Research, 2007. 313(9): p. 1820-1829.

Yoshikawa, HY, et al., Quantitative evaluation of mechanosensing of cells on dynamically tunable hydrogels. Journal of the American Chemical Society, 2011. 133(5): p. 1367-1374.

Young, JL and Engler, AJ, Hydrogels with time-dependent material properties enhance cardiomyocyte differentiation in vitro. Biomaterials, 2011. 32(4): p. 1002-1009.

Young, RJ, et al., Inhibition of inducible nitric oxide synthase by acetamidine derivatives of hetero-substituted lysine and homolysine. Bioorganic and Medicine Chemistry Letters, 2000. 10(6): p. 597-600.

Yu, H, et al., From a bodipy-rhodamine scaffold to a ratiometric fluorescent probe for nitric oxide. New Journal of Chemistry, 2013. 37(6): p. 1688-1691.

Yu, LM, Wosnick, JH, and Shoichet, MS, Miniaturized system of neurotrophin patterning for guided regeneration. Journal of Neuroscience Methods, 2008. 171(2): p. 253-263.

Zaman, MH, et al., Migration of tumor cells in 3d matrices is governed by matrix stiffness along with cell-matrix adhesion and proteolysis. Proceedings of the National Academy of Sciences, 2006. 103(29): p. 10889-10894.

Zander, NE and Beebe, TP, Jr., Immobilized laminin concentration gradients on electrospun fiber scaffolds for controlled neurite outgrowth. Biointerphases, 2014. 9(1): p. 011003.

Zhao, X-M, Xia, Y, and Whitesides, GM, Soft lithographic methods for nano-fabrication. Journal of Materials Chemistry, 1997. 7(7): p. 1069-1074.

Zheng, W, Zhang, W, and Jiang, X, Precise control of cell adhesion by combination of surface chemistry and soft lithography. Advanced Healthcare Materials, 2013. 2(1): p. 95-108.

Zhou, L and Zhu, DY, Neuronal nitric oxide synthase: Structure, subcellular localization, regulation, and clinical implications. Nitric Oxide, 2009. 20(4): p. 223-230.

Zicha, D, Dunn, GA, and Brown, AF, A new direct-viewing chemotaxis chamber. Journal of Cell Science, 1991. 99 (Pt 4): p. 769-775.

Zipfel, WR, Williams, RM, and Webb, WW, Nonlinear magic: Multiphoton microscopy in the biosciences. Nature Biotechnology, 2003. 21(11): p. 1369-1377.